Wang, Brian Z., *AMP-Activated Protein Kinase (AMPK) signaling regulates the age-related decline of hippocampal neurogenesis*. Doctor of Philosophy (Biomedical Sciences), 4 April, 2018, 113 pp., 6 tables, 48 illustrations, bibliography, 119 titles.

Aging is the progressive decline of physiological function and increased vulnerability to disease and death. By the year 2050, 2 billion people will be over the age of 60. Accompanying this, the incidence of age-associated neurological diseases is expected to rise. Thus, there is an urgent need to find therapies to promote healthy brain aging. The finding that neurogenesis continues into adulthood allows us to target endogenous neurogenesis as a potential therapeutic. However, the number of stem cells can decrease by about 80% in the aged brain and is a main cause for the decrease in brain function. The reasons for the age-related decline in neurogenesis can be due to intrinsic factors such as cell metabolism, which have been studied but its role in neurogenesis remains largely unexplored. Interestingly, neural stem cells (NSCs) possess metabolically different characteristics from their differentiated progeny, suggesting the need for a shift in cellular metabolism to accommodate the requirements for neurogenesis. In the process of the metabolic shift, the AMP-activated protein kinase (AMPK) plays a pivotal role for controlling stem cell proliferation and differentiation as a cell's master metabolic regulator. Additionally, AMPK has been reported to control the functions of signaling pathways that regulate the aging process, which suggests its potential involvement in the age-related decline of neurogenesis.

Therefore, we hypothesize that inhibition of AMPK signaling activation (phosphorylation) in the old brain will cause a concomitant increase in hippocampal neurogenesis. Our specific aim is to establish whether AMPK signaling plays a critical role in the age-related decline of hippocampal neurogenesis. Our objectives for this aim are to (i) determine the expression pattern of AMPK in the subgranular and subventricular zones of young-adult and old mice using immunohistochemistry and Western blotting; and (ii) examine the impact of loss or gain of AMPK activation on hippocampal neurogenesis in young-adult and old mice using pharmacological agents Compound C (AMPK inhibitor) and 5-Aminoimidazole-4-carboxamide ribonucleotide (AICAR, AMPK activator). Our results show that (i) AMPK subunit isoforms are differentially expressed in the neurogenic regions – most are localized to the cytoplasm in the subgranular zone (SGZ) with the exception of α2 and β1, while most isoforms are found in the nucleus in the subventricular zone (SVZ) except α1; (ii) AMPK signaling activation was significantly increased in the SGZ and SVZ; and (iii) short-term but not long-term pharmacological inhibition of AMPK signaling could partially rescue hippocampal neurogenesis in the old brain. Taken together, these results indicate that AMPK is a critical mediator in the regulation of downstream processes for the age-related decline in hippocampal neurogenesis.

AMP-ACTIVATED PROTEIN KINASE (AMPK) SIGNALING REGULATES

THE AGE-RELATED DECLINE OF HIPPOCAMPAL NEUROGENESIS

Brian Z. Wang, B.Sc. (Hons)

APPROVED:

Major Professor

Committee Member

Committee Member

Committee Member

University Member

Chair, Department of Pharmacology & Neuroscience

Dean, Graduate School of Biomedical Science

AMP-ACTIVATED PROTEIN KINASE (AMPK) SIGNALING REGULATES THE AGE-RELATED DECLINE OF HIPPOCAMPAL NEUROGENESIS

DISSERTATION

Presented to the Graduate Council of the

Graduate School of Biomedical Sciences

University of North Texas

Health Science Center at Fort Worth

in Partial Fulfillment of the Requirements

For the Degree of

DOCTOR OF PHILOSOPHY

By

Brian Z. Wang, B.Sc. (Hons)

Fort Worth, Texas

April 2018

TABLE OF CONTENTS

LIST OF TABLES

Tables

LIST OF ILLUSTRATIONS

Figures

ACKNOWLEDGMENTS

I would like to acknowledge my advisory committee members Drs. Lisa Hodge, Meharvan Singh, Nathalie Sumien, Shaohua Yang and especially, my mentor, Dr. Kunlin Jin. I am deeply grateful for how each of you has poured into my life. Your words of wisdom are simple and life-changing, and I can say I have grown into a well-rounded scientist and a better person because of you. Thank you so much.

I also want to recognize past and present members of Jin lab (Jiang Lei, Jixian, Kaijing, Changhong, Jane, Shengwei, Jiangnan, Hongxia) and friends here in Fort Worth (Charity, Faith, Hope) and back in the UK (Mateusz) and Singapore (DLCC family). Your friendships have molded me into the person I am today.

To my dad (Timothy), mum (Theresa), sister (Eunice), granddad (Daniel) and grandma (Elizabeth), I would have struggled through this tremendously if not for your unceasing prayers and encouragement. I give thanks to God for each of you.

CHAPTER I

INTRODUCTION

Aging is the progressive decline of physiological function and increased vulnerability to disease and death (*1*). By the year 2050, one-fifth of the world population, that is, 2 billion people, will be over the age of 60 (*2*). With this increase in the proportion of elderly people, the incidence of age-associated neurological diseases and the economic burden are also expected to rise. For example, the number of Americans living with Alzheimer's disease (AD) will increase from 5.7 million in 2018 to 14 million in 2050 and the economic burden for AD is projected to rise to $1.1 trillion in 2050 from $277 billion in 2018 [Taken from: Alzheimer's Association, 2018 Alzheimer's Diseases Facts & Figures, https://www.alz.org/facts/ (Accessed April 3, 2018)]. Similarly, stroke, which is the leading cause of serious long-term disability in the US, is reported to have 610,000 new cases every year. The cost of stroke to the US is estimated to be about $34 billion each year (*3*). Thus, there is an urgent need to find therapies to promote healthy brain aging.

The finding that neurogenesis, the birth of new and functional neurons, continues into adulthood (*4, 5*) guides the current stem cell and regeneration field in targeting endogenous neurogenesis as a therapeutic for healthy brain aging (*6, 7*). It is well established that progressive

aging is associated with changes in brain structure, cellular and metabolic changes, increased oxidative stress, decreased self-repair capacities, reduced sensorimotor and cognitive functions, and dramatically increased susceptibility to neurodegenerative diseases (*8*). One such decline that is prominent with increasing age is the decrease in neurogenesis (*9*). An increasing number of studies show that neurogenesis in the adult brain is controlled by key molecules implicated in AD pathogenesis (*6*). For example, mutations in the presinilin-1 gene impaired hippocampus-dependent associative learning as early as 3 months of age (*10*), while significant reductions in cell proliferation and differentiation were evident as early as 2 months of age (*11*). Therefore, AD pathogenesis and neurogenesis may have a reciprocal relationship instead of solely being the result of neural dysfunction. With regards to stroke, a recent study showed that conditionally inhibiting neurogenesis after stroke impeded functional recovery in the long-term, indicating that neurogenesis in the adult brain is critical for functional recovery after stroke (*12*). Taken together, these highlight the importance of neurogenesis in the adult brain in coping with the increased vulnerability to neurological diseases with age. However, studies have shown that the number of stem cells in the aged brain dramatically decrease by about 80% in the subgranular zone (SGZ) of the dentate gyrus in the hippocampus (*13, 14*) and about 50% in the subventricular zone (SVZ) of the lateral ventricles (*15-17*), which suggests that the capacity to regenerate neurons is also decreased in response to aging. Therefore, while neurogenesis continues into adulthood, the aged brain's aptitude to repair itself is restricted, due to a dramatic decrease of cell renewal. Nevertheless, even with fewer stem cells in the aged brain, these can still produce similar numbers of newborn neurons compared with the young albeit at slower rates (*18, 19*). The reasons for the age-related decline in neurogenesis can be due to intrinsic factors such as cell metabolism, which have been studied but its role in neurogenesis remains largely unexplored.

Interestingly, it is reported that stem cells possess metabolically different characteristics from their differentiated progeny (*20, 21*). Proteomic analyses by Kuchinsky's group (*22, 23*) showed that almost half of the differentially expressed proteins identified in differentiated neurons versus (*vs.*) non-differentiated neural stem cells (NSCs) were proteins involved in metabolic pathways, suggesting the need for a shift in cellular metabolism to accommodate the requirements for neurogenesis. In the process of the metabolic shift, the AMP-activated protein kinase (AMPK) plays a pivotal role for controlling stem cell proliferation and differentiation as a cell's master metabolic regulator (*24, 25*). AMPK is a serine/threonine kinase and its structure and function in maintenance of at whole-body and cellular levels have been elucidated (*24-26*). However, its molecular role in neurogenesis has not been comprehensively studied at present, which is the aim of this research study.

To elaborate, AMPK exists as a heterotrimer that can form different combinations of α, β, and γ subunits (*Figure 1*), which are encoded by distinct genes to produce two α subunits (α1 and α2) that mediate AMPK's catalytic activity, two β (β1 and β2) and three γ (γ1, γ2, and γ3) subunits that regulate AMPK's phosphorylation and activity (*26, 27*). Differential combinations of these subunit proteins can generate twelve heterotrimeric configurations of AMPK, whose structures are essential to cope with the diverse roles in regulating metabolic processes in response to various stimuli. AMPK subunits also exhibit distinctive tissue-specific expression and activation. In the rat, AMPKα1 is uniformly distributed across the heart, liver, kidney, brain, spleen, lung, and skeletal muscle, but higher levels are found in adipose tissue (*27*). The AMPKα2 isoform, however, is most abundant in rat skeletal muscle compared with the heart, liver, brain, kidney, and lung (*28*).

In the mouse, qRT-PCR analysis indicates that the AMPKα2 isoform is highly expressed in the red and white vastus, heart, kidney, liver and to a lesser extent the lung, brain and adipose tissue (*26*). The AMPKβ1 isoform shows widespread expression in the liver while the β2 isoform is expressed highly in skeletal muscle and to a lesser extent the heart (*29, 30*). AMPKγ1 is expressed in most tissues while AMPKγ3 is restricted to the skeletal muscle (*31*) and AMPK γ2 is highly expressed in the heart (*32*).

AMPK is regulated by three main upstream kinases – liver kinase B1 (LKB1) (*33, 34*), calmodulin-dependent kinase kinase β (CaMKKβ) (*35, 36*), and the transforming growth factor beta-activated kinase 1 (TAK1) (*37, 38*) (*Figure 2*). When energy (ATP) levels are low in the cell, AMP binds to the γ subunit of AMPK, which facilitates the phosphorylation by LKB1, CaMKKβ or TAK1 at the Thr-172 site in the activation loop of the α-subunit catalytic domain thus activating AMPK to restore energy to equilibrium (*39-41*); AMPK achieves this by triggering energy-producing metabolic processes such as glycolysis and fatty acid oxidation, while simultaneously inhibiting energy-consuming metabolic pathways such as protein and fatty acid synthesis (*24*). Additionally, there are several proposed potential inhibitory mechanisms of AMPK activation. AMPK phosphorylation is also regulated by several protein phosphatases such as PP1, PP2A, and PP2C. These phosphatases eliminate the phosphate group from the phosphorylated Thr172 residue, and thus inactivate the AMPK complex (*42*). Other signaling protein kinases can also inhibit AMPK activity through the phosphorylation of Ser487 residue on the AMPKα1 isoform and Ser491 residue on the AMPKα2 isoform in humans (*43, 44*). Lastly, the presence of the autoinhibitory domain (AID) positioned between the catalytic and carboxy-terminal of the α subunit allows AMPK to regulate its own activity (*45, 46*).

Several studies have shown that AMPK is implicated in caloric restriction, which extends lifespan and delays the aging process (*47-49*). Furthermore, AMPK controls the functions of other metabolic regulators such as the Sirtuins and FoxO signaling pathways, which have direct effects on aging (*47, 50, 51*). Taken together, these suggest that the AMPK signaling pathway is involved in the aging process. However, with advancing age, AMPK signaling responsiveness to various stimuli declines (*47, 52*), indicating that effective activation of AMPK is essential to regulate an organism's metabolism to manage both internal and external environmental stimuli (*42*). Specifically, 5-Aminoimidazole-4-carboxamide ribonucleotide (AICAR) treatment and physical exercise significantly increased AMPKα2 activity in young rats but not in the old (*52*), and similar results have been reported (*53, 54*). Moreover, AMPK's sensitivity declines as we age, which evokes age-related cardiovascular disease and metabolic syndrome. The age-related dysregulation of activated AMPK and suppression of insulin-stimulated glucose uptake in rat skeletal muscles led to the development of metabolic syndrome (*55*), while a similar study showed its implication in myocardial dysfunction (*56*).

Since AMPK (i) is the master metabolic regulator coordinating the shift in cellular metabolism to accommodate the requirements for neurogenesis; (ii) is affected in its activity in aged tissues such as the brain (*54*), myocardium (*57*), and skeletal muscle (*52, 58*); (iii) AMPK activation suppress embryonic NSC proliferation *in vitro* (*59*) and dentate gyrus NSC proliferation *in vivo* (*60*), we, therefore, determined whether optimal AMPK activation plays a critical role in the age-related decline of hippocampal neurogenesis. We hypothesize that inhibition of AMPK signaling activation (phosphorylation) in the old brain will cause a concomitant increase in hippocampal neurogenesis.

Here, we demonstrated that AMPK subunit isoforms were differentially expressed with age in the hippocampal neural stem cell niche and uncovered a new role for the inhibition of AMPK signaling, namely its ability of partial rescue of hippocampal neurogenesis in the old brain via pharmacological inhibition with Compound C, suggesting AMPK's critical involvement in the regulation of downstream processes for the age-related decline in hippocampal neurogenesis.

CHAPTER II

MATERIALS & METHODS

Ethics statement

All animal procedures were approved by the Institutional Animal Care and Use Committee at the University of North Texas Health Science Center (UNTHSC). The study was conducted according to the NIH Guide for the Care and Use of Laboratory Animals. Every effort was made to reduce the number of animals used as well as to minimize suffering to the animals.

Chemicals

AICAR (AMPK activator, Cat. # A611700) and Compound C dihydrochloride (AMPK inhibitor, Cat. # CD0339) were obtained from Toronto Research Chemicals (ON, Canada) and Chemdea (NJ, USA), respectively. 5-bromo-2'-deoxyuridine (BrdU, Cat. # B5002) and paraformaldehyde (Cat. # P6148) were obtained from Millipore-Sigma (MO, USA).

Animals

A total of 132 young-adult (2-3 months; body weight 20-25 g, Charles River) and old (19-20 months; body weight 35-42 g, National Institute of Aging) male C57BL/6 mice were randomly divided into the following schedules:

Schedule I – short term intraperitoneal drug administration for a duration of 7 days (Figure 4A): Young-vehicle-7d group (n = 10), Young-activator-7d group (n = 10), Young-inhibitor-7d group (n = 10); Old-vehicle-7d group (n = 10), Old-activator-7d group (n = 10), Old-inhibitor-7d group (n = 10).

Schedule II – long term intraperitoneal drug administration for a duration of 28 days (Figure 4B): Young-vehicle-28d group (n = 10), Young-activator-28d group (n = 10), Young-inhibitor-28d group (n = 10); Old-vehicle-28d group (n = 10), Old-activator-28d group (n = 10), Old-inhibitor-28d group (n = 10).

Schedule III – short term intracerebroventricular drug administration for a duration of 3 days (Figure 5): Young-vehicle group (n = 4), Young-activator group (n = 4), Young-inhibitor group (n = 4).

For each group in Schedules I and II, n = 6 animals were allocated for immunohistochemical studies, while n = 4 animals were used for Western blotting. For each group in Schedule II, n = 4 mice were randomly selected to measure their body weights and blood glucose levels weekly (at 9 am) for the duration of the drug administration using a Bayer Contour glucometer (USA) (*61, 62*). All animals were housed in the UNTHSC vivarium and maintained at 23 ± 1 °C on a 12-hr light/dark cycle starting at 0700 hours with ad libitum access to food and water.

BrdU administration

To visualize proliferating cells, mice used for immunohistochemical studies were administered BrdU (50 mg/kg, twice a day, i.p.) for seven days, as described (*19, 63, 64*). BrdU (10 mg/mL) was dissolved in 0.9% saline with its final pH adjusted to 7.4.

Administration of AMPK signaling activator and inhibitor

0.9% saline was used as a vehicle for all experiments. Stock solutions of AICAR (100 mg/mL) and Compound C (2 mg/mL) were made by dissolving the drugs in 0.9% saline. The pH of AICAR and Compound C stock solutions were adjusted to 7.4 and 7.0, respectively, then aliquoted and stored in -20 °C until further use. Mice were administered AICAR (500 mg/kg/day) or Compound C (10 mg/kg/day) via the intraperitoneal route for 7 or 28 consecutive days. The intraperitoneal doses for AICAR and Compound C were selected based on a review of the literature that administered AICAR and Compound C (Table 1 and Table 2, respectively) through the intraperitoneal route.

For intracerebroventricular administration, young-adult male C57BL/6 mice were anesthetized and implanted with an Alzet® osmotic minipump (Cat. # 1003D, Durect Corporation, CA, USA). The cannula was placed into the right lateral ventricle: 1 mm lateral to the midline, 0.34 mm posterior to the bregma, and 3.5 mm deep into the pial surface (Figure 5). AICAR (4 mM) and Compound C (1 μM) were dissolved in 0.9% saline and pH adjusted to 7.4 and 7.0, respectively. Doses were selected based on an *in vitro* pilot study (not shown). Each mouse was infused for 3 days with 1 μL/hour of either: (1) 0.9% saline (vehicle), (2) AICAR, or (3) Compound C. Mice were sacrificed on day 4, and their brain tissues were collected for Western blotting analyses.

Immunohistochemistry

Mice were deeply anesthetized and sacrificed the day after their last injection. After perfusion with 0.9% saline and 4% PFA (pH adjusted to 7.4), their brains were collected, embedded in paraffin, and cut into 5 μm sections.

Immunohistochemistry was performed as previously described (*65*) with modifications. In brief, sections were cleared in xylene, rehydrated through graded alcohols, and rinsed. These were then subjected to 0.3% Triton X-100 for 15 minutes, rinsed and incubated in citrate-based pH 6.0 antigen retrieval at 95-100 ºC for 10 minutes using the microwave method and allowed to cool to room temperature for an hour. To detect BrdU-labeled cells, sections were incubated in 2N HCl at 37 ºC for 30 minutes and rinsed with 0.1M boric acid (pH 8.5) for 10 minutes followed by PBS. To block endogenous peroxidase activity, sections were incubated in 3% H_2O_2 in ddH_2O for 15 minutes after which they were blocked in blocking solution (3% horse serum, 1% bovine serum albumin in 1X PBS, pH 7.4) for 1 hour at room temperature and subsequently incubated with the appropriate primary antibodies (Table 3) at 4 ºC overnight (~16 hours). The following day, sections were washed with PBS and incubated with the appropriate horse biotinylated secondary antibodies (Table 4) (Vector, CA, USA) for 1 hour at room temperature. After washing, the VECTASTAIN Elite ABC HRP solution was applied to the sections for 1 hour at room temperature. Finally, the HRP reaction was detected with DAB ImmPACT (Cat. # SK-4105, Vector, CA, USA) until the desired brown staining intensity is achieved. The reaction was stopped by rinsing the sections under running tap water for 5 minutes. Sections were then dehydrated, cleared in xylene, cover-slipped with permanent mounting medium (Vector, CA, USA), and air-dried overnight. Sections were examined and photographed with a Nikon Ti-E microscope and Nikon DS-Fi1 color camera (Nikon, NY, USA). Controls included omitting the primary antibodies.

Double-label immunostaining

Double-label immunostaining was performed as previously described (*65*) with modifications. Briefly, sections were blocked in blocking solution (3% donkey serum, 1% bovine serum albumin (BSA) in 1X PBS, pH 7.4) for 1 hour at room temperature and incubated with the appropriate primary antibodies (Table 3) at 4 ºC overnight. Sections were then washed with PBS, incubated with the appropriate donkey secondary antibodies (Life Technologies, USA) (Table 4) for 1 hour at room temperature, rinsed, and cover-slipped with Prolong Gold Antifade with DAPI, according to the manufacturer's instructions (Cat. # P36931, Life Technologies, USA). The sections were cured overnight in the dark. Controls included omitting the primary antibodies. Fluorescence signals were detected using a Nikon Ti-E microscope and Nikon DS-Qi MC camera (Nikon, NY, USA), and images were acquired using the NIS-Elements Basic Research software (Nikon, NY, USA).

Cell counting

An observer blinded to the experimental conditions counted BrdU- , MCM2- , DCX-positive, and double-labeled cells in the dentate gyrus of the hippocampus (beginning bregma -1.64 mm) from four to six coronal sections per animal (n = 5-6 animals per group) spaced 100 µm apart. An average cell count was obtained by totaling the number of cells from each coronal section dividing by the total number of coronal sections. The results are expressed as a percentage of the control.

Western blot analysis and densitometry

Mice were deeply anesthetized and sacrificed by cervical dislocation the day after their last injection. The subventricular zone (SVZ) and hippocampus were dissected on ice from young and aged mice as previously described (*66*), using a Zeiss V8 dissecting microscope. The brains were removed, placed in a coronal brain matrix, and cut into 1 mm thick coronal sections throughout the area of the SVZ (from bregma -0.30 to -1.2 mm), while the entire hippocampus was dissected by removing the surrounding cortex that encapsulates it. The dissected SVZ and hippocampi were flash frozen immediately in liquid nitrogen and stored at -80 °C for further analysis. Each dissection was timed from the start of cervical dislocation and performed within 8-10 minutes. The timing was crucial because AMPK activity reaches to the peak at 15 minutes (*67*).

Tissues were lysed through sonication using lysis buffer (13.5 mM NaCl, 2.7 mM KCl, 4.3 mM $NaPO_4$, 1.4 mM KPO_4, 0.5% NP-40, 0.5% sodium deoxycholate, pH 7.4) containing 1X Halt™ protease and phosphatase inhibitor cocktail (Cat. # 78444, Thermo Fisher Scientific, USA). Protein concentration was determined using the Pierce 660 nm protein assay (Cat. # 22660, Thermo Fisher Scientific, USA) with BSA as a standard. Protein samples (30 µg) were boiled at 95-100 °C for 10 minutes, resolved on 10% SDS-PAGE gels, transferred onto polyvinylidene difluoride (PVDF) membranes, blocked with 5% non-fat dry milk in TBST (containing 0.1% Tween-20), and incubated overnight (~14 hours) with gentle shaking at 4 °C with either of the following primary antibodies from Cell Signaling Technology (MA, USA): (1) rabbit monoclonal anti-phospho-AMPKα (Thr 172) (Cat. # 2535, 1:1000), (2) rabbit monoclonal anti-AMPKα (Cat. # 5831, 1:1000), (3) rabbit monoclonal anti-pan-Actin (Cat. # 8456, 1:10,000). Membranes were then washed with TBST, incubated at room temperature for two hours with horseradish peroxidase conjugated anti-rabbit secondary antibody (Cell Signaling Technology, 1:5000), and washed 5 ×

7 minutes with TBST. Peroxidase activity was visualized by chemiluminescence with SuperSignal West Femto Maximum Sensitivity Substrate (Cat. # 34095, Thermo Fisher Scientific, USA) using Bio-Rad's Chemidoc MP imaging system. Antibodies were then removed by incubating with a homemade stripping buffer (0.2 mM Glycine, 0.1% SDS, ddH_2O, adjusted to pH 2.0 with HCl) with gentle rocking at room temperature for 30 minutes. Following washing with TBST, the membranes were blocked and reprobed with Actin. Densitometry measurements were obtained using the Image Lab v. 6.0 software by Bio-Rad. Bands were automatically selected by the software and default background subtraction of disk size 10.0 mm was applied to all bands. The "Adjusted Total Band Volumes" were then normalized to the densities of the housekeeping gene, Actin, of the same lane and blot to obtain relative expression.

Open field test

Spontaneous locomotor activity was measured weekly for a period of one month using the ANY-Maze (v. 5.3, Stoelting Co., IL, USA) software. During a 5-minute test period, a mouse's movement was recorded by a camera linked to the software to yield variables that described horizontal and spatial components of spontaneous activity.

Statistical analysis

Sample sizes using 80% power were determined with G*Power (Universität Düsseldorf, Germany). Statistical analyses were performed using GraphPad Prism 7 (GraphPad Software, CA, USA). Cell counts were subjected to a two-way analysis of variance (ANOVA) followed by Fisher's Least Significant Difference post-hoc test with Treatment (Vehicle, Inhibitor or Activator) and Duration of treatment (7 or 28 days) as between-groups factors. Distance traveled in the open field test was subjected to two-way repeated measures ANOVA with Treatment (Vehicle, Inhibitor or Activator) and Duration of treatment (7 or 28 days) as between-groups factors. Densitometry measurements (1) between three groups of mice (Vehicle, Inhibitor, Activator) were subjected to a one-way ANOVA followed by Fisher's Least Significant Difference post-hoc test; (2) between two groups of mice (Young and Old) were subjected to the Student's t-test. All data are expressed as mean ± s.e.m. A p value of less than 0.05 was regarded as statistically significant.

CHAPTER III

RESULTS

Expression pattern of AMPK subunit isoforms in the cortex and hippocampus of young-adult and old mice

AMPKα subunit isoforms

The expression pattern for the AMPKα1 subunit isoform in the cortex and hippocampus are shown for the young-adult (Figure 6) and old (Figure 7) mice. The α1 isoform was localized to the cytoplasm and observed in all areas except the hilus and granular cell layer (GCL) of the dentate gyrus (DG). With respect to age, its expression level in the young-adult was higher than in the old in all regions studied. The expression pattern for the AMPKα2 subunit isoform in the cortex and hippocampus are shown for the young-adult (Figure 8) and old (Figure 9) mice. The α2 isoform was localized to the nucleus. Unlike the α1 isoform, it was found in all areas of the cortex and hippocampus. However, similar to the α1 isoform, the expression level in the young-adult was higher than in the old in all regions studied. Its higher expression in the SGZ *vs.* the GCL is more distinct in the old mouse brain (Figure 9C).

Next, we were interested in the expression pattern of activated (i.e., phosphorylated) AMPKα (pAMPKα) since the activated form sets off a series of downstream metabolic processes that occur in the cell. The expression pattern for pAMPKα in the cortex and hippocampus are shown for the young-adult (Figure 10) and old (Figure 11) mice. Similar to its inactive (non-phosphorylated) form, pAMPKα was found to be localized to the nucleus. The expression level for pAMPKα is higher in the old *vs.* the young in all regions studied. Western blotting analysis confirmed that pAMPKα was indeed significantly higher in the hippocampus of the old *vs.* young mouse ($p < 0.05$, Figure 12).

AMPKβ subunit isoforms

The expression pattern for the AMPKβ1 subunit isoform in the cortex and hippocampus are shown for the young-adult (Figure 13) and old (Figure 14) mice. The β1 isoform was found in all regions studied and observed to be mainly localized to the nucleus with some cytoplasmic expression in pyramidal cells in the cortex (Figure 13A). With respect to age, its expression level in the young-adult was higher than in the old in all areas studied. The expression pattern for the AMPKβ2 subunit isoform in the cortex and hippocampus are shown for the young-adult (Figure 15) and old (Figure 16) mice. The β2 isoform was also found in all areas and was mainly localized to the cytoplasm although some nuclear expression was also present in cortical cells (Figure 15A and Figure 16A). Similar to the β1 isoform, the expression level in the young-adult was higher than in the old in all regions studied.

AMPKγ subunit isoforms

The expression pattern for the AMPKγ1 subunit isoform in the cortex and hippocampus are shown for the young-adult (Figure 17) and old (Figure 18) mice. The γ1 isoform was localized to the cytoplasm in all regions studied. With respect to age, the expression level in the young-adult was higher than in the old. The expression pattern for the AMPKγ2 subunit isoform in the cortex and hippocampus are shown for the young-adult (Figure 19) and old (Figure 20) mice. The γ2 isoform was mainly found in the cytoplasm in all areas of the cortex and hippocampus. Its expression level in the young-adult was higher than in the old in all regions studied. The expression pattern for the AMPKγ3 subunit isoform in the cortex and hippocampus are shown for the young-adult (Figure 21) and old (Figure 22) mice. The γ3 isoform was mainly localized to the cytoplasm. Its expression level in the young-adult was higher than in the old in all regions studied.

Expression pattern of AMPK subunit isoforms in the subventricular zone of young-adult and old mice

AMPKα subunit isoforms

The expression pattern for the AMPKα1 subunit isoform in the SVZ is shown for the young-adult (Figure 23A) and old (Figure 24A) mice. The α1 isoform was localized to the cytoplasm and its expression level in the anterior SVZ (aSVZ) of the young-adult was higher than in the old. The expression pattern for the AMPKα2 subunit isoform in the SVZ is shown for the young-adult (Figure 23B) and old (Figure 24B) mice. The α2 isoform was localized to the nucleus. Unlike the α1 isoform, it was found to be more widely expressed in all regions studied. However, similar to the α1 isoform, the expression level in the young-adult was higher than in the old aSVZ

in all regions studied. Next, we were interested in the expression pattern of activated (i.e., phosphorylated) AMPKα (pAMPKα) since the activated form sets off a series of downstream metabolic processes that occur in the cell. The expression pattern for pAMPKα in the SVZ are shown for the young-adult and old mice (Figure 25). Similar to its inactive (non-phosphorylated) form, pAMPKα was found to be localized to the nucleus. Qualitatively, the expression level for pAMPKα did not seem to change with respect to age. However, further investigation with Western blotting revealed that the level of pAMPKα trended towards being higher in the young-adult *vs.* old SVZ (Figure 26).

AMPKβ subunit isoforms

The expression patterns for the AMPKβ1 and AMPKβ2 subunit isoforms in the SVZ are shown for the young-adult (Figure 27) and old (Figure 28) mice. Both isoforms were found in all regions studied and observed to be localized to the nucleus. With respect to age, the expression level of β1 in the young-adult was higher than in the old while expression level of β2 in the old was higher than in the young-adult.

AMPKγ subunit isoforms

The expression patterns for the AMPKγ1, AMPKγ2 and AMPKγ3 subunit isoforms in the SVZ are shown for the young-adult (Figure 29) and old (Figure 30) mice. The three isoforms were found in all regions studied except the striatum and observed to be localized to the nucleus. With respect to age, the expression levels of all three isoforms seem to be higher in the old compared with the young-adult in all regions studied.

Effects of Compound C administration on hippocampal neurogenesis in the young-adult and old mice

To study the effects of the loss of function of AMPK activation on the age-related decline in hippocampal neurogenesis, young-adult and old mice were subjected to short- and long-term administration of the AMPK inhibitor, Compound C, at a dose of 10 mg/kg/day for 7 and 28 days via the intraperitoneal (i.p.) route. We evaluated the number of newly generated cells ($BrdU^+$) as well as Type I ($GFAP/Sox2^+$), Type II ($MCM2^+$), and Type III (DCX^+) cells after 7 and 28 days of i.p. treatment. With respect to $BrdU^+$ cells, there were significant increases in the inhibitor-treated young-adult ($p < 0.01$, *vs.* vehicle) and old ($p < 0.05$, *vs.* vehicle) groups after 7 days of administration (Figure 31). No significant changes were seen for Type I cells (Figure 32). On the other hand, the inhibitor-treated young-adult group had about 50% increase in Type II cells after 28 days of treatment ($p < 0.05$, *vs.* vehicle) while the inhibitor-treated old group had approximately 100% increase after 7 days of treatment ($p < 0.05$, *vs.* vehicle) (Figure 33). Likewise, inhibitor-treated young-adult mice experienced about 50% increase in Type III cells after 28 days of treatment ($p < 0.05$, *vs.* vehicle) while old mice had an approximately 200% increase after 7 days of treatment ($p < 0.05$, *vs.* vehicle) (Figure 34). To confirm whether intraperitoneal administration of the inhibitor resulted in a decrease in AMPK activation in the hippocampus, we performed Western blotting and found a significant decrease in AMPK activation in the young-adult hippocampus after 7 days of inhibitor treatment ($p < 0.05$, *vs.* vehicle, Figure 35 and Figure 36C). Similarly, intracerebroventricular (i.c.v.) administration with the inhibitor for 3 days showed a robust decrease in AMPK activation in the young-adult hippocampus ($p < 0.0001$, *vs.* vehicle, Figure 37 and Figure 38C).

Effects of AICAR administration on hippocampal neurogenesis in the young-adult and old mice

To study the effects of the gain of function of AMPK activation on the age-related decline in hippocampal neurogenesis, young-adult and old mice were subjected to short- and long-term administration of the AMPK activator, AICAR, at a dose of 500 mg/kg/day for 7 and 28 days via the i.p. route. We evaluated the number of newly generated cells ($BrdU^+$) as well as Type I ($GFAP/Sox2^+$), Type II ($MCM2^+$), and Type III (DCX^+) cells after 7 and 28 days of i.p. treatment. Compared with control, no significant changes in the numbers of newly generated cells (Figure 39) as well as Type I (Figure 40), Type II (Figure 41) and Type III (Figure 42) cells were observed for activator-treated young-adult and old groups after 7 and 28 days of treatment. To confirm whether i.p. administration of the activator resulted in an increase in AMPK activation in the hippocampus, we performed Western blotting and found no significant increase in AMPK activation in the young-adult hippocampus after 7 days of activator treatment (Figure 43 and Figure 44C). However, i.c.v. administration with the activator for 3 days showed a robust increase in AMPK activation in the young-adult hippocampus ($p < 0.0001$, *vs.* vehicle, Figure 45 and Figure 46A).

Effects of long-term Compound C and AICAR intraperitoneal administration on general health and behavior of young-adult and old mice

Long-term administration of an AMPK-altering drug such as Compound C and AICAR have the potential to affect glucose metabolism, which may subsequently affect an animal's body weight and spontaneous locomotor activity. Therefore, we monitored the body weight, blood glucose level and spontaneous locomotor activity of inhibitor- and activator-treated young-adult and old mice for a period of 28 days. Measurements were taken at baseline (Day 1) and every 7 days following that till the day of sacrifice (Day 29). No significant changes were observed in all parameters studied (Figure 47).

CHAPTER IV

DISCUSSION

Understanding the fundamental processes that regulate the age-related decline of neurogenesis has long been a goal in the stem cell and aging fields. The idea of increasing the number of endogenous stem cells as a potential therapy for brain aging is particularly enticing when a similar outcome could be accomplished without the need for invasive procedures such as cell transplantation.

Our results revealed that the activation of AMPK signaling was pivotal in the age-related decline of neurogenesis in the hippocampus, which was substantiated with our finding that AMPK subunit isoforms were expressed in the two neurogenic regions, subgranular zone (SGZ) and subventricular zone (SVZ) (Table 5), levels of active (phosphorylated) AMPK were increased in the old SGZ and SVZ, and treatment known to decrease AMPK activation (Compound C) increased neurogenesis in the old hippocampus after 7 but not 28 days of administration (Table 6). Taken together, these results indicated that the increase in AMPK signaling with age is a key step in the regulation of downstream processes, leading to the age-related decline of neurogenesis (Figure 48).

Age-related changes in AMPK subunit expression and signaling

The heterotrimeric complex of AMPK is made up of different subunit isoforms in the ratio of 1:1:1 (α:β:γ), which lends itself to the formation of at least twelve different AMPK complexes. These subunits were differentially expressed in a tissue-specific manner with distinct subcellular localization (nuclear *vs.* cytoplasmic, or both) in various tissues, which was important in regulating specific responses at the cellular and even whole-body level. To date, there has been only one study that performed an extensive interrogation of AMPK subunit isoform expression pattern and localization in the mouse central nervous system (*68*), while others merely focused on a specific subunit isoform in different parts of the brain (*27, 69-72*). Thus, information regarding their expression patterns in the SGZ and SVZ in young-adult and old mice was deficient. Our study is the first demonstration on the expression pattern of all seven AMPK subunit isoforms in the SGZ and SVZ of young-adult and old mice.

Overall, the expression levels of all subunit isoforms in the SGZ and SVZ were higher in the young-adult *vs.* old mice with the exception of (i) activated AMPKα (pAMPKα) in the old SGZ and SVZ; (ii) AMPKβ2 subunit isoform in the SVZ (discussed later). Activating AMPKα is critical in mediating downstream signaling cascade, which is dependent on the isoform's location. Once activated, in the cytoplasm, it triggers metabolic processes such as fatty acid oxidation and glycolysis while simultaneously inhibit fatty acid synthesis and gluconeogenesis. If in the nucleus, it is involved in regulating gene expression (*73, 74*). The AMPKα isoforms showed the expected localization pattern demonstrated by Turnley et al. (*68*) and others (*75-77*). In the SGZ and SVZ, AMPKα1 was mainly localized to the cytoplasm while AMPKα2 was preferentially localized to the nucleus, suggesting that during neurogenesis, α1 controls cytoplasmic metabolic processes while AMPKα2 governs AMPK-mediated transcriptional events. Our finding regarding the

abundance of AMPKα2 expression in the regions studied corroborates with the idea that it is the predominant catalytic subunit isoform in the brain (*68*) and in our case, the SGZ and SVZ. The importance of the brain catalytic α2 isoform and by extension AMPK activation, have been implicated in age-related neurological disorders: (i) pharmacological inhibition of AMPK activity by Compound C (*78*) and deletion of AMPKα2 in the brain (*79*) provided neuroprotection after ischemic stroke; (ii) AMPK was hyper-activated in Alzheimer's disease (AD) human brains (*80*) and AMPKα2$^{-/-}$ mice had a reduction of endogenous tau phosphorylation (*81*) and inhibited Aβ-induced LTP failure (*82*). In the young and old SGZ and SVZ, pAMPKα was localized to the nucleus and its expression level was found to be consistently higher compared with other parts of the brain. Interestingly, a study conducted using human subjects (n =120) found that there is an age-related increase in resting metabolic rate in the brain (*83*). With increased energy consumption in the old brain, AMPK is activated to a greater extent, which corroborates with our data. In rodents, higher pAMPKα levels were found in the old brain (*54*), liver (*84*) and kidney (*85*). In the old brain, there was about a 40% increase in pAMPKα level (*54*) while in the old liver, the percentage increased to about 60% (*84*). Jin et al. also observed a low AMPKα content in the old kidney even though there was an increase in pAMPKα level (*85*), which supports our finding that total AMPKα expression levels in the old hippocampus (Figure 12) and old SVZ (Figure 26) were decreased compared with the young. However, this was not seen in the study by Liu et al. where total AMPKα expression level was found to be unchanged with age (*54*). This may be due to the utilization of the entire non-ischemic hemisphere so much so that subtle differences in specific regions were lost.

Apart from binding the α and γ subunits through its C-terminal domain thereby allowing the formation of a stable heterotrimer (Figure 1), another important role of the regulatory AMPKβ subunit is its ability to regulate AMPK substrate selection by directing the α subunit to its cellular compartment (*86, 87*). The AMPKβ1 subunit isoform showed the expected localization pattern by Turnley et al.; it was localized to the nucleus in the SGZ and SVZ regions. The group also reported that the AMPKβ2 subunit isoform was restricted to the cytoplasm in Purkinje cells of the cerebellum and pyramidal cells in the hippocampus. However, we found that it had a higher expression in the cytoplasmic *vs.* nuclear compartments of cells in the hippocampus and cortex but was predominantly expressed in the nucleus in the SGZ and SVZ regions. It is widely accepted that AMPKβ1 is the predominant subunit isoform in the brain, liver, pancreas, kidney and brown fat while AMPKβ2 is found mainly in the heart and skeletal muscle (*88*). However, Western blot analysis by Dasgupta et al. revealed that the levels of the two isoforms are relatively equal in the adult mouse brain and heart (*71*). In fact, toward the rostral part of the brain, we observed a higher expression of the β1 isoform in the cortex (data not shown), striatum, and subventricular zone. Moving caudally to where the hippocampal formation is prominent, we found a higher expression for the β2 isoform in the cortex and hippocampus instead. Together, these highlight a region-specific difference in the expression of AMPKβ subunit isoforms. It is interesting to note that the localization for both AMPKβ isoforms in the SGZ and SVZ are found in the nucleus, which suggests that the AMPKα2 isoform is able to associate with either of the AMPKβ isoforms regardless of cell compartment. This idea of subunit selection can be supported with the study by Chen et al. (*89*) where they performed immunoprecipitation and found that α2 in the extensor digitorum longus (EDL) muscle could associate with both β1 and β2 while α2 in the soleus muscle only associated with the β1 isoform. Furthermore, β2 was found to associate with α2 only and not

α1, indicating that β2 was the least promiscuous of the two β isoforms. However, the factors promoting the association of α2 with β1 or β2 isoforms are still unknown. We also found that the expression level of AMPKβ2 is increased in the old SVZ when compared with the young. This pattern was not seen in the old SGZ, which may suggest that the low expression or absence of the β2 isoform could play an important role in the age-related decline of neurogenesis. It has been shown that the β1 isoform was important in development and neurogenesis (*90*) and the β2 isoform was required for energy homeostasis in times of metabolic stress in the muscle (*71*). Since aging is an accumulation of stress from a variety of sources, one can then argue that the upregulation of the β2 isoform in the old SVZ may help in part to combat the age-related stress to NSCs thereby maintaining energy homeostasis to allow neurogenesis to continue.

The regulatory AMPKγ subunit acts as an allosteric activator of AMPK. It contains two Bateman domains (Figure 1) that allow the binding of AMP and ADP to result in the allosteric activation of AMPK. The AMPKγ subunit isoforms showed higher expression levels in the old *vs.* young-adult SVZ. This exception could have been better substantiated with an additional method such as Western blotting, which is useful for semi-quantitatively measuring protein expression levels. Strikingly, we observed a region-specific difference in the localization of AMPKγ subunit isoforms in the SGZ and SVZ. All AMPKγ subunit isoforms in the SGZ appear to be in the cytoplasm while those in the SVZ are localized to the nucleus. Moreover, the expression levels of AMPKγ subunits in the old SVZ were higher compared with the young. The localization of all γ isoforms in one cellular compartment has not been reported.

In the case of the β and γ subunits, the question remains as to whether AMPK subunit isoforms could be present in the same subcellular location, form a functional complex in a different compartment and still carry out their intended functions. One possibility could be that the

individual subunits are using a shuttling system to transport the subunit to its required location and bring it back to its original subcellular compartment. It was initially thought to be energy inefficient, but, on the contrary, it has been shown that tRNAs in yeast can be shuttled into the cytosol and back to the nucleus (*91*). Another study supports this nucleocytoplasmic transport reversibility and went further to demonstrate that shuttling is a fundamental feature when the accumulation of molecules in one cellular compartment was observed (*92*). One other probable reason relates to changes in the cell being dynamic and fast-paced. Since AMPK is known to be the master regulator of cellular metabolic processes, it needs to be quick and sensitive to respond to energy changes in the cell. Therefore, it is likely that the concept of subunit isoform switching, which is well-known in the field of receptor pharmacology, can be applied in this case especially when the subunit isoforms are aggregated or localized to the same subcellular compartment. Analogous to how a sport such as basketball can have an unlimited number of player substitutions to cope with changing situations on the court, AMPK, when faced with a certain stressor such as low energy levels in the cell, through a yet unknown mechanism of subunit isoform selection, can then choose which isoforms to recruit and switch out to ensure its maximum effectiveness of dealing with that stressor e.g., as discussed earlier, the α2 isoform was able to associate with either of the β isoform in the EDL muscle but only associates with the β1 isoform in the soleus muscle (*89*). It is also plausible to marry the two notions above for explaining the supposed conundrum. AMPK subunit isoforms can rely on reversible nucleocytoplasmic transport and form the most appropriate heterotrimeric AMPK complex for activating various downstream metabolic processes. Therefore, we hypothesize that the formation of the AMPK complex is dynamic and not static, an idea that has been recently shown to be possible in other protein complexes (*93, 94*).

Forced inhibition and activation of AMPK signaling on the age-related decline of hippocampal neurogenesis

We decided on (i) focusing on hippocampal neurogenesis because of the drastic decrease (~80%) in NSC numbers with age; (ii) administering the agents through the intraperitoneal (i.p.) route as it could be easily administered and is less invasive compared with intracerebroventricular (i.c.v.) injection; (iii) using a high dose of AICAR (500 mg/kg/day) as studies have shown that it could stimulate neurogenesis (Table 1) although it has limited permeability across the blood-brain barrier (*95*); (iv) using a low dose of Compound C (10 mg/kg/day) as this dose was sufficient to demonstrate inhibition of AMPK activation (Table 2); (v) a treatment duration of 7 and 28 days for studying the short- and long-term effects of forced inhibition and activation of AMPK signaling on neurogenesis; (vi) using well known markers such as GFAP/Sox2 for labeling Type I cells, MCM2 for labeling Type II cells and DCX for labeling Type III cells (Figure 5).

Compound C is a well-known and widely used inhibitor of AMPK activation that acts as an ATP-competitive inhibitor (*96*) by binding reversibly to the AMPKα subunit kinase domain (*97*). In our study, Compound C significantly inhibited AMPK activation in the hippocampus through the i.p. and i.c.v. routes as well as increase hippocampal neurogenesis in the young and old mice, indicating that Compound C-mediated increase of neurogenesis was AMPK-dependent. We observed that Compound C increased hippocampal neurogenesis in young and old mice after 7 days of treatment only. Furthermore, Compound C treatment increased NSC proliferation in the old hippocampus after 7 days of treatment while in the young hippocampus after 28 days of treatment. However, treatment with Compound C did not increase the number of quiescent (Type I) NSCs in the young and old hippocampus. Therefore, it seems at this point, that inhibition of AMPK signaling is very likely to be involved in augmenting the proliferative events of the

neurogenic process whereas the effect on NSC differentiation remains unknown. Indeed, this is congruent with the idea that when AMPK signaling is inhibited (decrease in AMPK activation), downstream metabolic pathways such as glycolysis and fatty acid oxidation are downregulated while protein and fatty acid synthesis are upregulated, which allow for cell proliferation (*Figure 2*). The short- and long-term effects of Compound C on cell proliferation have not been studied *in vivo*. It has been suggested that the age-related decrease in neurogenesis with age may be a consequence of several processes that control NSC dynamics such as quiescence, terminal differentiation, increase in cell cycle length, senescence or death (*98*). One study reported that decreased neurogenesis in the old mouse was due to proliferating NSCs becoming quiescent via the Wnt signaling pathway and they found that this process was reversible (*99*). However, this was not true in our case as Type I cells, which are quiescent, did not increase with short- and long-term Compound C treatment. Furthermore, it could not have been due to the prolongation of the cell cycle length since we did not witness an increase in cell proliferation in Types II and III cells with long-term Compound C treatment. Thus, we speculate that with already low numbers and very limited divisions left in old hippocampal NSCs, inhibition of AMPK signaling increased cell proliferation in the short-term only possibly due to the exhaustion of the stem cell pool.

AICAR is an analog of adenosine that is taken up by cells through adenosine transporters then phosphorylated by adenosine kinase, which gives rise to the AMP-mimetic, AICAR monophosphate (ZMP) (*100*). Its mechanism of action is similar to that of AMP where it allosterically activates AMPK by binding with the cystathione-β-synthase (CBS) domain 3 on the AMPKγ subunit (*Figure 1*). AICAR acts as a direct activator of AMPK in that it does not alter the ADP:ATP ratio or oxygen uptake like many other AMPK activators do by inhibiting mitochondrial function (*101*). Therefore, AICAR was used as our AMPK activator of choice. To demonstrate

gain of function of AMPK signaling, we administered AICAR through the i.p. route and expected AMPK activation to increase in the young hippocampus and consequently observe a decrease in cell proliferation. We also expected no change to cell proliferation in the old hippocampus since an increasing body of evidence have shown that AMPK is not as sensitive to changes in the cell and could not effectively respond to the stimuli with advancing age (*52, 54, 84*). Surprisingly, we found (i) an absence of increased AMPK activation compared with vehicle and (ii) no decrease in cell proliferation in the young hippocampus. However, two separate reports from the same group using the same dose (500 mg/kg/day) and route of administration (via i.p.), demonstrated that AICAR had an effect on neurogenesis in young and old female mice (*102, 103*). The authors cited a piece of report showing that only <1% of AICAR could cross the blood-brain barrier (*95*), which could have contributed to the absence of increased AMPK activation in our male mouse model. Possible reasons for this disparity in our study and theirs will be discussed in the *Future Directions* section. Additionally, to rule out the possibility of a "bad" lot of the drug, we infused AICAR (4 mM) for 3 days using a minipump that delivers the drug directly into the brain and found a significant increase in AMPK activation.

Future directions

We propose performing additional experiments using gene-deletion mice e.g., a brain-specific AMPKα2 conditional knockout (CKO) to provide further evidence of a causal relationship between the loss of AMPK activation on increased hippocampal neurogenesis and potential crosstalk of other signaling pathways with AMPK. The Notch signaling pathway has been increasingly suggested as a metabolic regulator in its own right (*104*). Notch has been implicated in the regulation of adipocyte homeostasis (*105*), production of glucose (*106*) and lipogenesis

(*107*) in the liver. In fact, studies have reported (i) an age-related decrease in Notch signaling causing a concomitant decrease in SVZ neurogenesis (*64*); (ii) SIRT1, another metabolic regulator, could suppress Notch signaling under metabolic stress thereby promoting neurogenesis (*108*); and (iii) SIRT1 could bind to a downstream target of Notch, Hes1, to promote astrogliogenesis (*109*). Thus, there could be a case for studying the interaction of the Notch and AMPK signaling pathways and how they might affect the age-related decline of neurogenesis. Furthermore, it would be interesting to examine sex-specific differences since it is emerging as an important topic in the aging field for researchers to address. Significant sex differences exist in the regulation of behavior and metabolism as well as development and progression of metabolic diseases such as cardiovascular diseases (*110*). Our study is limited to the male mouse but others have shown that there are sex-specific differences with regards to AMPK's activation (*111*) and that estrogen could activate AMPK through the direct interaction of estrogen receptors α and β with AMPKα2's βγ-binding domain (*112*), suggesting that estrogens may be a potential novel activator of AMPK. Moreover, the two studies by van Praag's group reported the use of female C57BL/6J mice and showed that intraperitoneal administration of AICAR for 7 and 14 days at the same dose used in our study (500 mg/kg/day) could increase neurogenesis (*102, 103*), suggesting that (i) the AMPK complex in the female mouse could be more responsive to the <1% of AICAR that crossed the blood-brain-barrier compared with the male mouse of the same strain and age; (ii) there may be a sex-specific difference in the composition of the blood brain barrier that allowed them to witness such a substantial increase in neurogenesis that even affected spatial memory and motor coordination. At the time of writing, an NIH grant was awarded to Dr. Robyn Klein of Washington University in St. Louis who proposed that the sphingosine 1-phosphate receptor 2 (S1PR2) found in the central nervous system vasculature of SJL mice (a model for studying sex differences in

multiple sclerosis) destabilizes adherens junctions in endothelial cells, which contributes to disease development in females *vs.* males. Another group reported that S1PR2 is exclusively upregulated in microvessels in stroke to induce cerebrovascular permeability while inhibition resulted in a decrease in gelatinase and matrix metalloproteinase (MMP)-9 activities (*113*). Taken together, these suggest that females may have a more permeable blood-brain barrier compared with males.

TABLES & FIGURES

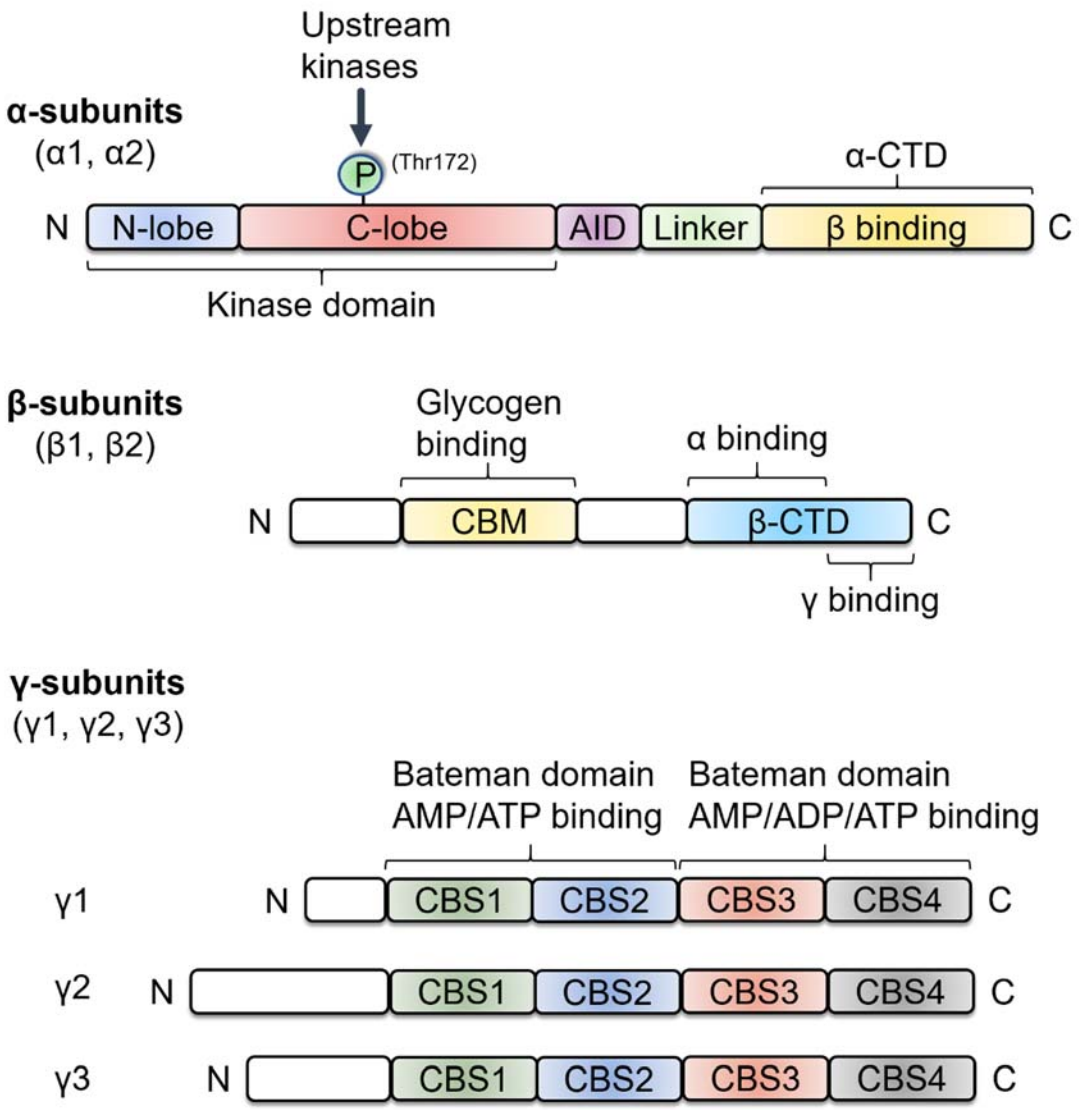

Figure 1. Schematic of mammalian AMPK subunits. The AMPK complex is a heterotrimer made up of α-, β-, and γ-subunits in a 1:1:1 ratio. The β-CTD of the β subunit forms the core of the complex, which binds to the N-terminus of the γ-subunit just before CBS1 and the α-CTD of the α-subunit. AID: Autoinhibitory domain; CBM: Carbohydrate-binding module; CTD: carboxy-terminal domain; CBS: Cystathione-β-synthase.

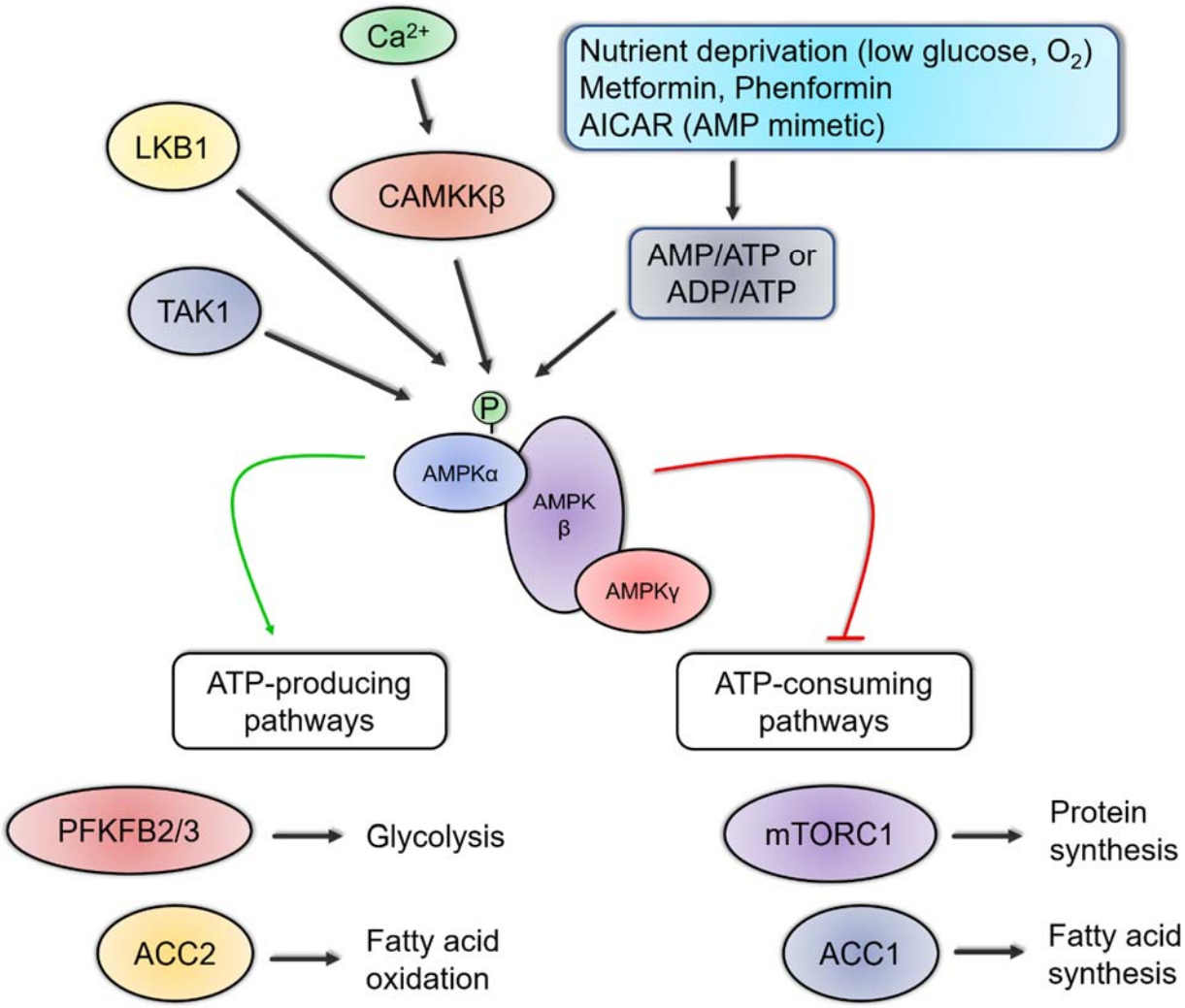

Figure 2. AMPK signaling and select downstream effects. AMPK is regulated by three main upstream kinases such as liver kinase B1 (LKB1), calmodulin-dependent kinase kinase β (CaMKKβ), and the transforming growth factor beta-activated kinase 1 (TAK1). When energy (ATP) levels are low in the cell, AMPK is phosphorylated at the Thr-172 on the α subunit catalytic domain by either of the upstream kinases thus activating AMPK to restore energy to equilibrium. AMPK does this by triggering (green arrow) energy-producing metabolic processes such as glycolysis and fatty acid oxidation while simultaneously inhibiting (red arrow) energy-consuming metabolic pathways such as protein and fatty acid synthesis.

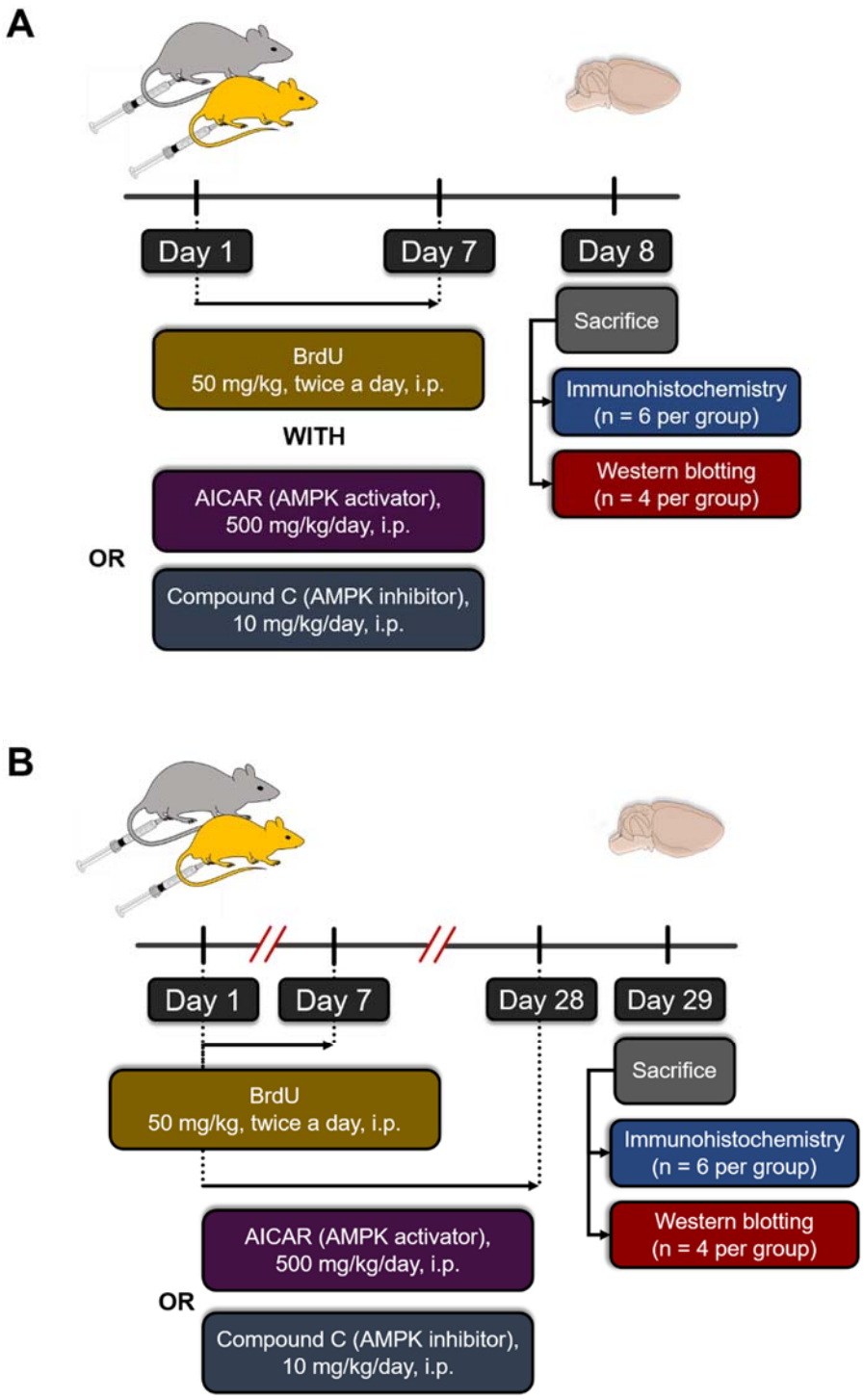

Figure 3. Experimental design. Young-adult (2-3 months, orange mouse) and old (19-20 months, grey mouse) male C57BL/6 mice were randomly divided into the groups outlined in the Methods section. The infographic here describes the design and timeline for studying the short-term (A) and long-term (B) effects of forced inhibition and activation of AMPK signaling on hippocampal neurogenesis.

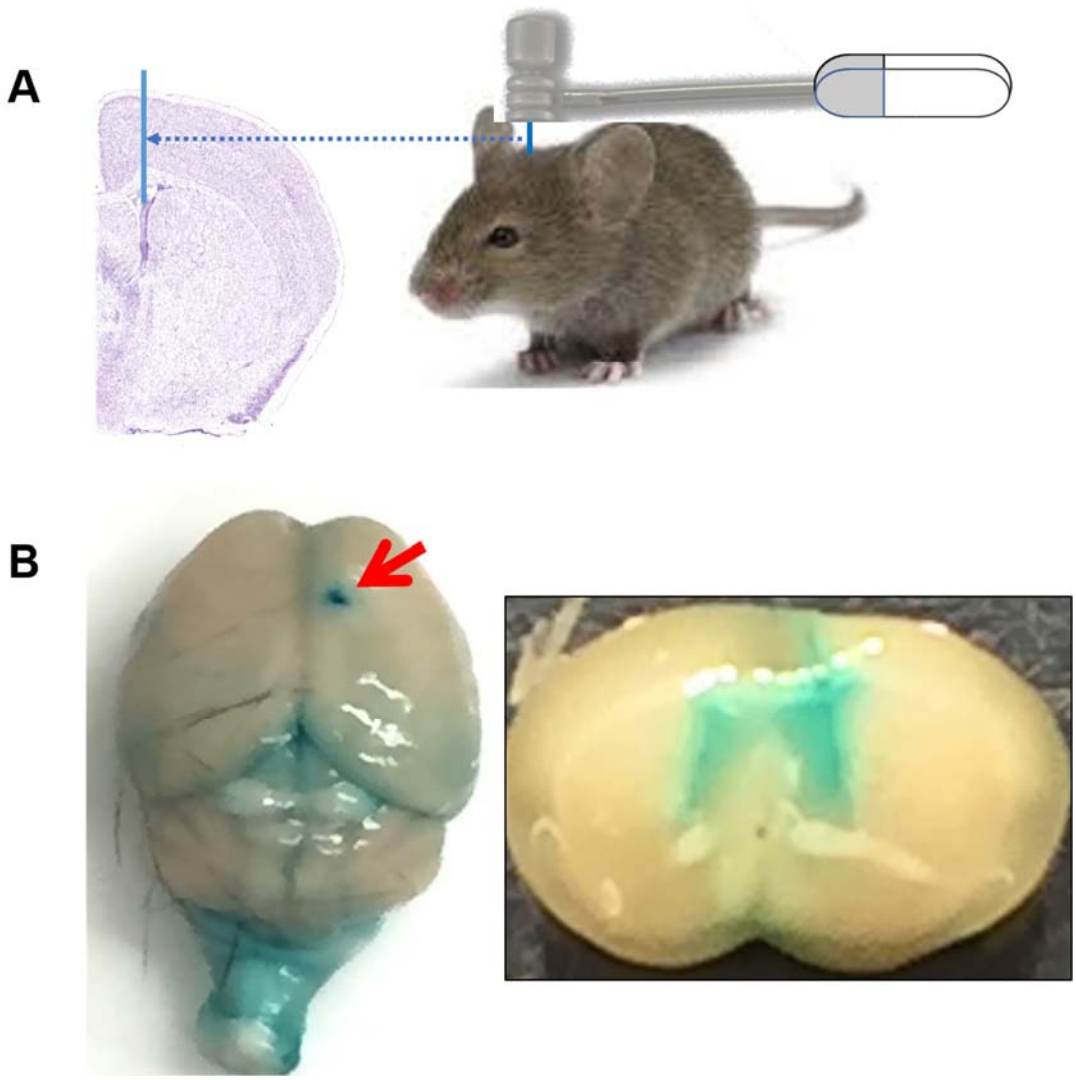

Figure 4. Intracerebroventricular infusion schematic. A 3-day minipump from Alzet® was used to infuse Vehicle, Compound C, or AICAR into the lateral ventricle of the mouse (A). The brain was stained with methyl green, the red arrow indicates the site of injection (B, left panel) to visualize the needle track into the lateral ventricle (B, right panel).

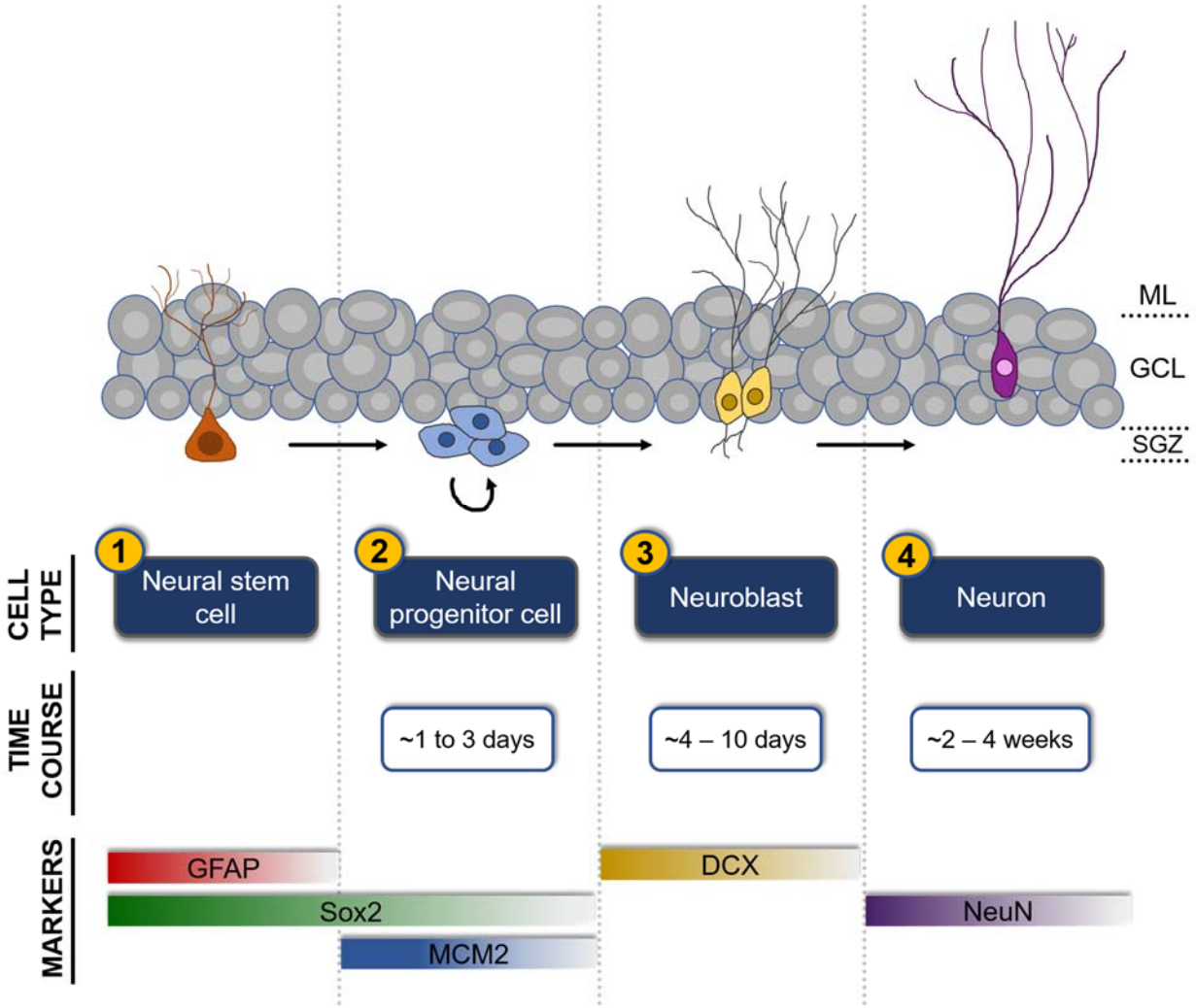

Figure 5. Illustration of hippocampal neurogenesis in the adult brain. Summary of the four developmental stages during adult hippocampal neurogenesis: (1) quiescent radial glia-like (Type I) cells in the subgranular zone (SGZ) are activated; (2) proliferation of non-radial progenitor (Type II) cells; (3) generation of neuroblasts (Type III) cells; (4) maturation of neurons. Also shown are the time course for each stage and expression of stage-specific markers. DCX: doublecortin; GCL: granule cell layer; GFAP: glial fibrillary acidic protein; MCM2: minichromosome maintenance complex component 2; ML: molecular layer; NeuN: neuronal nuclei; SGZ: subgranular zone; Sox2: SRY (sex determining region Y)-box 2.

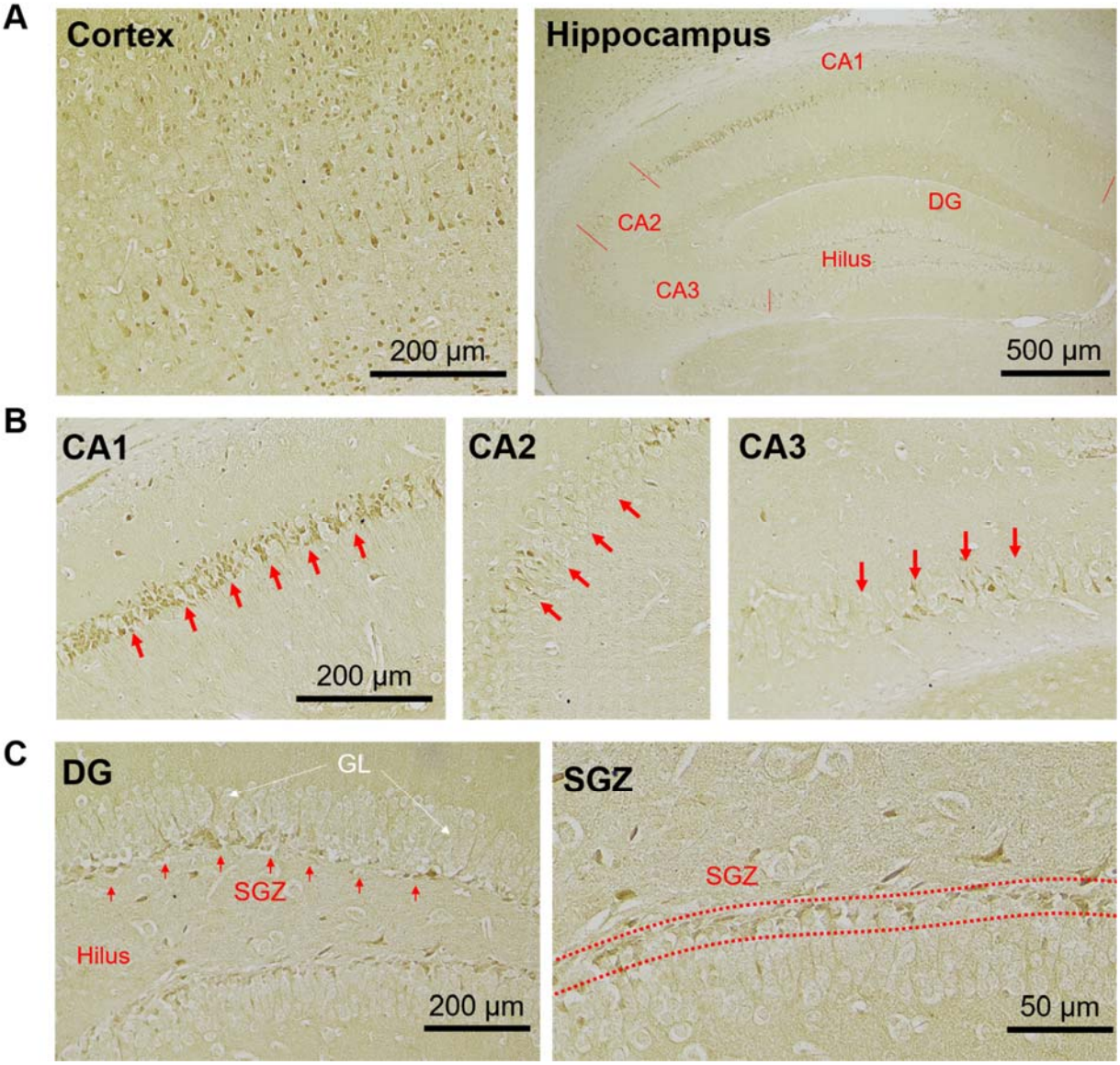

Figure 6. Immunohistochemical analysis of AMPKα1 expression in the young-adult hippocampus and cortex. 5 µm coronal sections of 2-month old mouse brains (n = 4) were immunostained for AMPKα1 expression. The representative section shows cortex (left panel, A) and hippocampus (right panel, A), CA1-3 (B), dentate gyrus and subgranular zone (C). DG: dentate gyrus; GL: granular layer; SGZ: subgranular zone.

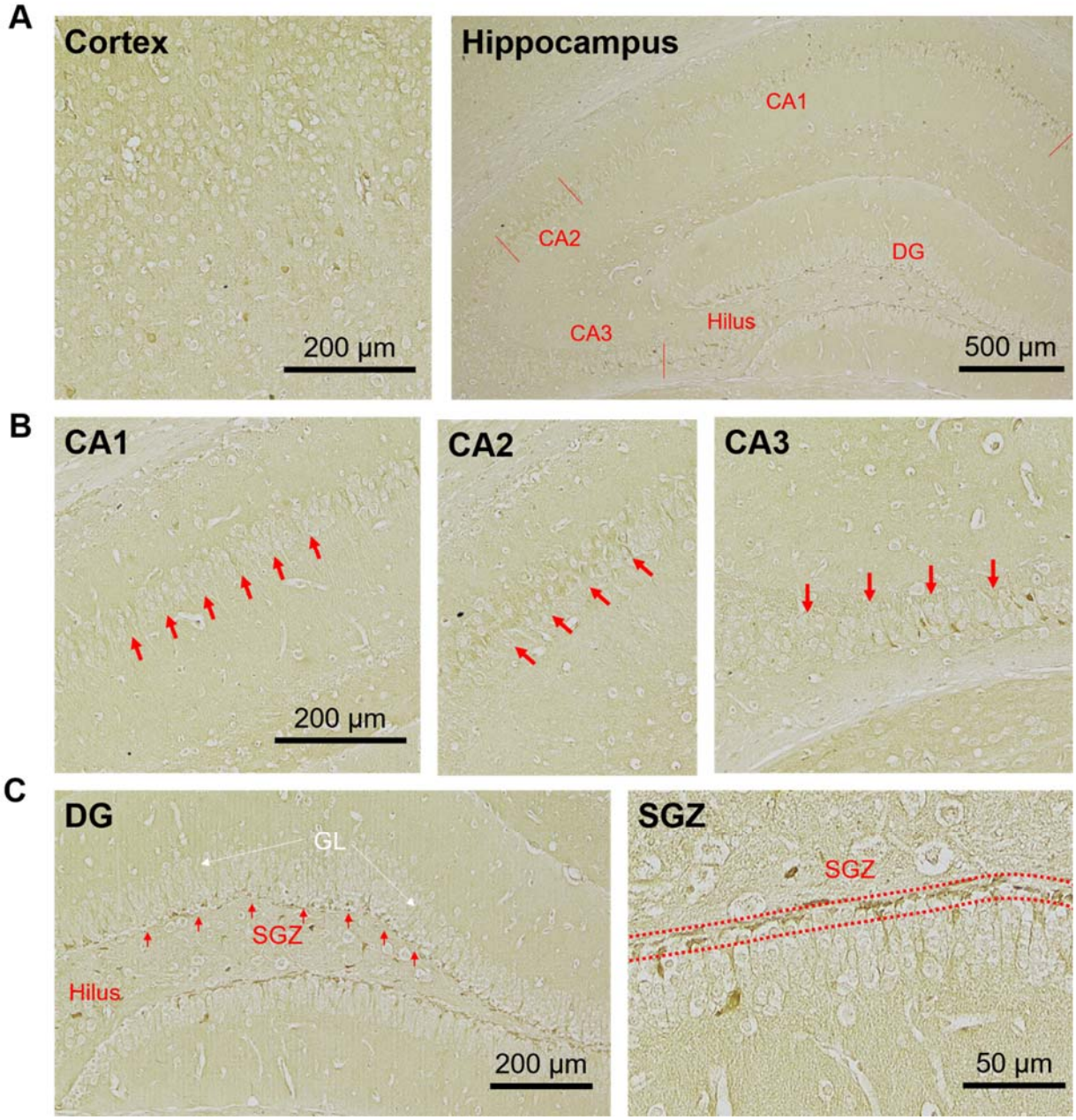

Figure 7. Immunohistochemical analysis of AMPKα1 expression in the old hippocampus and cortex. 5 µm coronal sections of 19-month old mouse brains (n = 4) were immunostained for AMPKα1 expression. The representative section shows cortex (left panel, A) and hippocampus (right panel, A), CA1-3 (B), dentate gyrus and subgranular zone (C). DG: dentate gyrus; GL: granular layer; SGZ: subgranular zone.

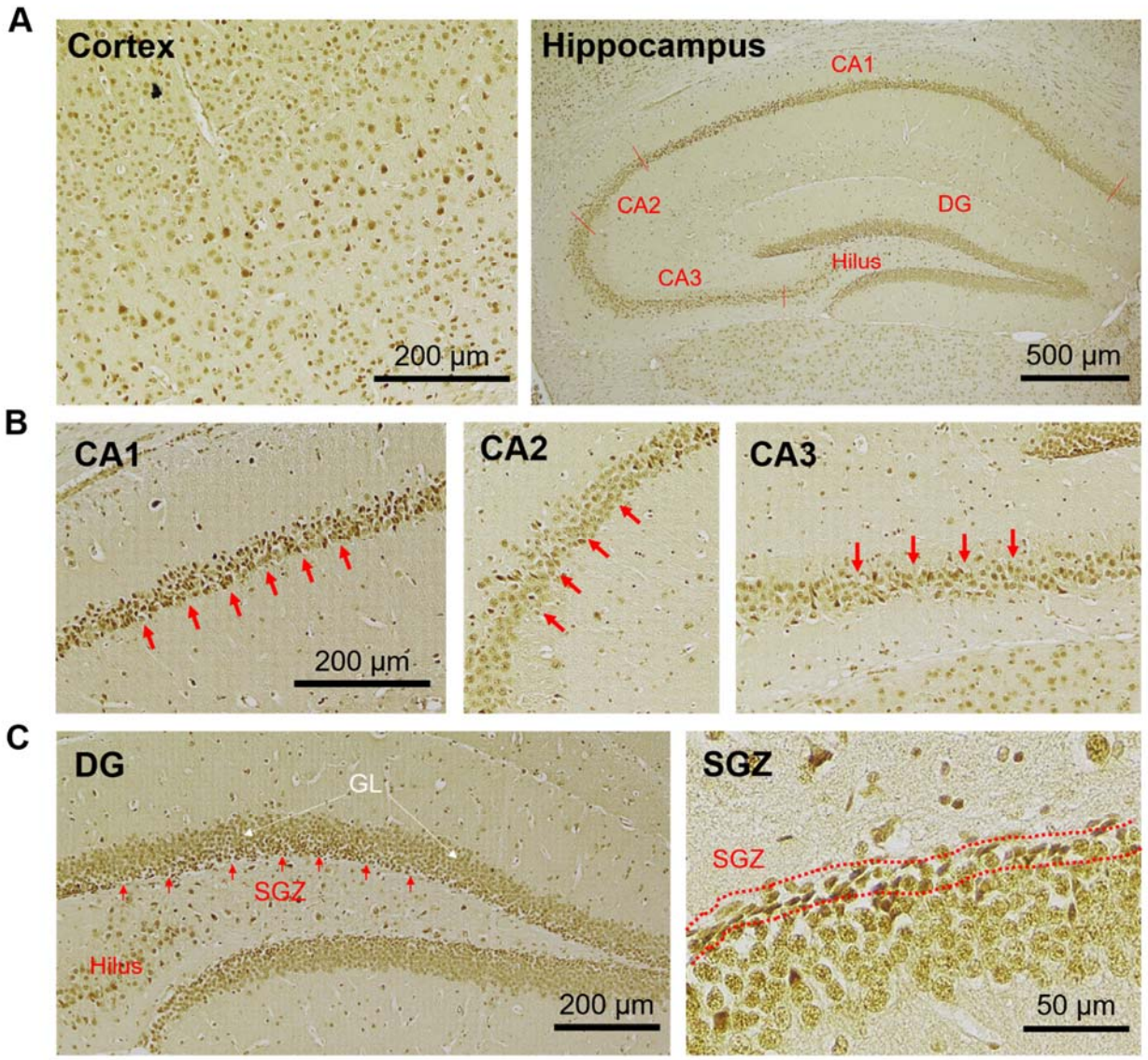

Figure 8. Immunohistochemical analysis of AMPKα2 expression in the young-adult hippocampus and cortex. 5 µm coronal sections of 2-month old mouse brains (n = 4) were immunostained for AMPKα2 expression. The representative section shows cortex (left panel, A) and hippocampus (right panel, A), CA1-3 (B), dentate gyrus and subgranular zone (C). DG: dentate gyrus; GL: granular layer; SGZ: subgranular zone.

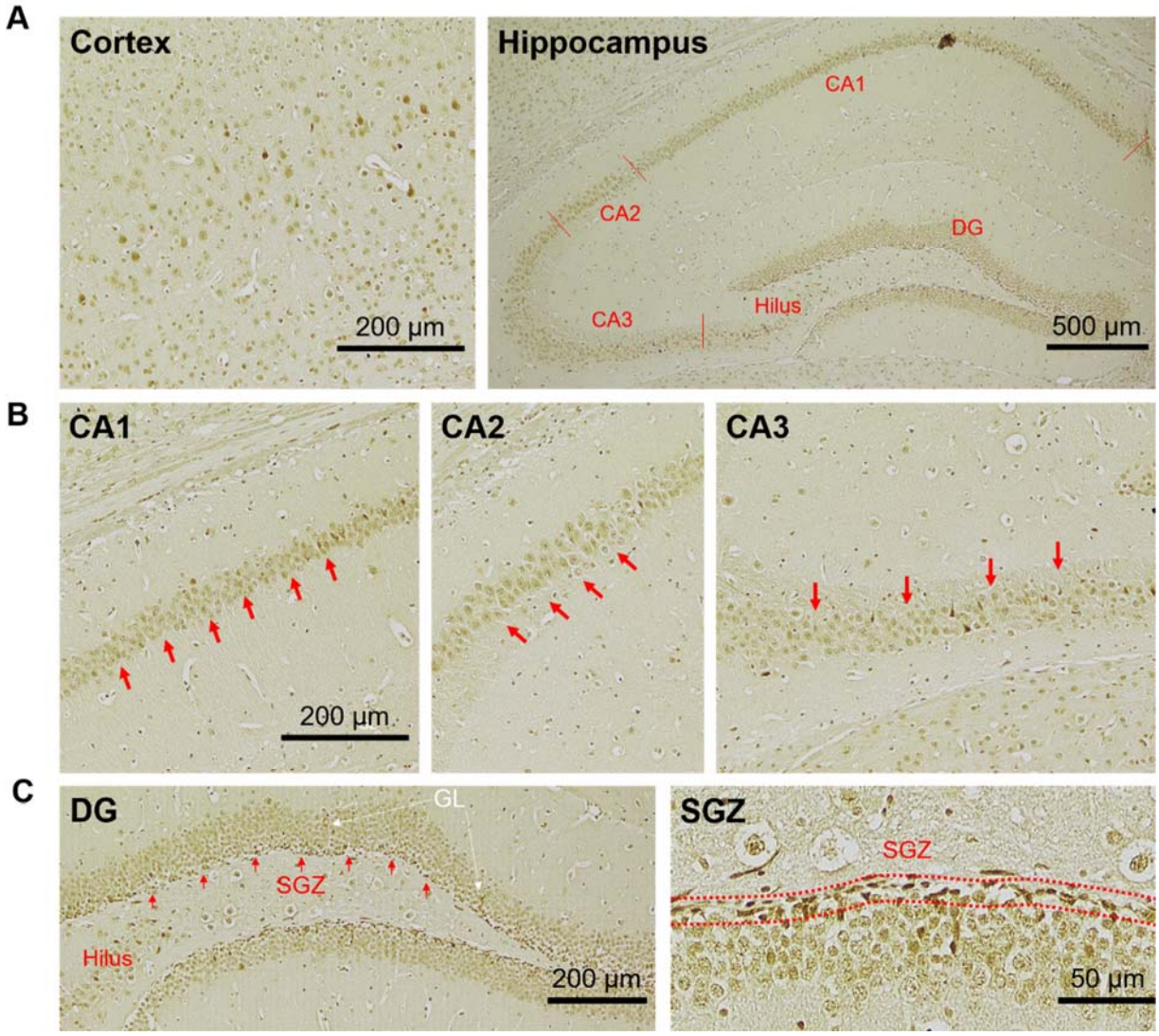

Figure 9. Immunohistochemical analysis of AMPKα2 expression in the old hippocampus and cortex. 5 µm coronal sections of 19-month old mouse brains (n = 4) were immunostained for AMPKα2 expression. The representative section shows cortex (left panel, A) and hippocampus (right panel, A), CA1-3 (B), dentate gyrus and subgranular zone (C). DG: dentate gyrus; GL: granular layer; SGZ: subgranular zone.

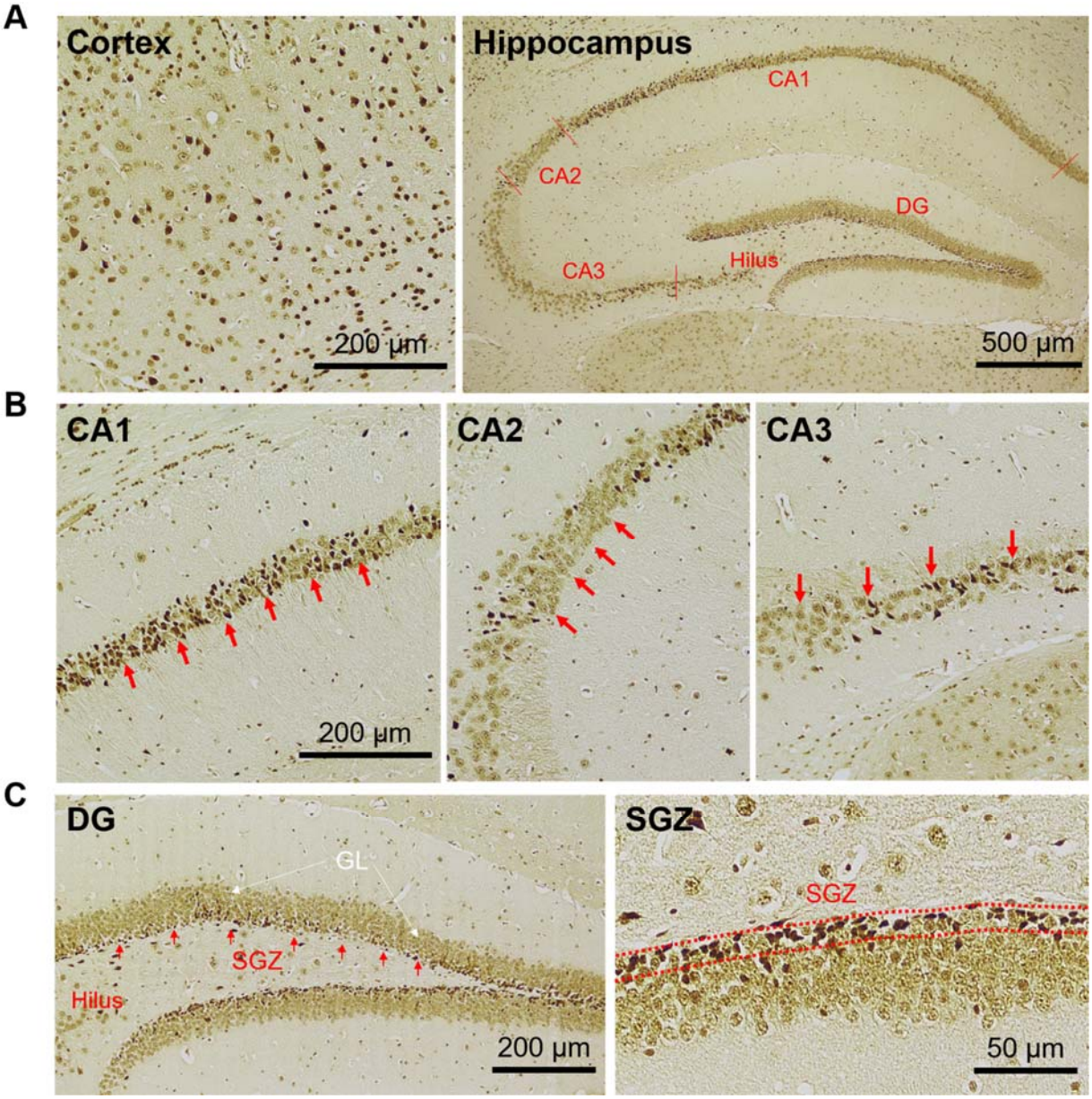

Figure 10. Immunohistochemical analysis of AMPKα phosphorylation (pAMPKα) expression in the young-adult hippocampus and cortex. 5 µm coronal sections of 2-month old mouse brains (n = 4) were immunostained for pAMPKα expression. The representative section shows cortex (left panel, A) and hippocampus (right panel, A), CA1-3 (B), dentate gyrus and subgranular zone (C). DG: dentate gyrus; GL: granular layer; SGZ: subgranular zone.

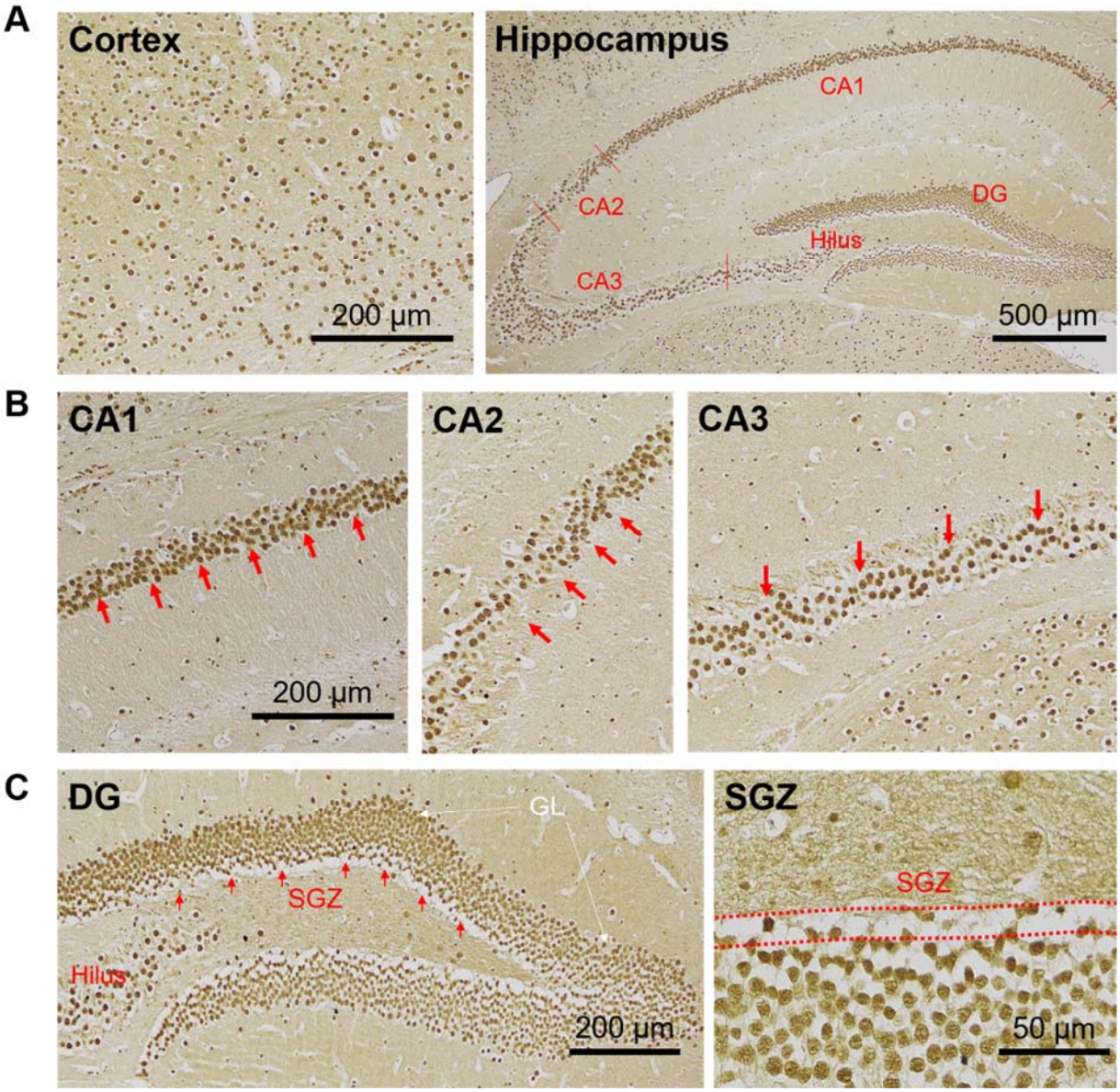

Figure 11. Immunohistochemical analysis of AMPKα phosphorylation (pAMPKα) expression in the old hippocampus and cortex. 5 µm coronal sections of 19-month old mouse brains (n = 4) were immunostained for pAMPKα expression. The representative section shows cortex (left panel, A) and hippocampus (right panel, A), CA1-3 (B), dentate gyrus and subgranular zone (C). DG: dentate gyrus; GL: granular layer; SGZ: subgranular zone.

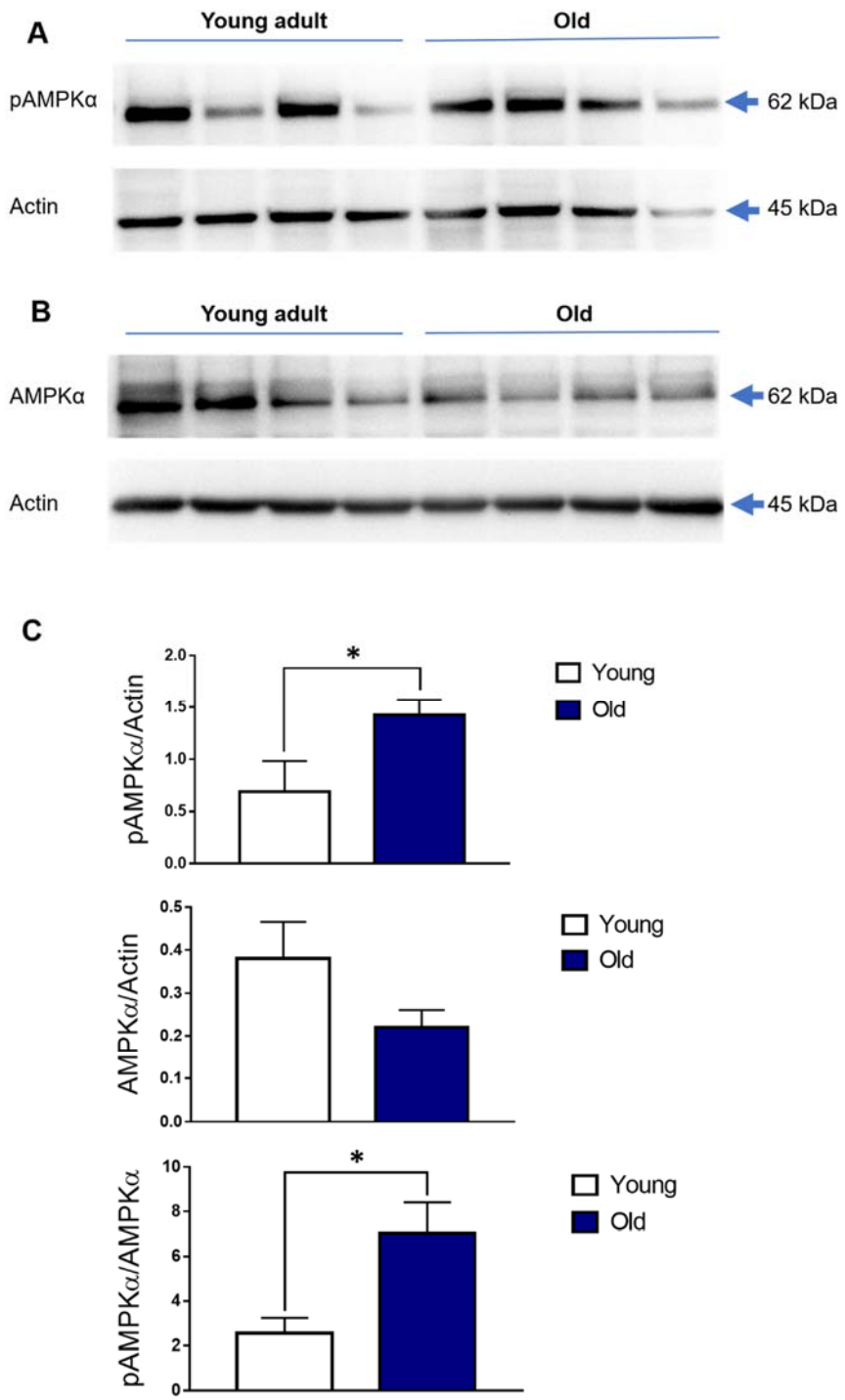

Figure 12. AMPK activation (pAMPKα) in the young-adult and old hippocampus. Protein lysates (30 µg) obtained from 2- and 19-month old hippocampi (n = 4 per group) were resolved on 10% SDS-PAGE gels, transferred onto PVDF membranes and probed with the appropriate primary and secondary antibodies. Representative Western blots showing pAMPKα (A) and total AMPKα (B) protein levels. Actin was used as the loading control. Statistical analysis of protein levels of pAMPKα and total AMPKα in the young and old hippocampus (C). *$p < 0.05$.

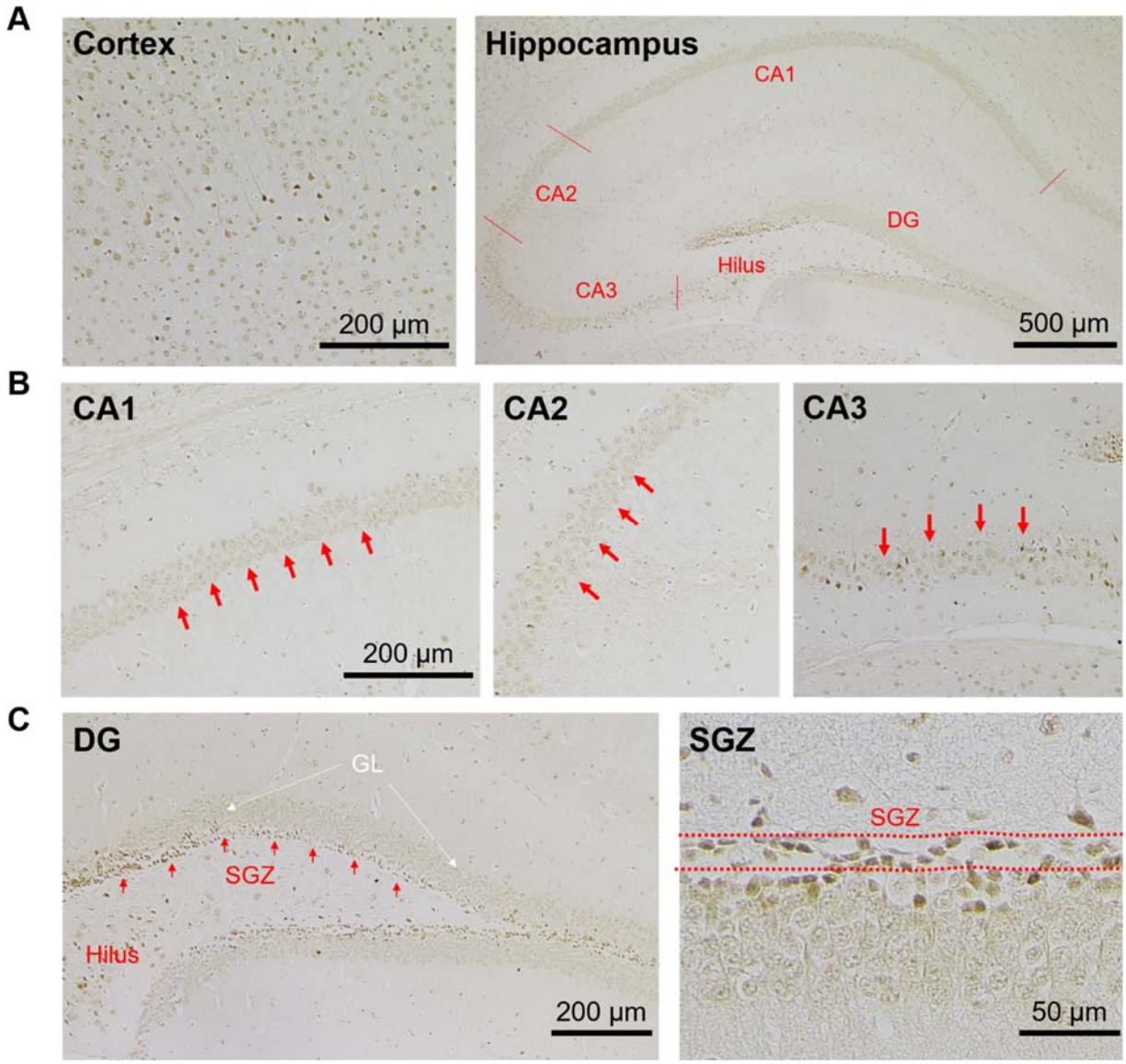

Figure 13. Immunohistochemical analysis of AMPKβ1 expression in the young-adult hippocampus and cortex. 5 µm coronal sections of 2-month old mouse brains (n = 4) were immunostained for AMPKβ1 expression. The representative section shows cortex (left panel, A) and hippocampus (right panel, A), CA1-3 (B), dentate gyrus and subgranular zone (C). DG: dentate gyrus; GL: granular layer; SGZ: subgranular zone.

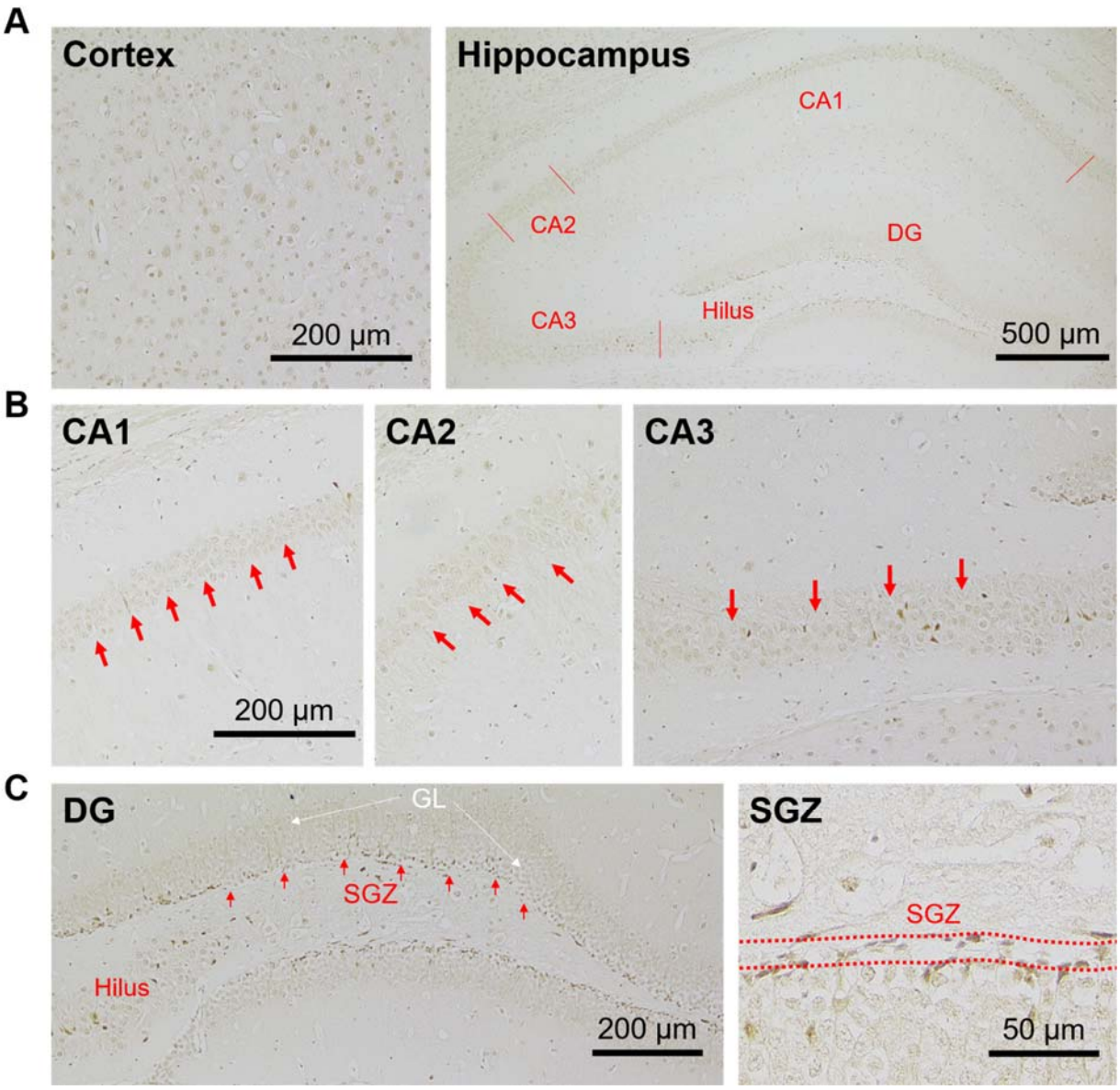

Figure 14. Immunohistochemical analysis of AMPKβ1 expression in the old hippocampus and cortex. 5 µm coronal sections of 19-month old mouse brains (n = 4) were immunostained for AMPKβ1 expression. The representative section shows cortex (left panel, A) and hippocampus (right panel, A), CA1-3 (B), dentate gyrus and subgranular zone (C). DG: dentate gyrus; GL: granular layer; SGZ: subgranular zone.

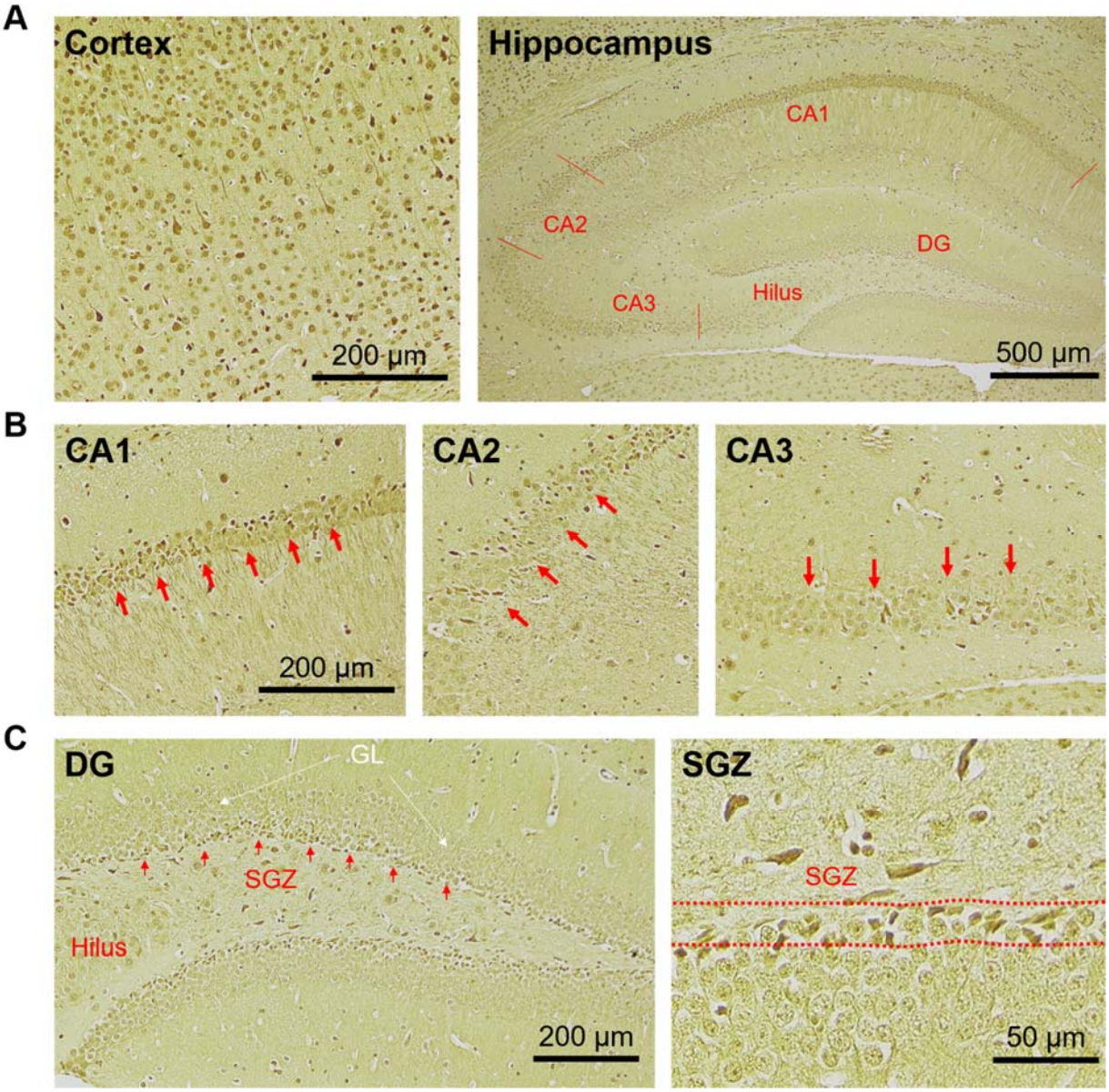

Figure 15. Immunohistochemical analysis of AMPKβ2 expression in the young-adult hippocampus and cortex. 5 µm coronal sections of 2-month old mouse brains (n = 4) were immunostained for AMPKβ2 expression. The representative section shows cortex (left panel, A) and hippocampus (right panel, A), CA1-3 (B), dentate gyrus and subgranular zone (C). DG: dentate gyrus; GL: granular layer; SGZ: subgranular zone.

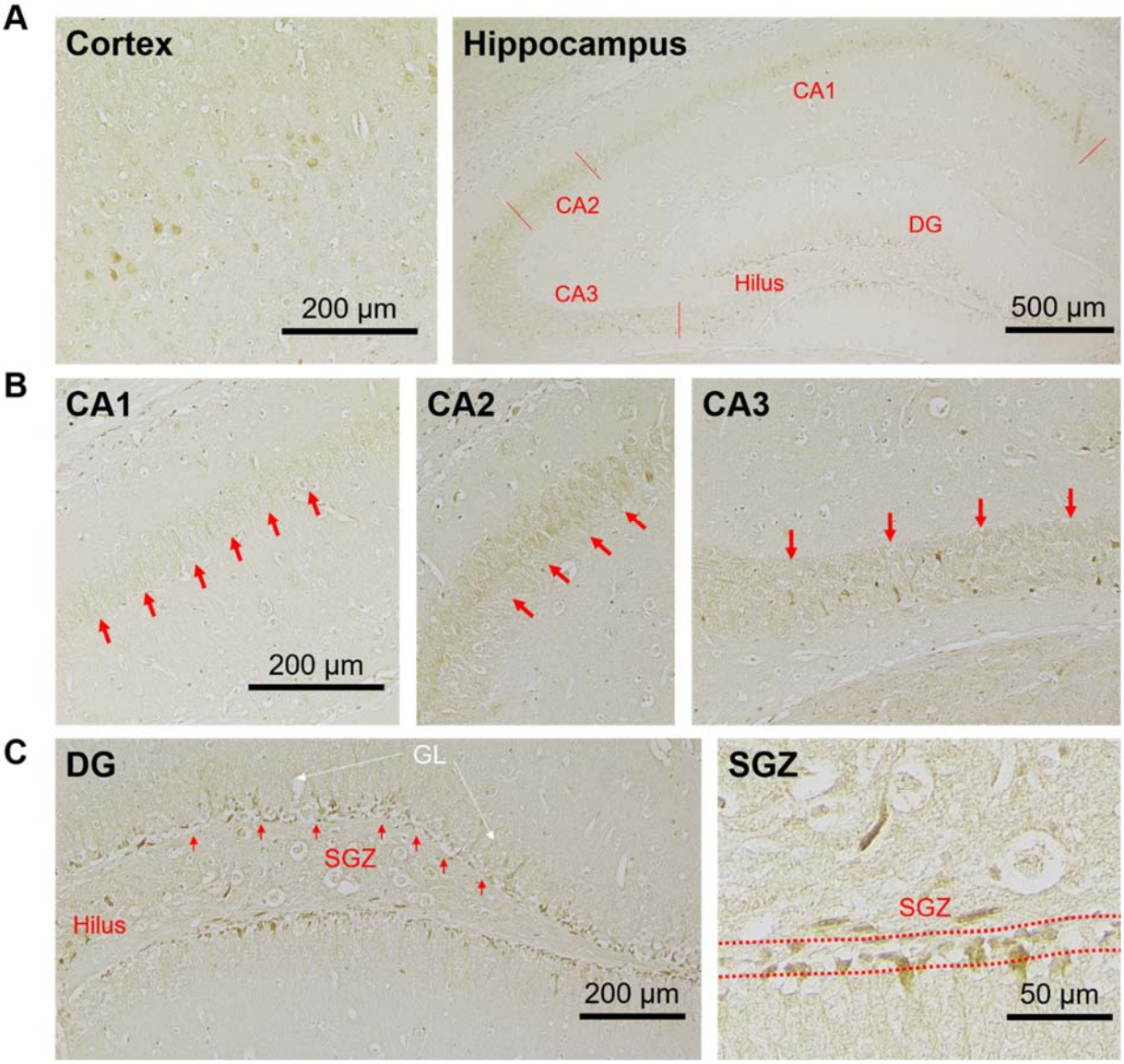

Figure 16. Immunohistochemical analysis of AMPKβ2 expression in the old hippocampus and cortex. 5 µm coronal sections of 19-month old mouse brains (n = 4) were immunostained for AMPKβ2 expression. The representative section shows cortex (left panel, A) and hippocampus (right panel, A), CA1-3 (B), dentate gyrus and subgranular zone (C). DG: dentate gyrus; GL: granular layer; SGZ: subgranular zone.

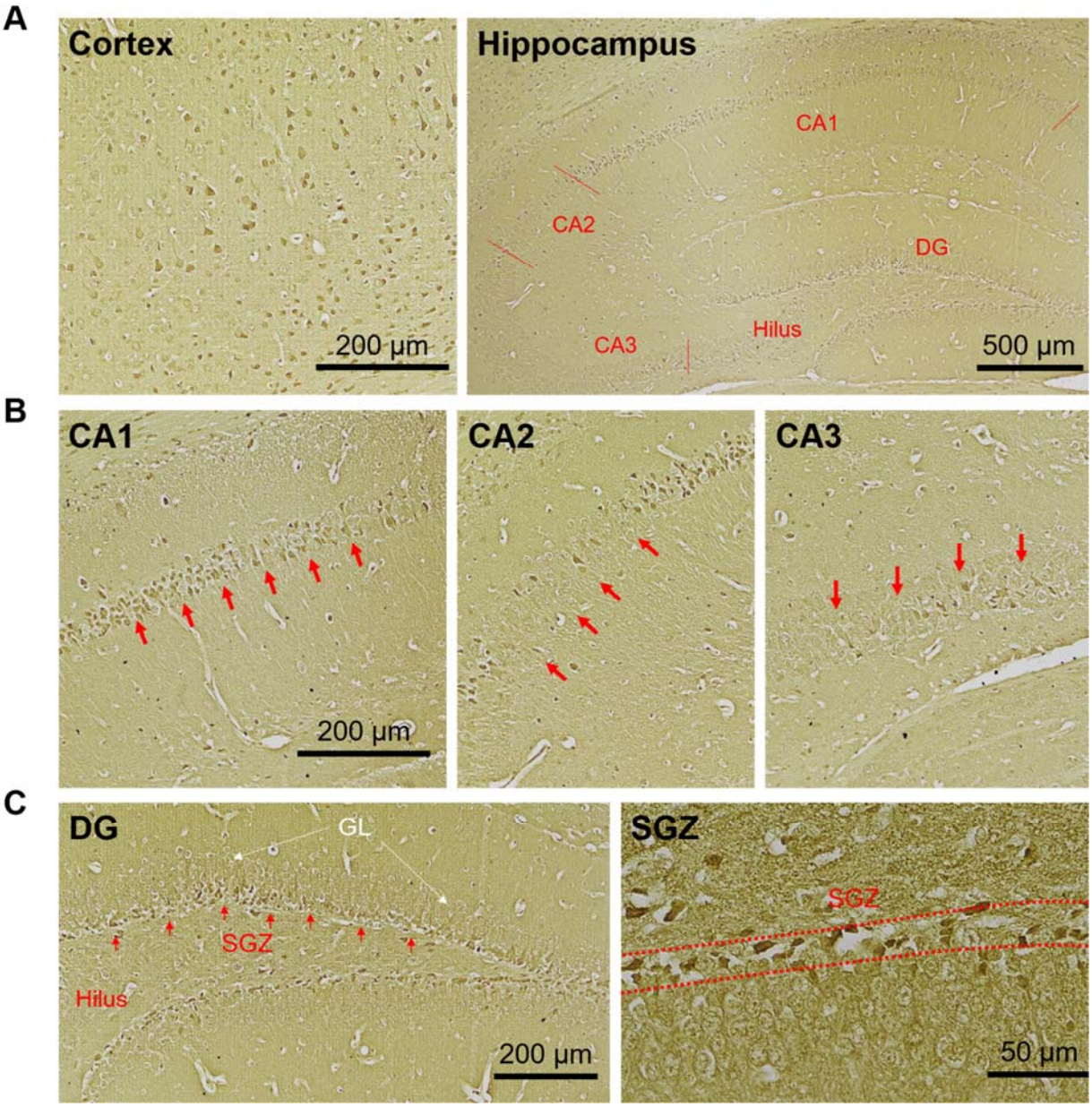

Figure 17. Immunohistochemical analysis of AMPKγ1 expression in the young-adult hippocampus and cortex. 5 µm coronal sections of 2-month old mouse brains (n = 4) were immunostained for AMPKγ1 expression. Representative section shows cortex (left panel, A) and hippocampus (right panel, A), CA1-3 (B), dentate gyrus and subgranular zone (C). DG: dentate gyrus; GL: granular layer; SGZ: subgranular zone.

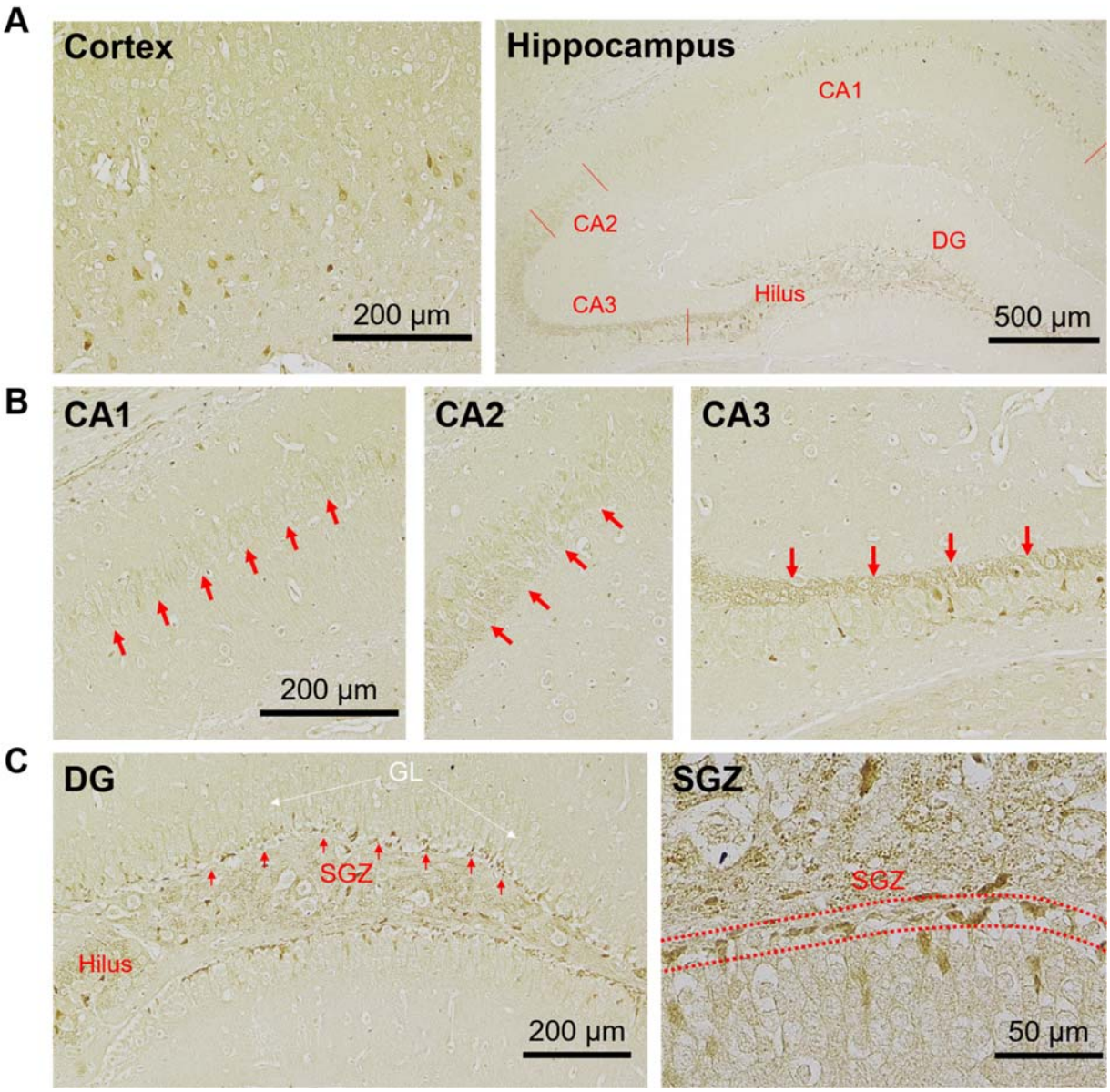

Figure 18. Immunohistochemical analysis of AMPKγ1 expression in the old hippocampus and cortex. 5 µm coronal sections of 19-month old mouse brains (n = 4) were immunostained for AMPKγ1 expression. The representative section shows cortex (left panel, A) and hippocampus (right panel, A), CA1-3 (B), dentate gyrus and subgranular zone (C). DG: dentate gyrus; GL: granular layer; SGZ: subgranular zone.

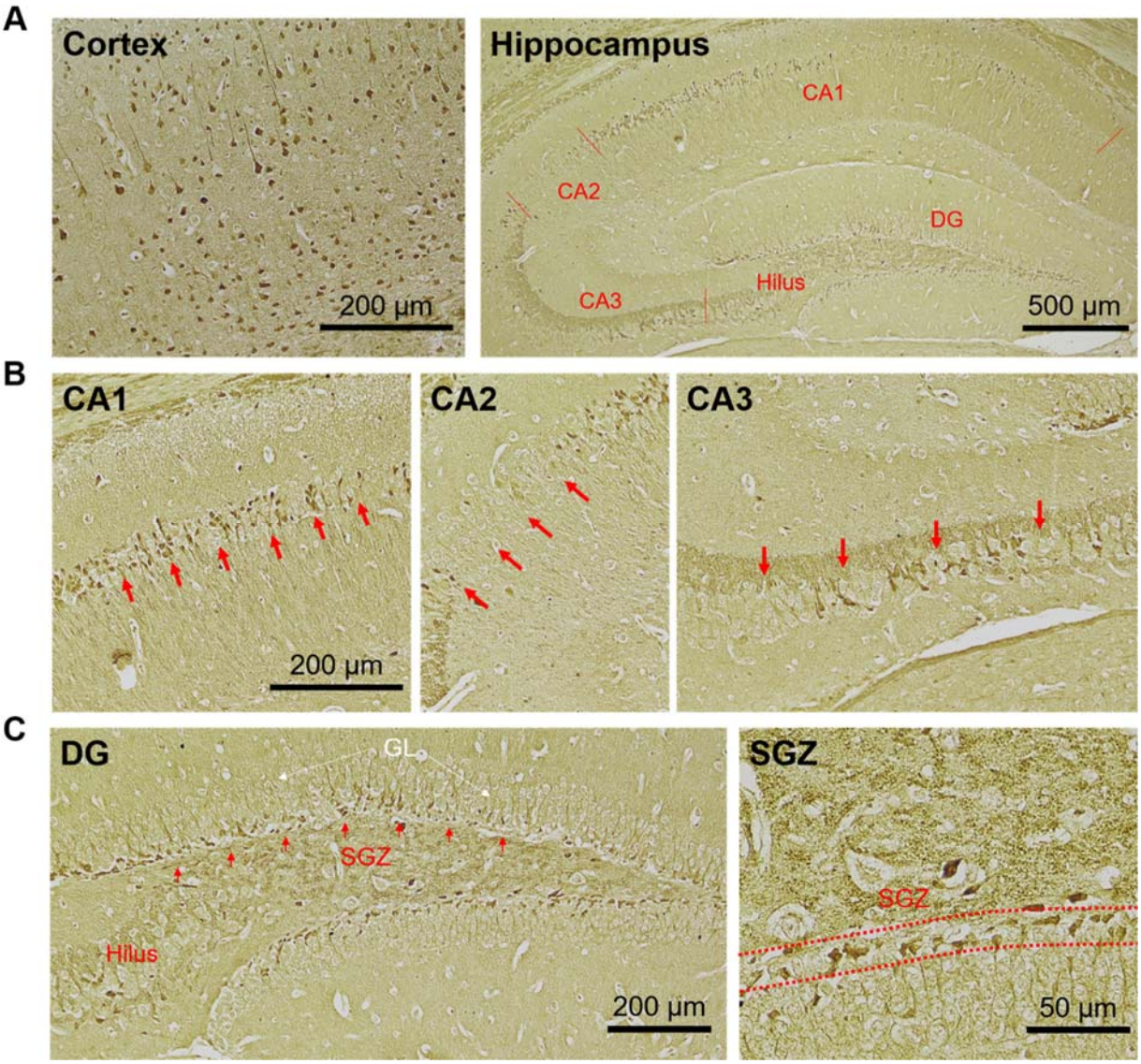

Figure 19. Immunohistochemical analysis of AMPKγ2 expression in the young-adult hippocampus and cortex. 5 µm coronal sections of 2-month old mouse brains (n = 4) were immunostained for AMPKγ2 expression. The representative section shows cortex (left panel, A) and hippocampus (right panel, A), CA1-3 (B), dentate gyrus and subgranular zone (C). DG: dentate gyrus; GL: granular layer; SGZ: subgranular zone.

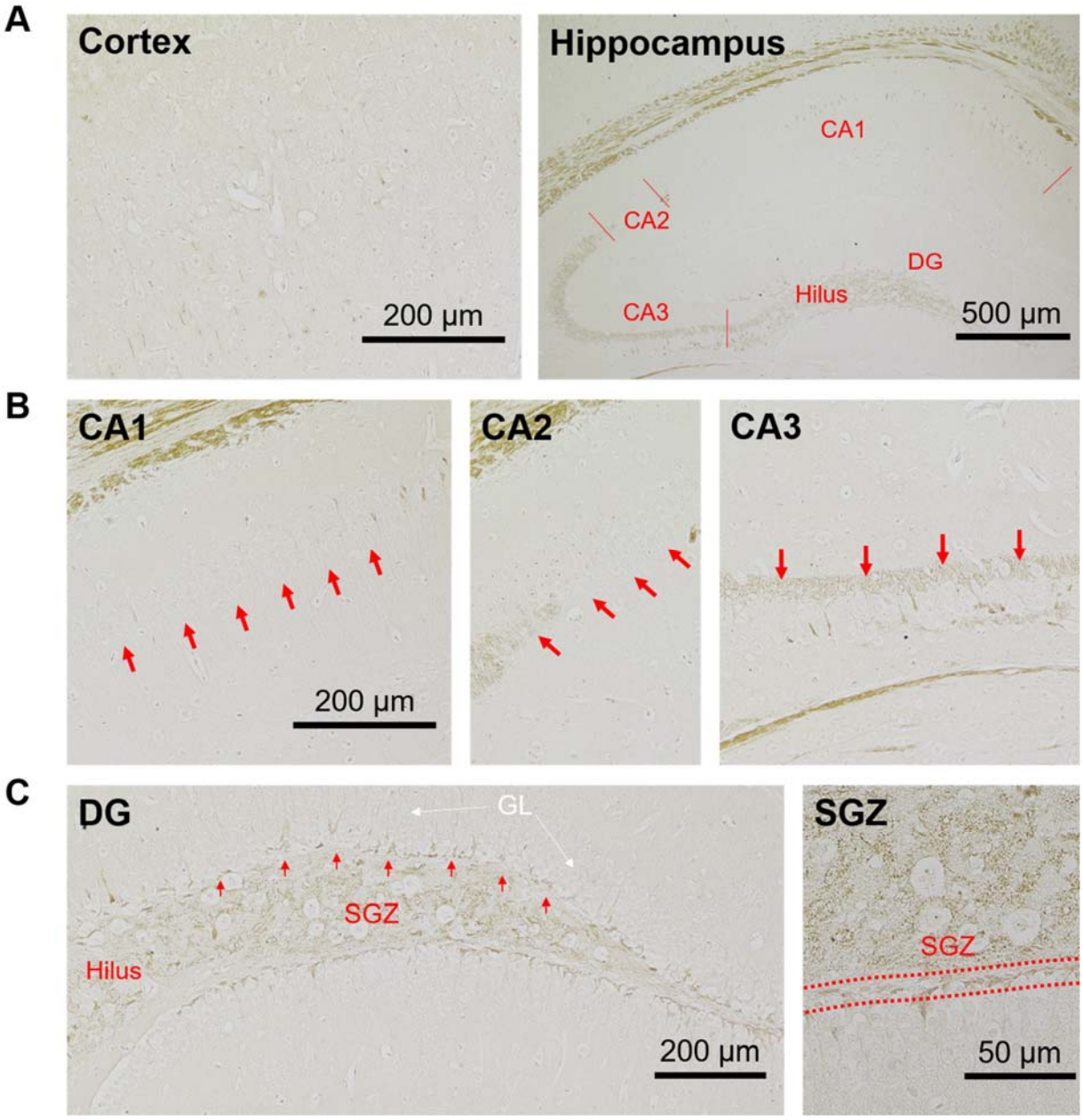

Figure 20. Immunohistochemical analysis of AMPKγ2 expression in the old hippocampus and cortex. 5 µm coronal sections of 19-month old mouse brains (n = 4) were immunostained for AMPKγ2 expression. The representative section shows cortex (left panel, A) and hippocampus (right panel, A), CA1-3 (B), dentate gyrus and subgranular zone (C). DG: dentate gyrus; GL: granular layer; SGZ: subgranular zone.

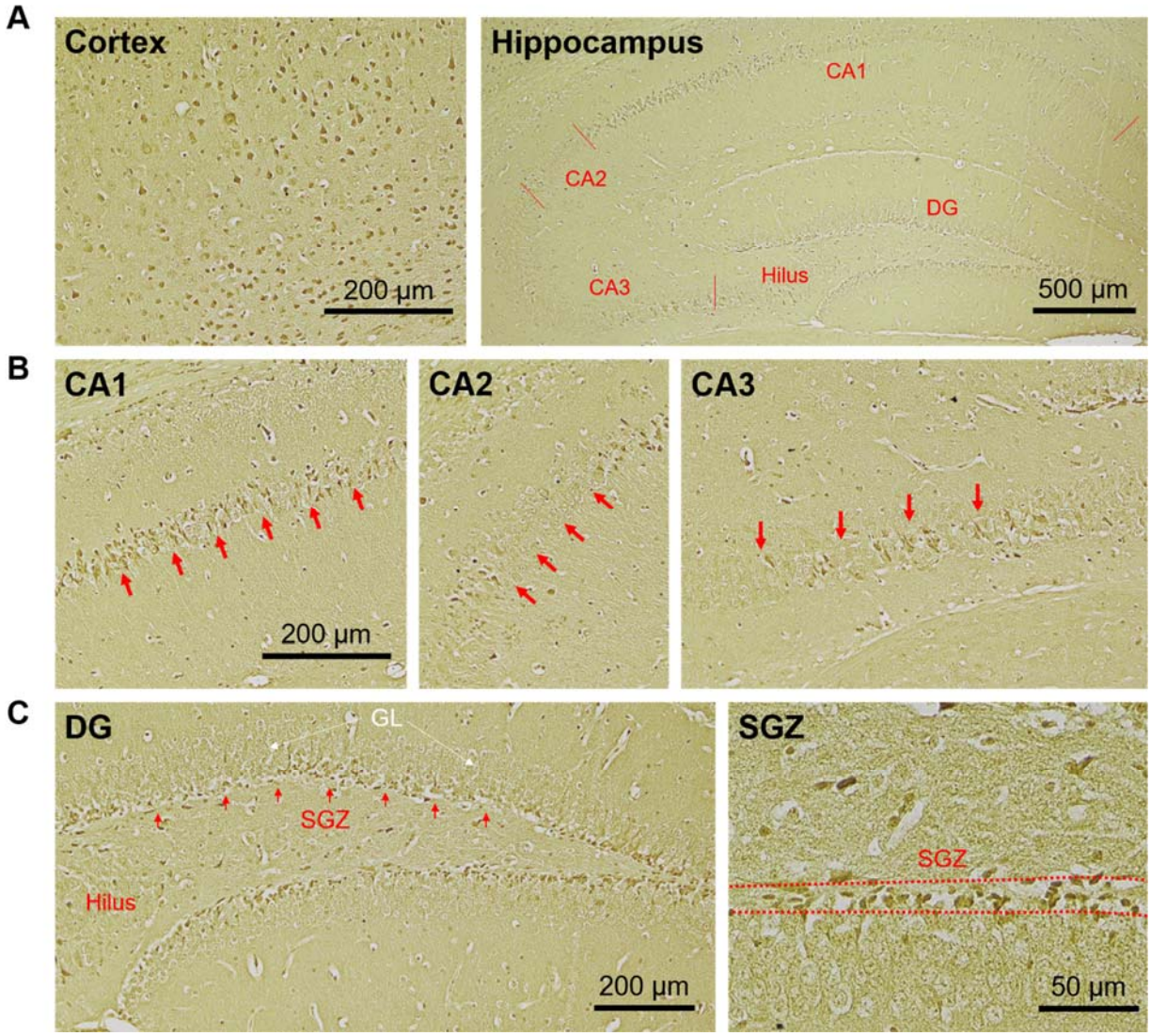

Figure 21. Immunohistochemical analysis of AMPKγ3 expression in the young-adult hippocampus and cortex. 5 µm coronal sections of 2-month old mouse brains (n = 4) were immunostained for AMPKγ3 expression. The representative section shows cortex (left panel, A) and hippocampus (right panel, A), CA1-3 (B), dentate gyrus and subgranular zone (C). DG: dentate gyrus; GL: granular layer; SGZ: subgranular zone.

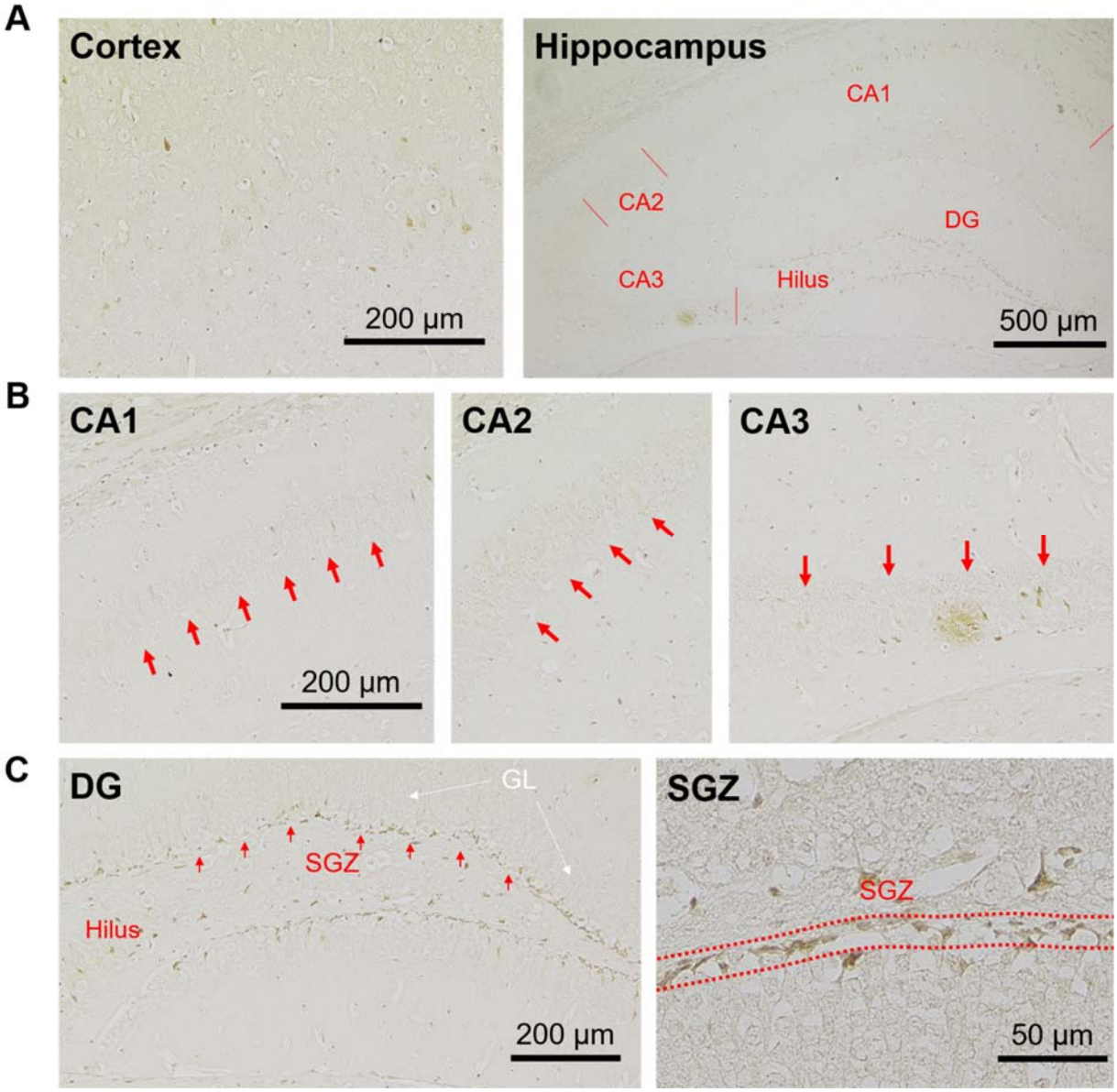

Figure 22. Immunohistochemical analysis of AMPKγ3 expression in the old hippocampus and cortex. 5 µm coronal sections of 19-month old mouse brains (n = 4) were immunostained for AMPKγ3 expression. The representative section shows cortex (left panel, A) and hippocampus (right panel, A), CA1-3 (B), dentate gyrus and subgranular zone (C). DG: dentate gyrus; GL: granular layer; SGZ: subgranular zone.

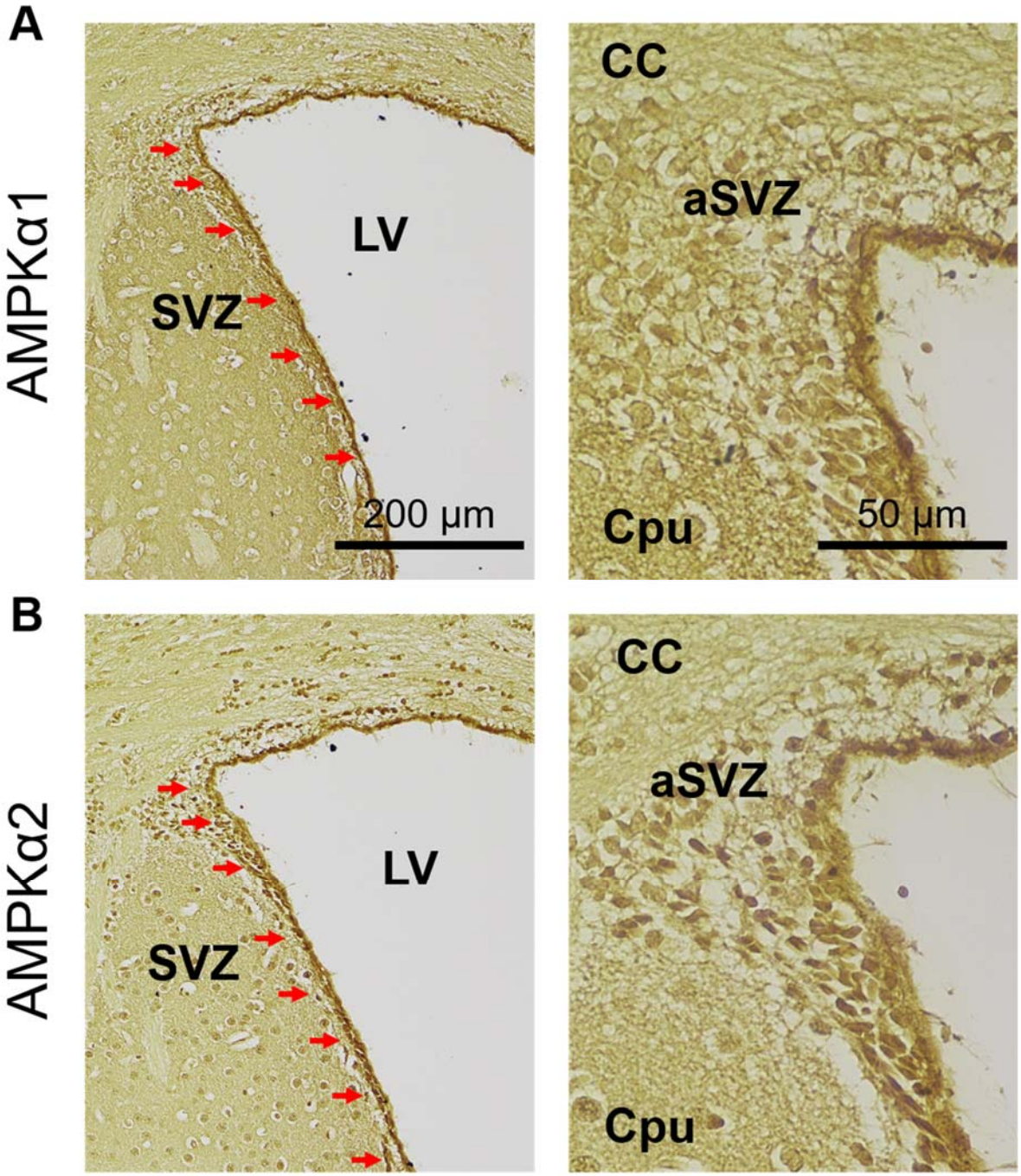

Figure 23. Immunohistochemical analysis of AMPKα expression in the young-adult subventricular zone. 5 µm coronal sections of 2-month old mouse brains (n = 4) were immunostained for AMPKα expression. The representaitve sections show AMPKα1 (A) and AMPKα2 (B) expressions. aSVZ: anterior subventricular zone, CC: corpus callosum; Cpu: striatum; LV: lateral ventricle, SVZ: subventricular zone.

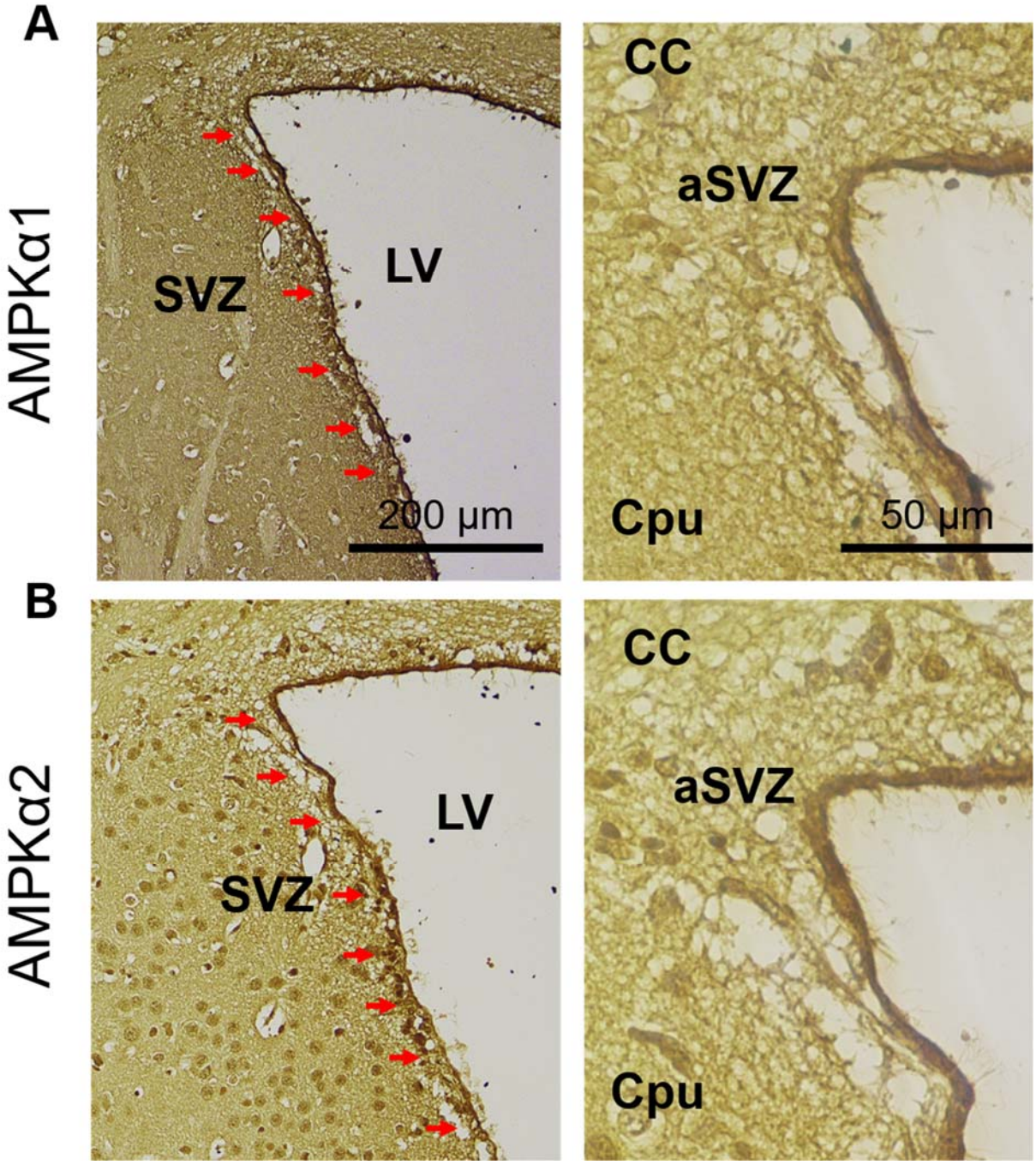

Figure 24. Immunohistochemical analysis of AMPKα expression in the old subventricular zone. 5 µm coronal sections of 19-month old mouse brains (n = 4) were immunostained for AMPKα expression. The representaitve sections show AMPKα1 (A) and AMPKα2 (B) expressions. aSVZ: anterior subventricular zone, CC: corpus callosum; Cpu: striatum; LV: lateral ventricle, SVZ: subventricular zone.

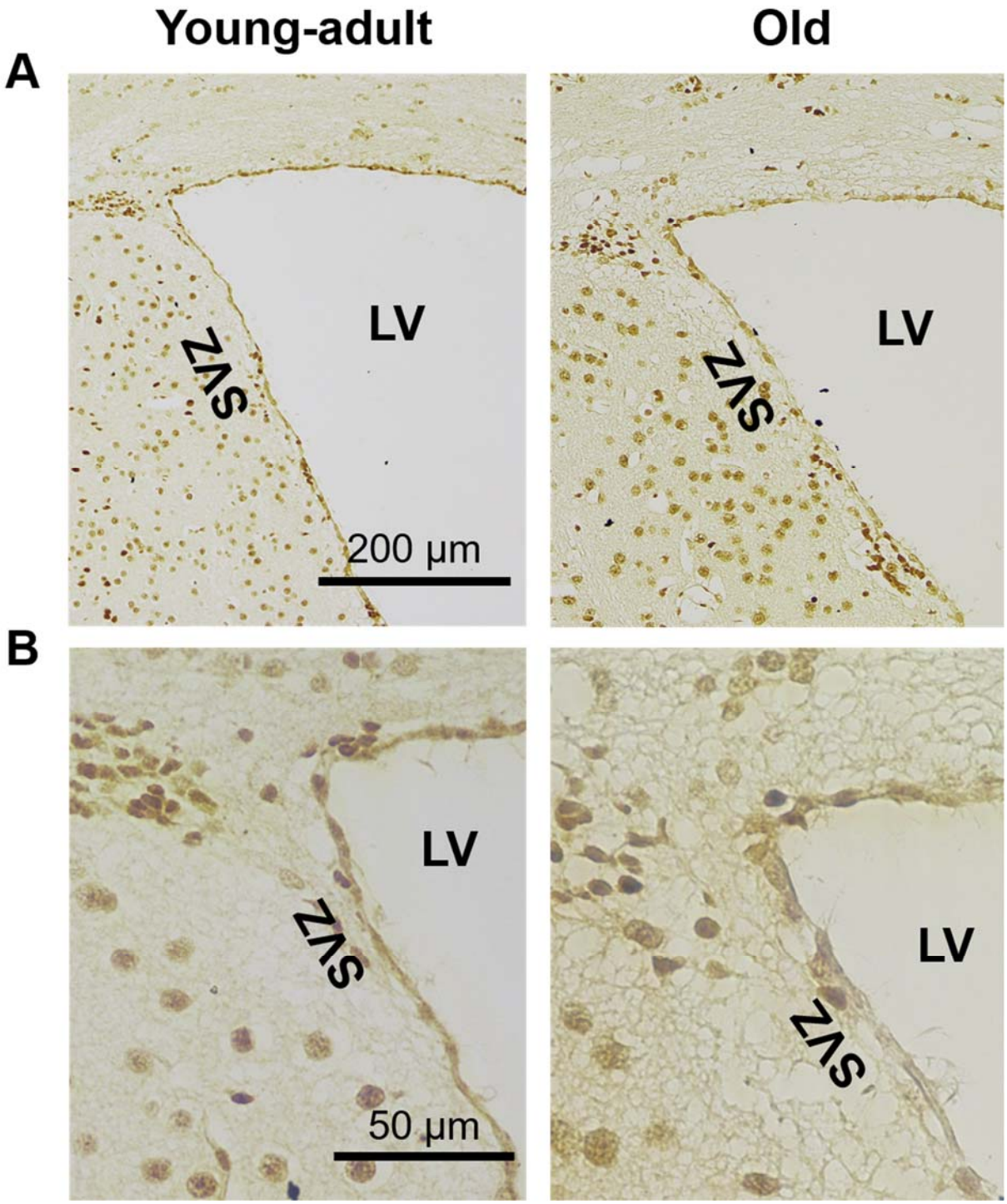

Figure 25. Immunohistochemical analysis of AMPKα phosphorylation (pAMPKα) expression in the young-adult and old subventricular zone. 5 µm coronal sections of 2- and 19-month old mouse brains (n = 4) were immunostained for pAMPKα expression. Representative sections show pAMPKα expression in low (A) and high (B) magnifications. LV: lateral ventricle, SVZ: subventricular zone.

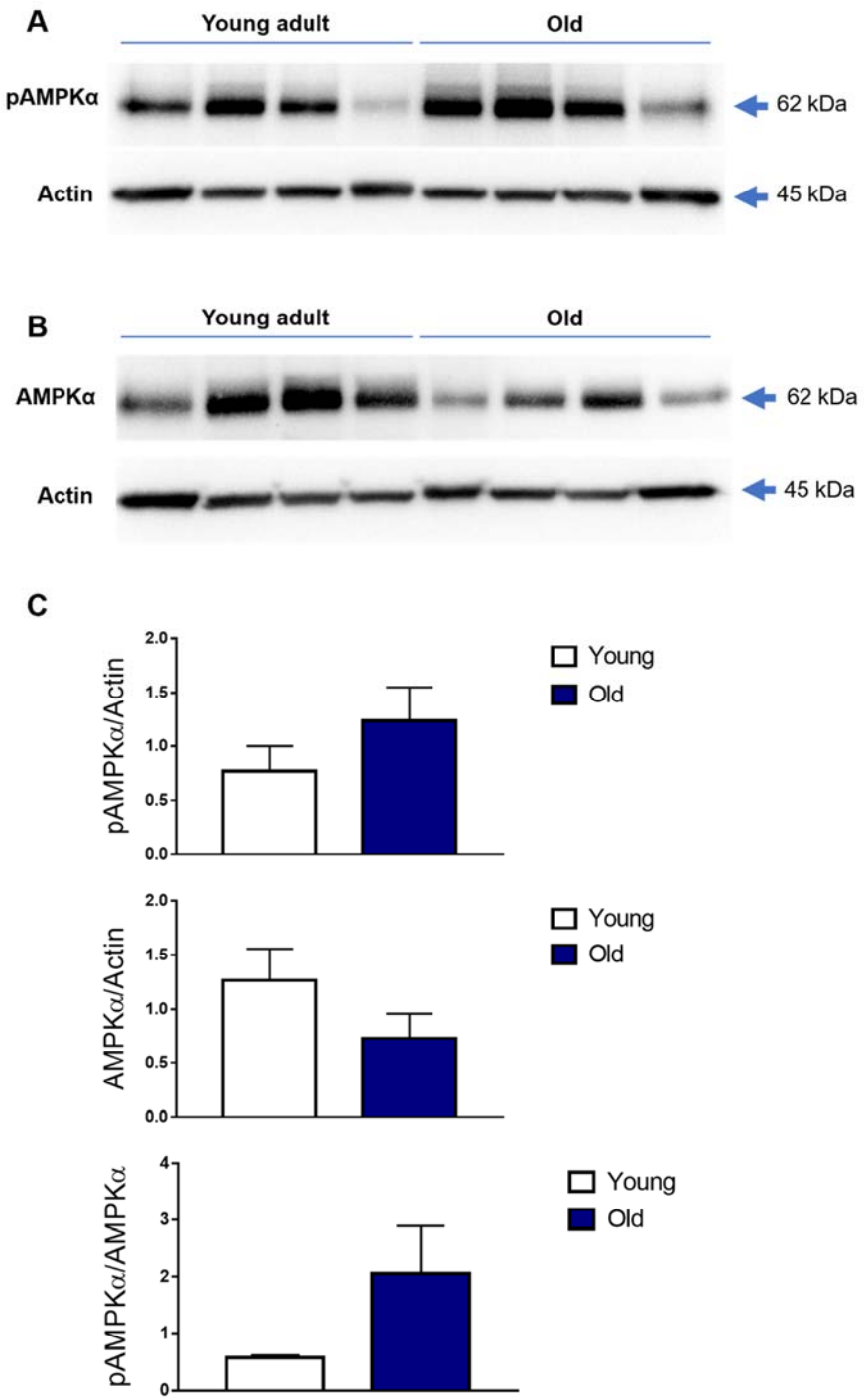

Figure 26. AMPK activation (pAMPKα) in the young-adult and old subventricular zone (SVZ). Protein lysates (30 µg) obtained from 2- and 19-month old SVZ (n = 4 per group) were resolved on 10% SDS-PAGE gels, transferred onto PVDF membranes and probed with the appropriate primary and secondary antibodies. Representative Western blots showing pAMPKα (A) and total AMPKα (B) protein levels. Actin was used as the loading control. Statistical analysis of protein levels of pAMPKα and total AMPKα in the young and old SVZ (C).

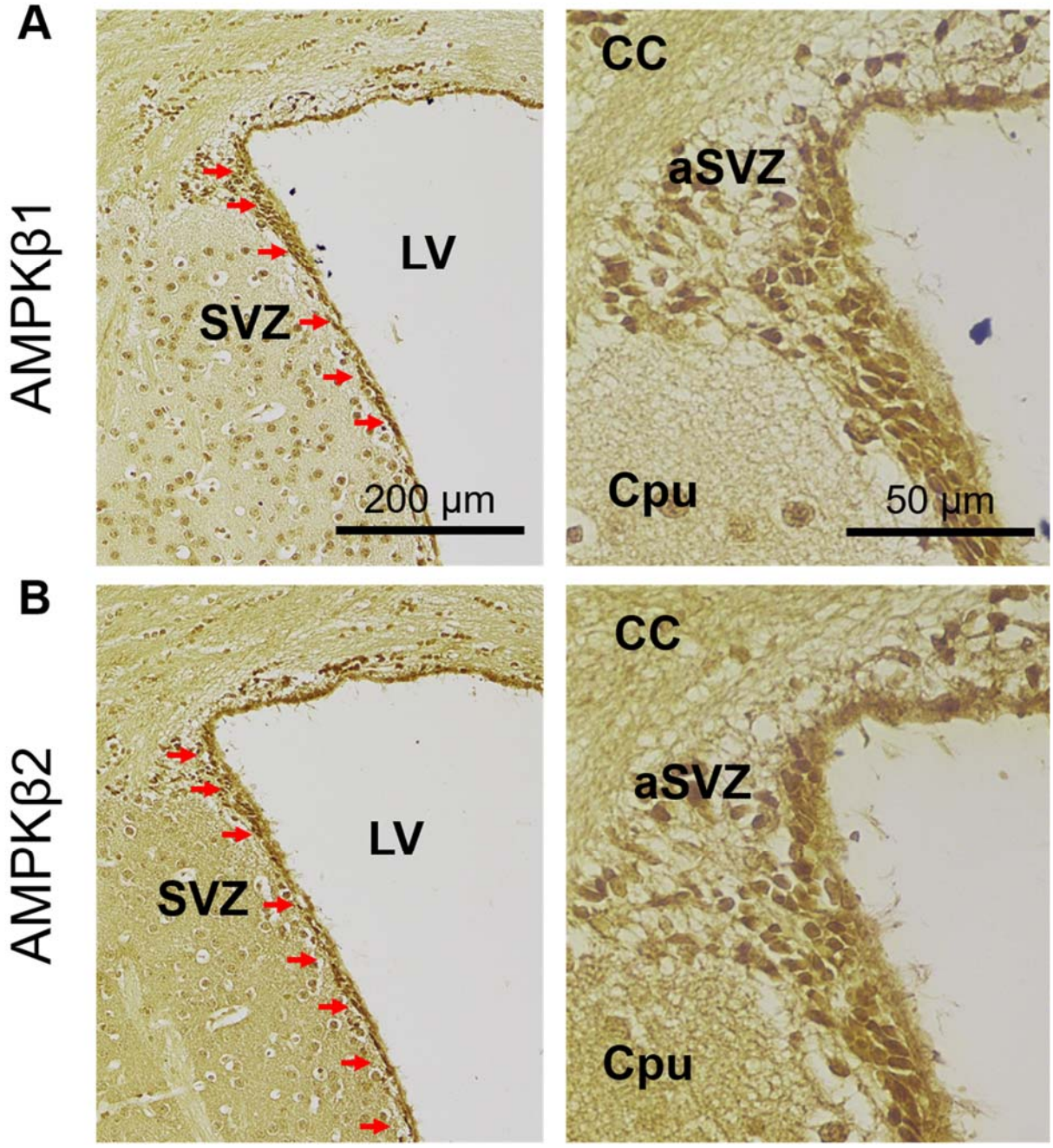

Figure 27. Immunohistochemical analysis of AMPKβ expression in the young-adult subventricular zone. 5 μm coronal sections of 2-month old mouse brains (n = 4) were immunostained for AMPKβ expression. Representative sections show AMPKβ1 (A) and AMPKβ2 (B) expressions. aSVZ: anterior subventricular zone, CC: corpus callosum; Cpu: striatum; LV: lateral ventricle, SVZ: subventricular zone.

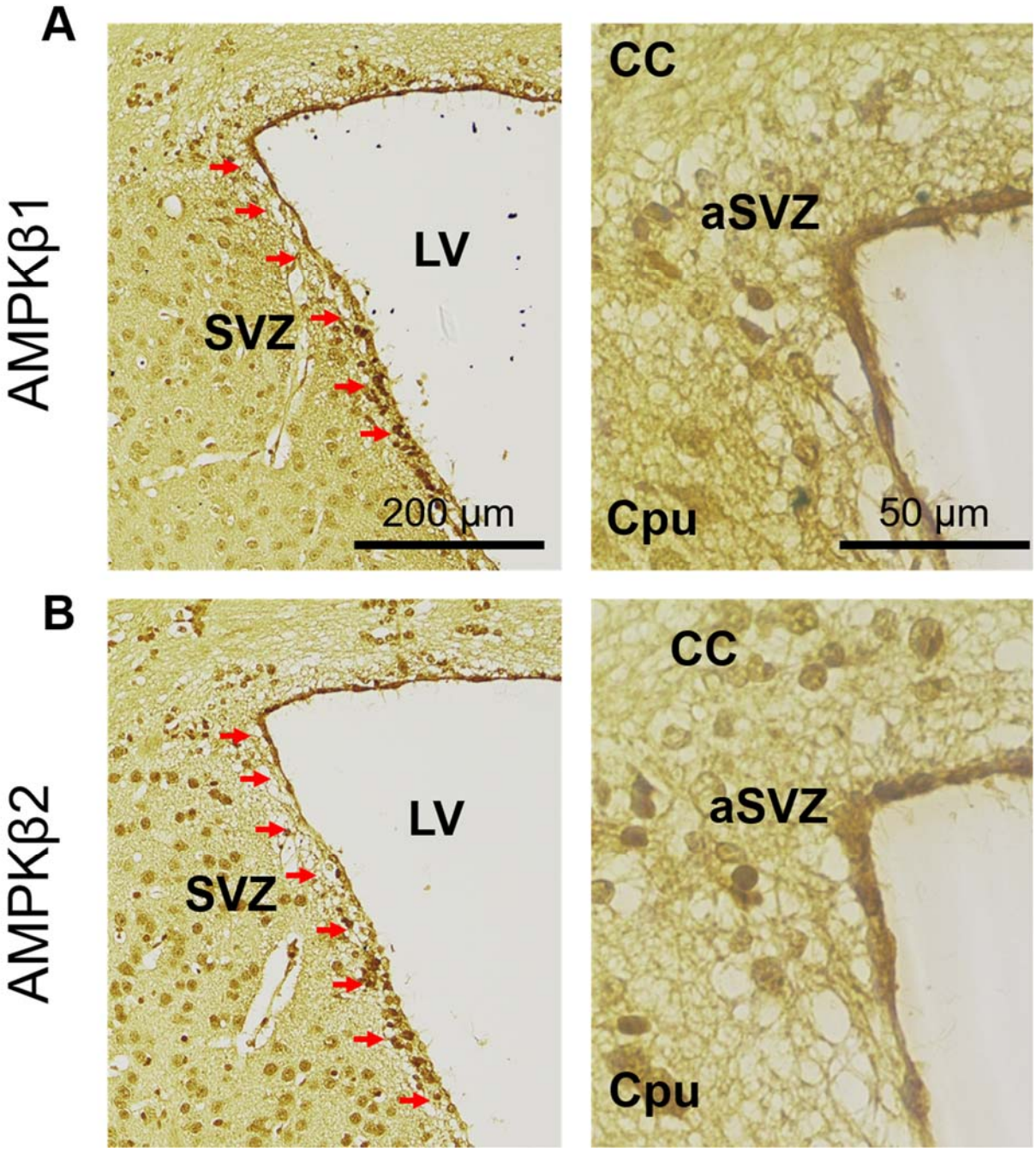

Figure 28. Immunohistochemical analysis of AMPKβ expression in the old subventricular zone. 5 µm coronal sections of 19-month old mouse brains (n = 4) were immunostained for AMPKβ expression. Representative sections show AMPKβ1 (A) and AMPKβ2 (B) expressions. aSVZ: anterior subventricular zone, CC: corpus callosum; Cpu: striatum; LV: lateral ventricle, SVZ: subventricular zone.

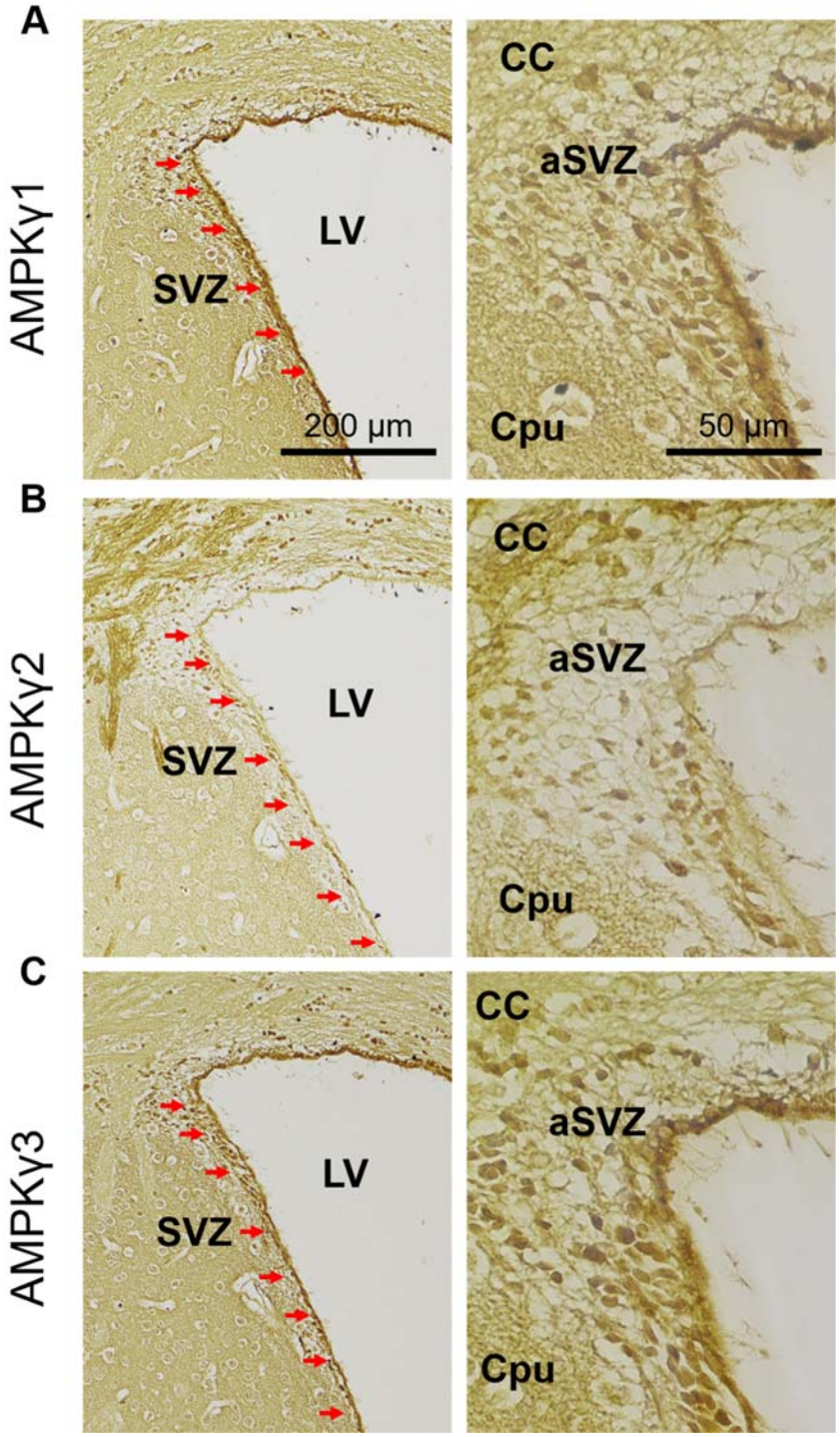

Figure 29. Immunohistochemical analysis of AMPKγ expression in the young-adult subventricular zone. 5 μm coronal sections of 2-month old mouse brains (n = 4) were immunostained for AMPKγ expression. Representative sections show AMPKγ1 (A), AMPKγ2 (B), and AMPKγ3 (C) expressions. aSVZ: anterior subventricular zone, CC: corpus callosum; Cpu: striatum; LV: lateral ventricle, SVZ: subventricular zone.

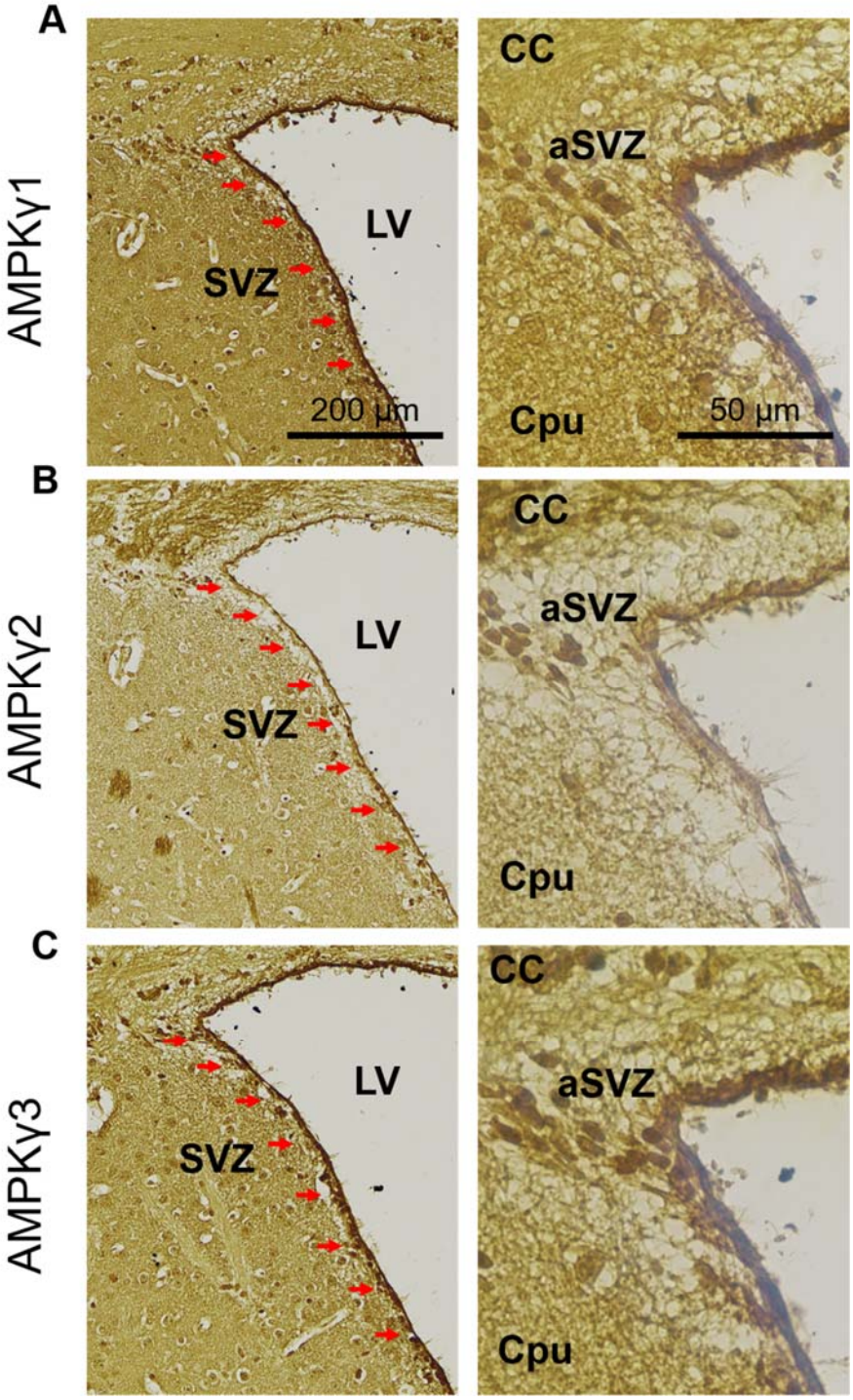

Figure 30. Immunohistochemical analysis of AMPKγ expression in the old subventricular zone. 5 µm coronal sections of 19-month old mouse brains (n = 4) were immunostained for AMPKγ expression. Representative sections show AMPKγ1 (A), AMPKγ2 (B), and AMPKγ3 (C) expressions. aSVZ: anterior subventricular zone, CC: corpus callosum; Cpu: striatum; LV: lateral ventricle, SVZ: subventricular zone.

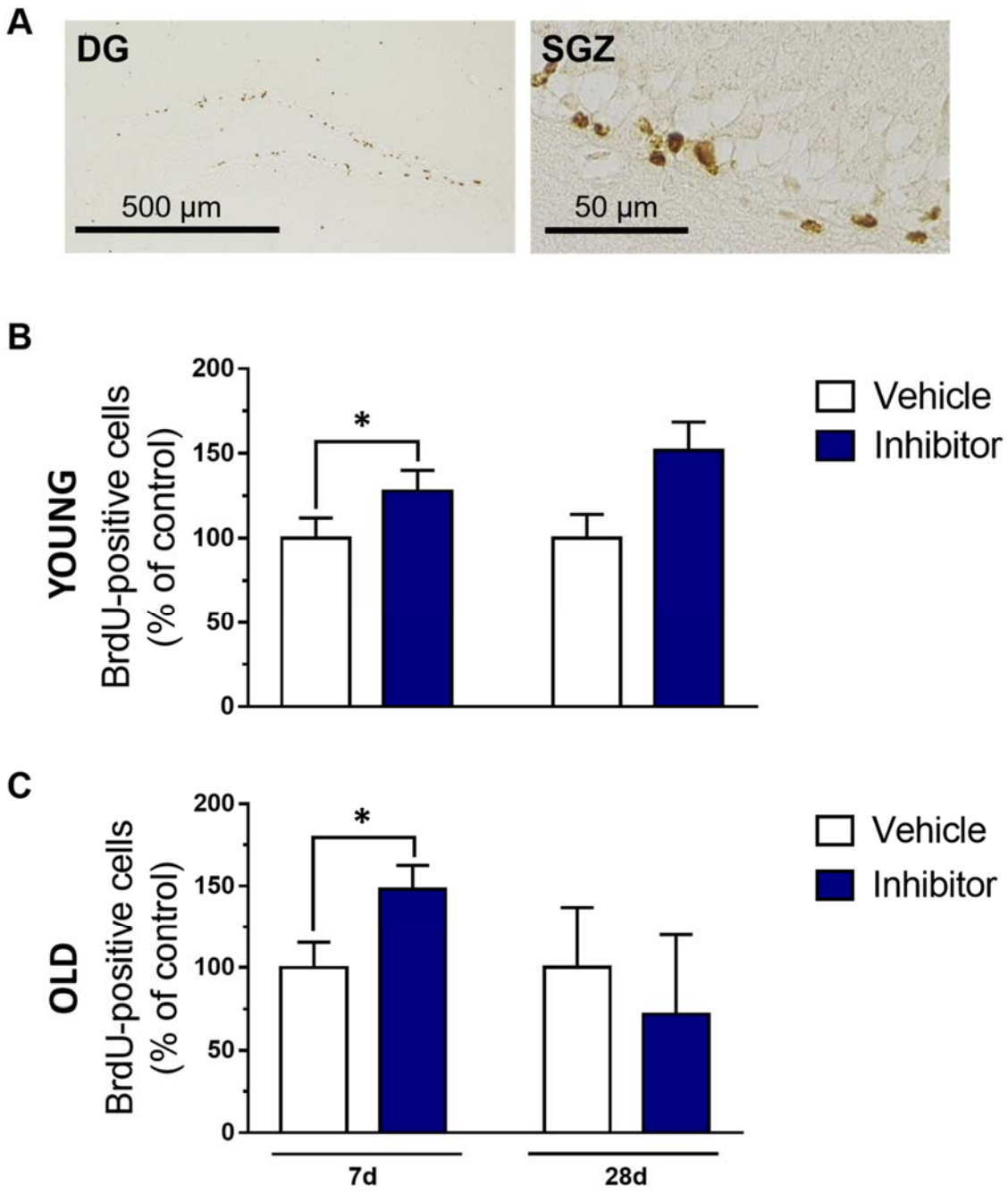

Figure 31. Effects of short- and long-term pharmacological inhibition of AMPK signaling on young-adult and old hippocampal neurogenesis. Young-adult (2 months) and old (19 months) mice were subjected to intraperitoneal administration of vehicle (0.9% saline) or AMPK inhibitor (Compound C, 10 mg/kg/day) for 7 and 28 days. Representative immunostaining with BrdU antibody in the DG and SGZ of young-adult mice (A). Quantification of BrdU-positive cells in the young-adult (B) and old (C) SGZ after 7 and 28 days of treatment. n = 5-6 mice/group/time point, 4-6 sections per animal. *$p < 0.05$.

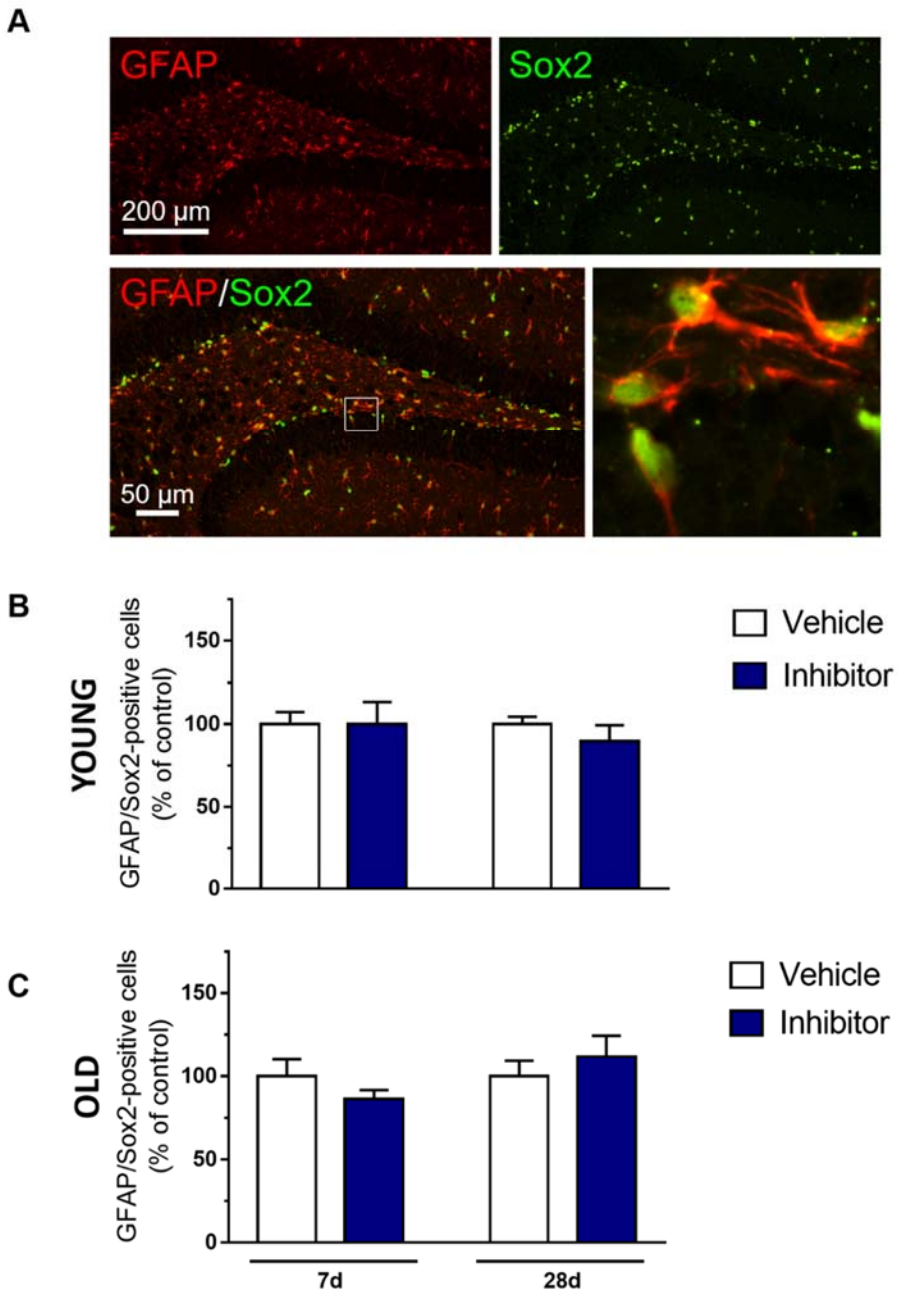

Figure 32. Effects of short- and long-term pharmacological inhibition of AMPK signaling on Type I neural stem cell numbers in the young-adult and old hippocampus. Young-adult (2 months) and old (19 months) mice were subjected to intraperitoneal administration of vehicle (0.9% saline) or AMPK inhibitor (Compound C, 10 mg/kg/day) for 7 and 28 days. Representative immunostaining with GFAP (red) and Sox2 (green) antibodies in the DG and SGZ of young-adult mice (A). High magnification of GFAP/Sox2-positive cells in the DG (Bottom right panel, A). Quantification of GFAP/Sox2-positive cells in the young-adult (B) and old (C) SGZ after 7 and 28 days of treatment. n = 5-6 mice/group/time point, 4-6 sections per animal.

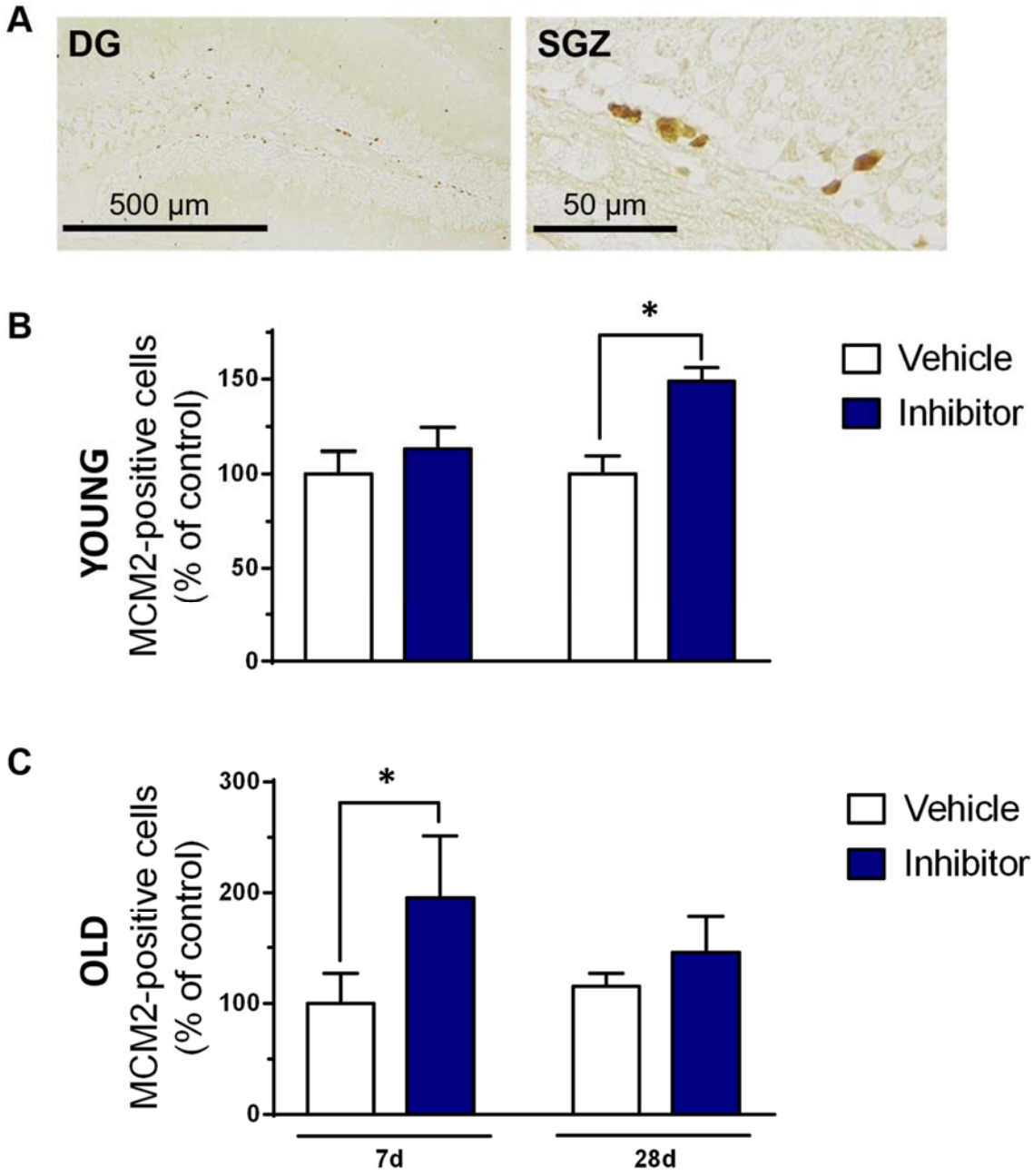

Figure 33. Effects of short- and long-term pharmacological inhibition of AMPK signaling on Type II neural stem cell numbers in the young-adult and old hippocampus. Young-adult (2 months) and old (19 months) mice were subjected to intraperitoneal administration of vehicle (0.9% saline) or AMPK inhibitor (Compound C, 10 mg/kg/day) for 7 and 28 days. Representative immunostaining with MCM2 antibody in the DG and SGZ of young-adult mice (A). Quantification of MCM2-positive cells in the young-adult (B) and old (C) SGZ after 7 and 28 days of treatment. n = 5-6 mice/group/time point, 4-6 sections per animal. *$p < 0.05$.

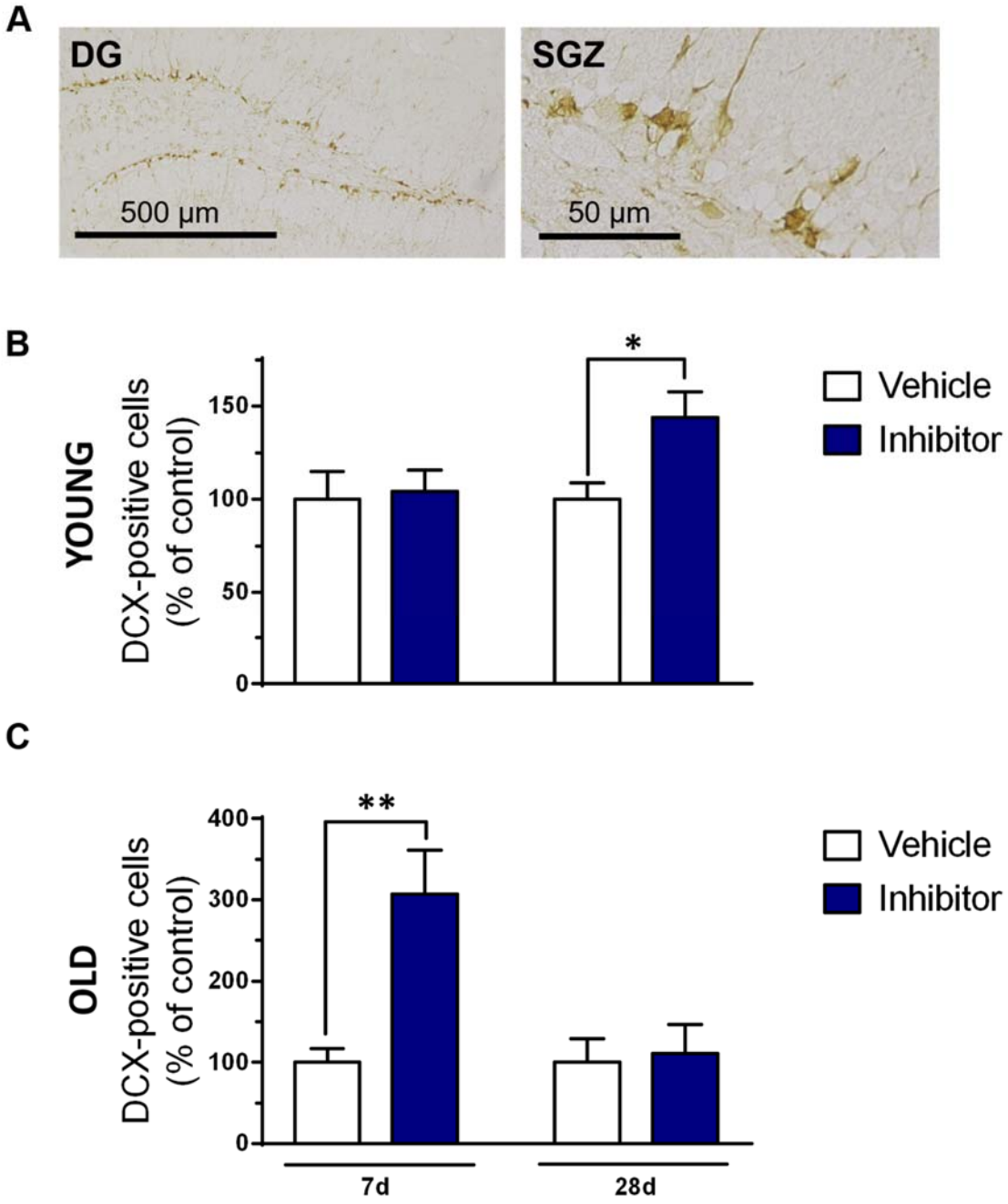

Figure 34. Effects of short- and long-term pharmacological inhibition of AMPK signaling on Type III neural stem cell numbers in the young-adult and old hippocampus. Young-adult (2 months) and old (19 months) mice were subjected to intraperitoneal administration of vehicle (0.9% saline) or AMPK inhibitor (Compound C, 10 mg/kg/day) for 7 and 28 days. Representative immunostaining with DCX antibody in the DG and SGZ of young-adult mice (A). Quantification of DCX-positive cells in the young-adult (B) and old (C) SGZ after 7 and 28 days of treatment. n = 5-6 mice/group/time point, 4-6 sections per animal. *$p < 0.05$.

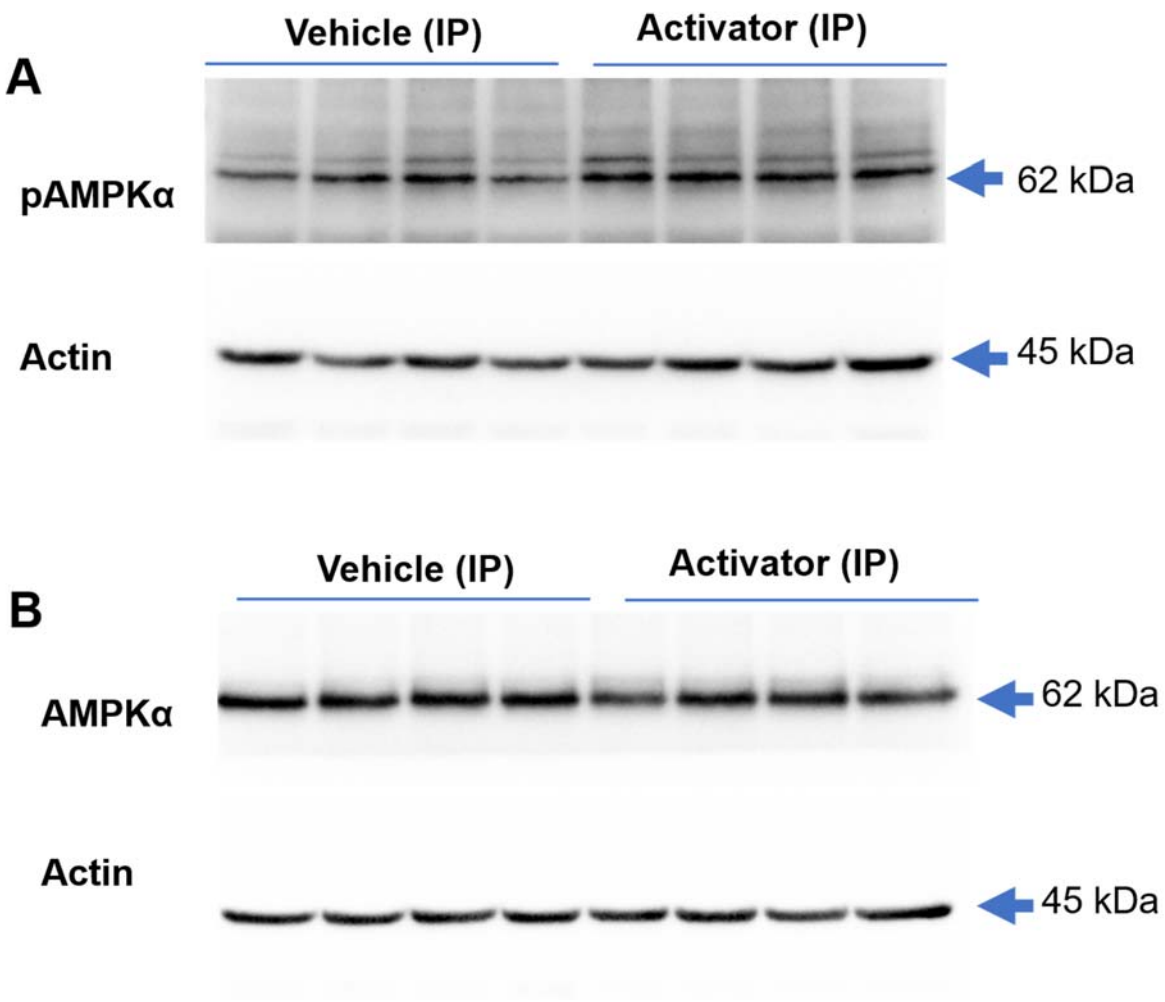

Figure 35. Forced inhibition of AMPK signaling in the young-adult hippocampus via IP administration. Mice were given vehicle (0.9% saline) or AMPK inhibitor (Compound C, 10 mg/kg/day) for 7 days via the IP route. Mice were sacrificed on day 8 and their hippocampi were collected for protein analysis. Protein lysates (30 µg) from the vehicle and inhibitor groups (n = 4 per group) were resolved on 10% SDS-PAGE gels, transferred onto PVDF membranes and probed with the appropriate primary and secondary antibodies. Representative Western blots showing pAMPKα (A) and total AMPKα (B) protein levels. Actin was used as the loading control. IP: intraperitoneal.

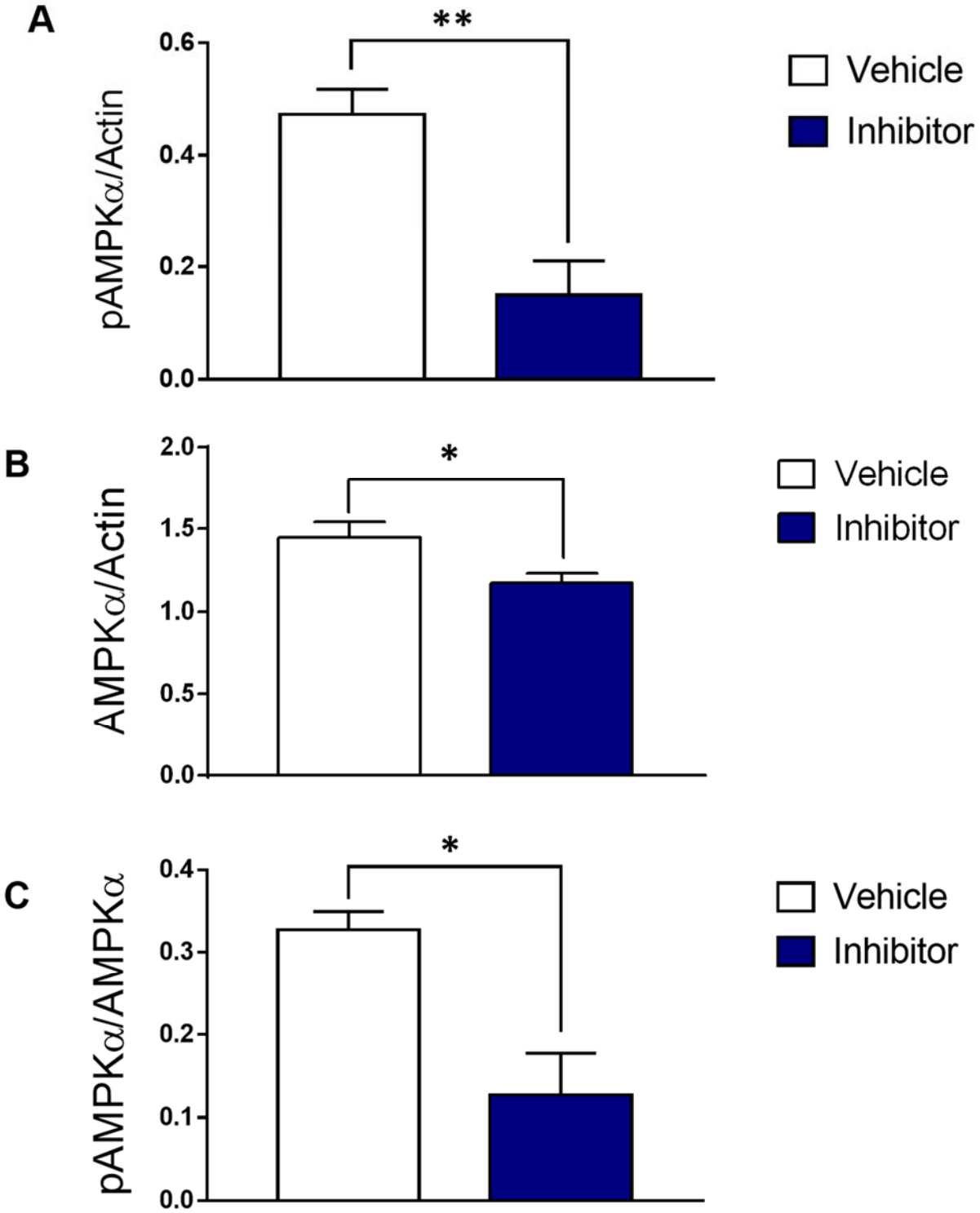

Figure 36. Statistical analysis for forced inhibition of AMPK signaling in the young-adult hippocampus via IP administration. Relative expressions of pAMPKα (A) and total AMPKα (B) after normalizing to Actin. Relative expression of pAMPKα versus total AMPKα content in the hippocampus. *$p < 0.05$, **$p < 0.01$.

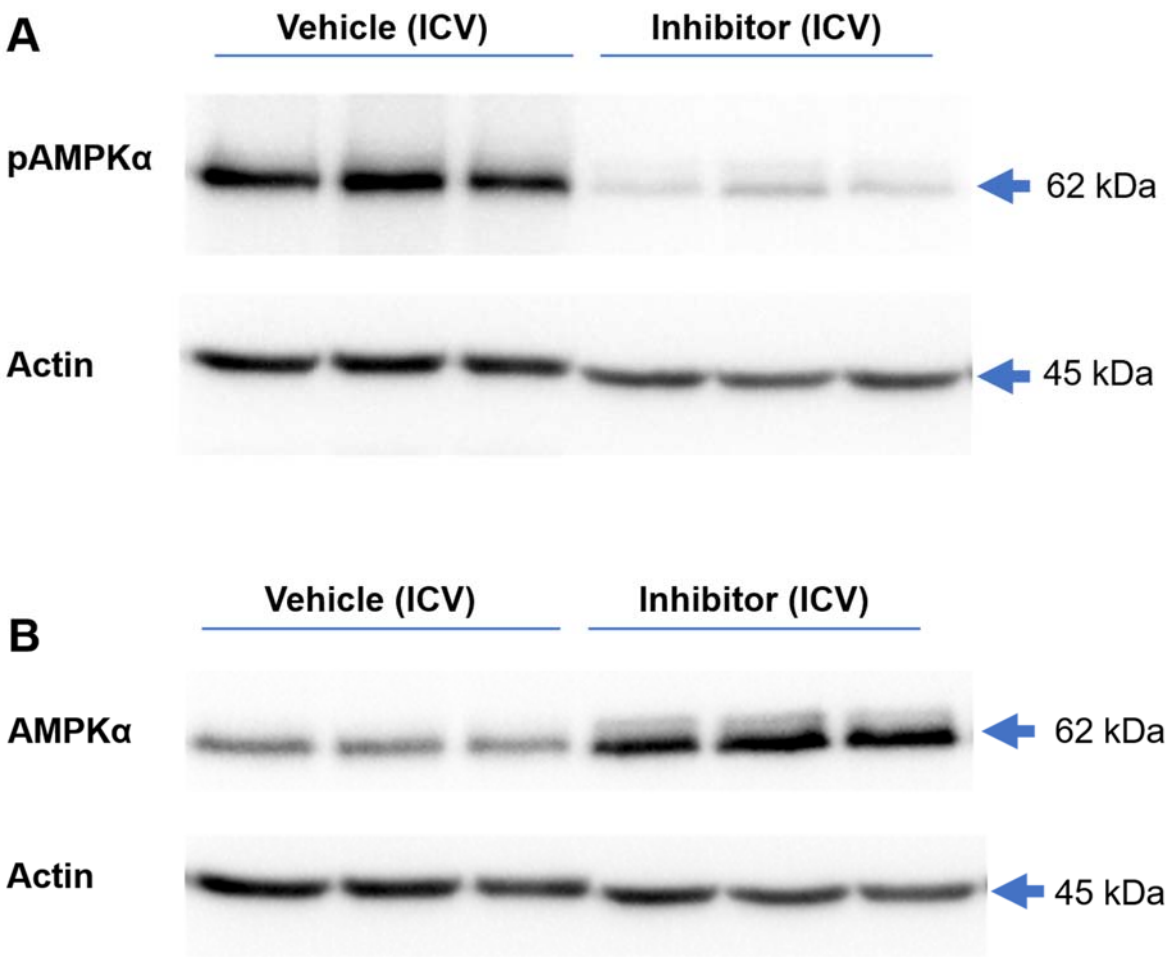

Figure 37. Forced inhibition of AMPK signaling in the young-adult hippocampus via ICV administration. Mice were infused via ICV administration with vehicle (0.9% saline) or AMPK inhibitor (Compound C, 1 μM) for 3 days. They were sacrificed on day 4 and their hippocampi were collected for protein analysis. Protein lysates (30 μg) from the vehicle and inhibitor groups (n = 3 per group) were resolved on 10% SDS-PAGE gels, transferred onto PVDF membranes and probed with the appropriate primary and secondary antibodies. Representative Western blots showing pAMPKα (A) and total AMPKα (B) protein levels. Actin was used as the loading control. ICV: intracerebroventricular.

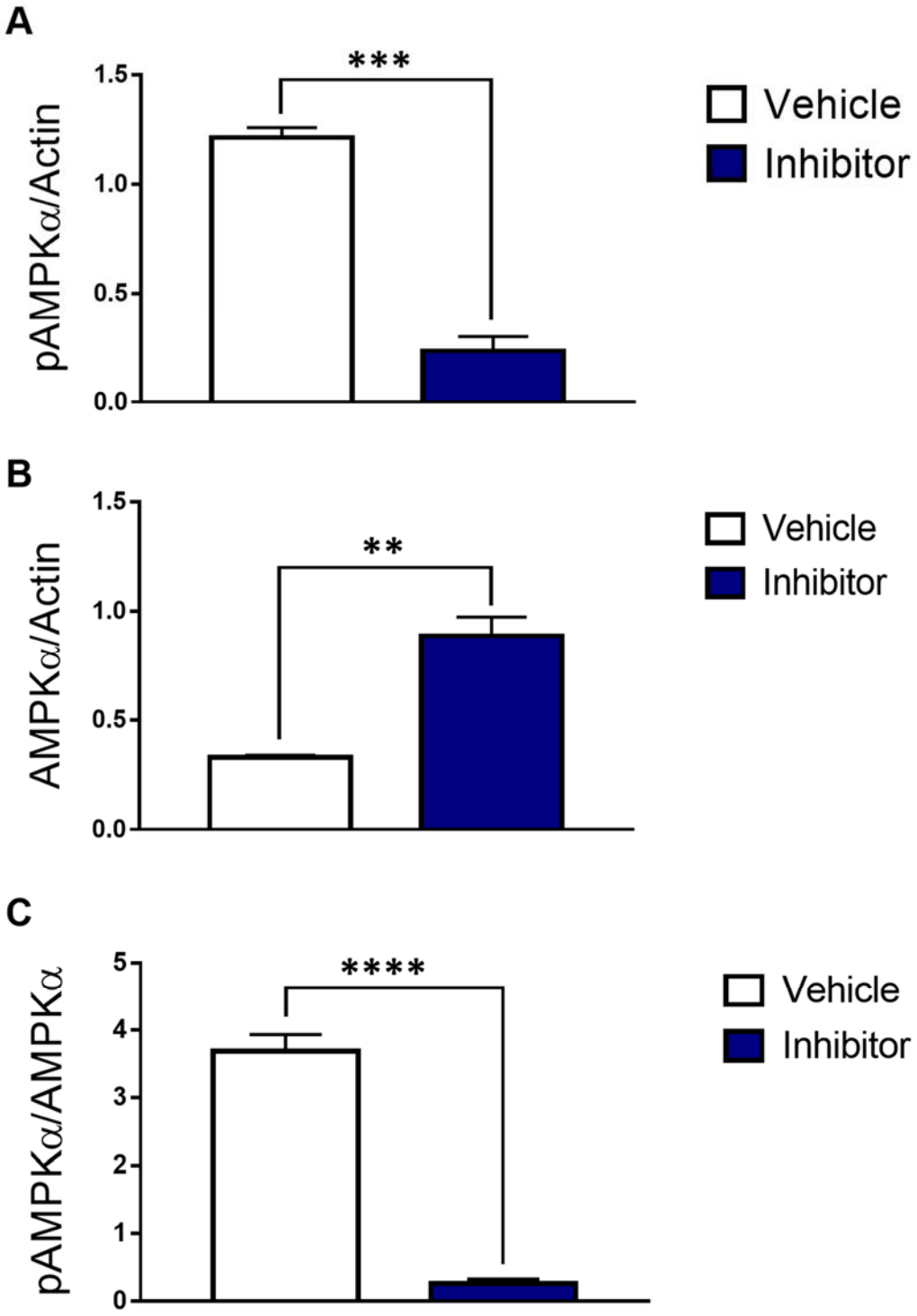

Figure 38. **Statistical analysis for forced inhibition of AMPK signaling in the young-adult hippocampus via ICV administration.** Relative expressions of pAMPKα (A) and total AMPKα (B) after normalizing to Actin. Relative expression of pAMPKα versus total AMPKα content in the hippocampus. $^{**}p < 0.01$, $^{***}p < 0.001$, $^{****}p < 0.0001$. ICV: intracerebroventricular.

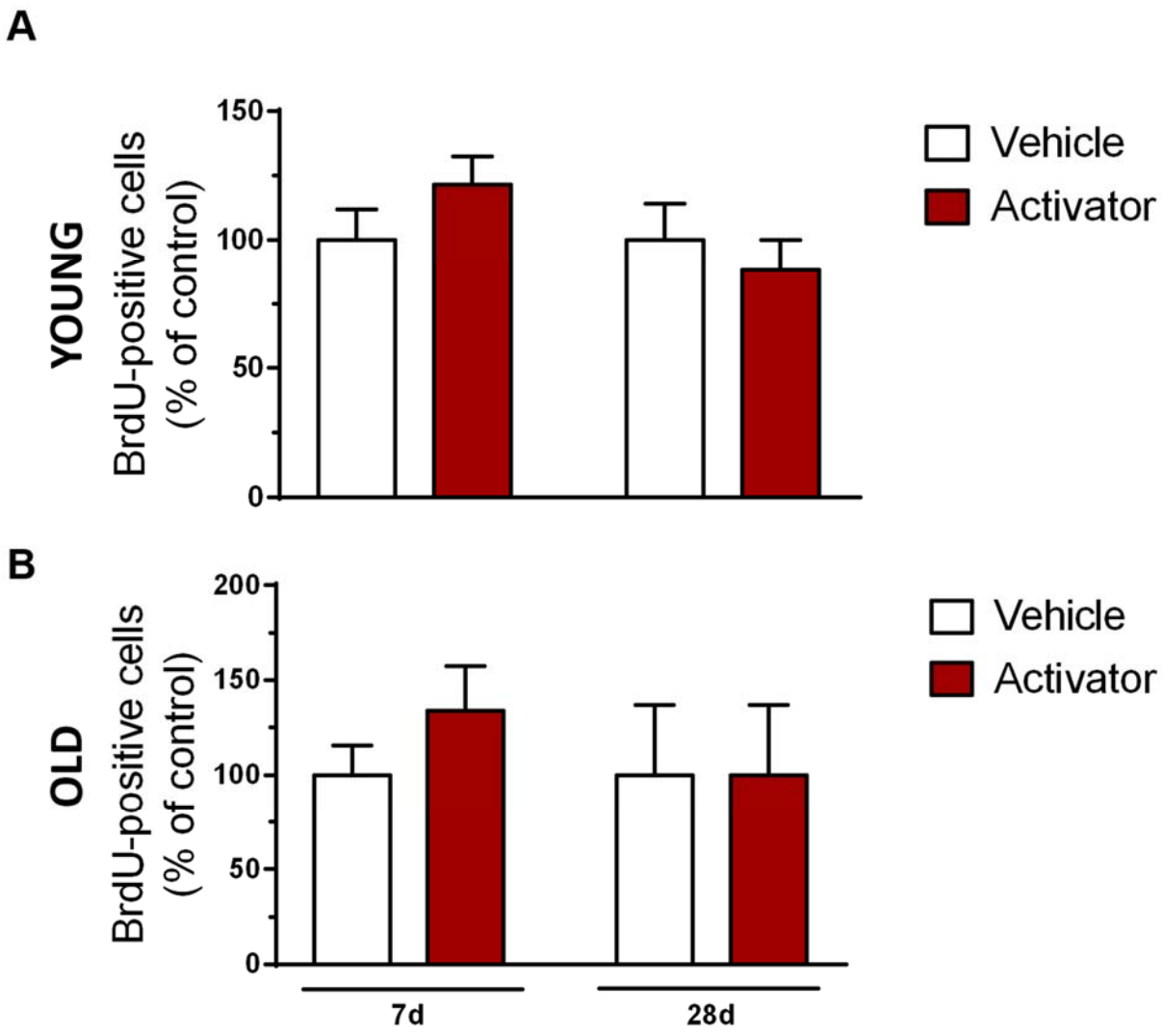

Figure 39. Effects of short- and long-term pharmacological activation of AMPK on young-adult and old hippocampal neurogenesis. Young-adult (2 months) and old (19 months) mice were subjected to intraperitoneal administration of vehicle (0.9% saline) or AMPK activator (AICAR, 500 mg/kg/day) for 7 and 28 days. Quantification of BrdU-positive cells in the young-adult (A) and old (B) SGZ after 7 and 28 days of treatment. n = 5-6 mice/group/time point, 4-6 sections per animal.

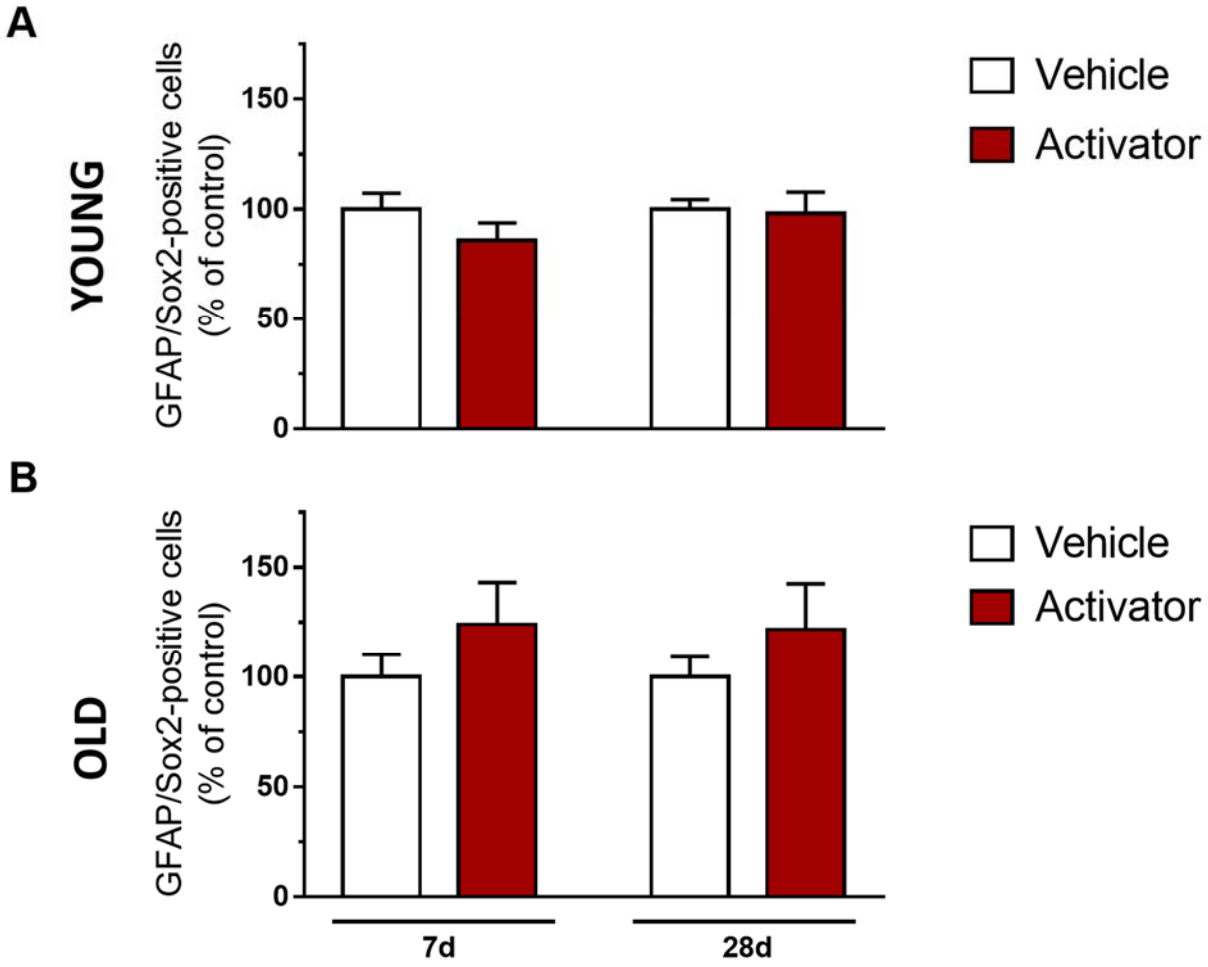

Figure 40. Effects of short- and long-term pharmacological activation of AMPK on Type I neural stem cell numbers in the young-adult and old hippocampus. Young-adult (2 months) and old (19 months) mice were subjected to intraperitoneal administration of vehicle (0.9% saline) or AMPK activator (AICAR, 500 mg/kg/day) for 7 and 28 days. Quantification of GFAP/Sox2-positive cells in the young-adult (A) and old (B) SGZ after 7 and 28 days of treatment. n = 5-6 mice/group/time point, 4-6 sections per animal.

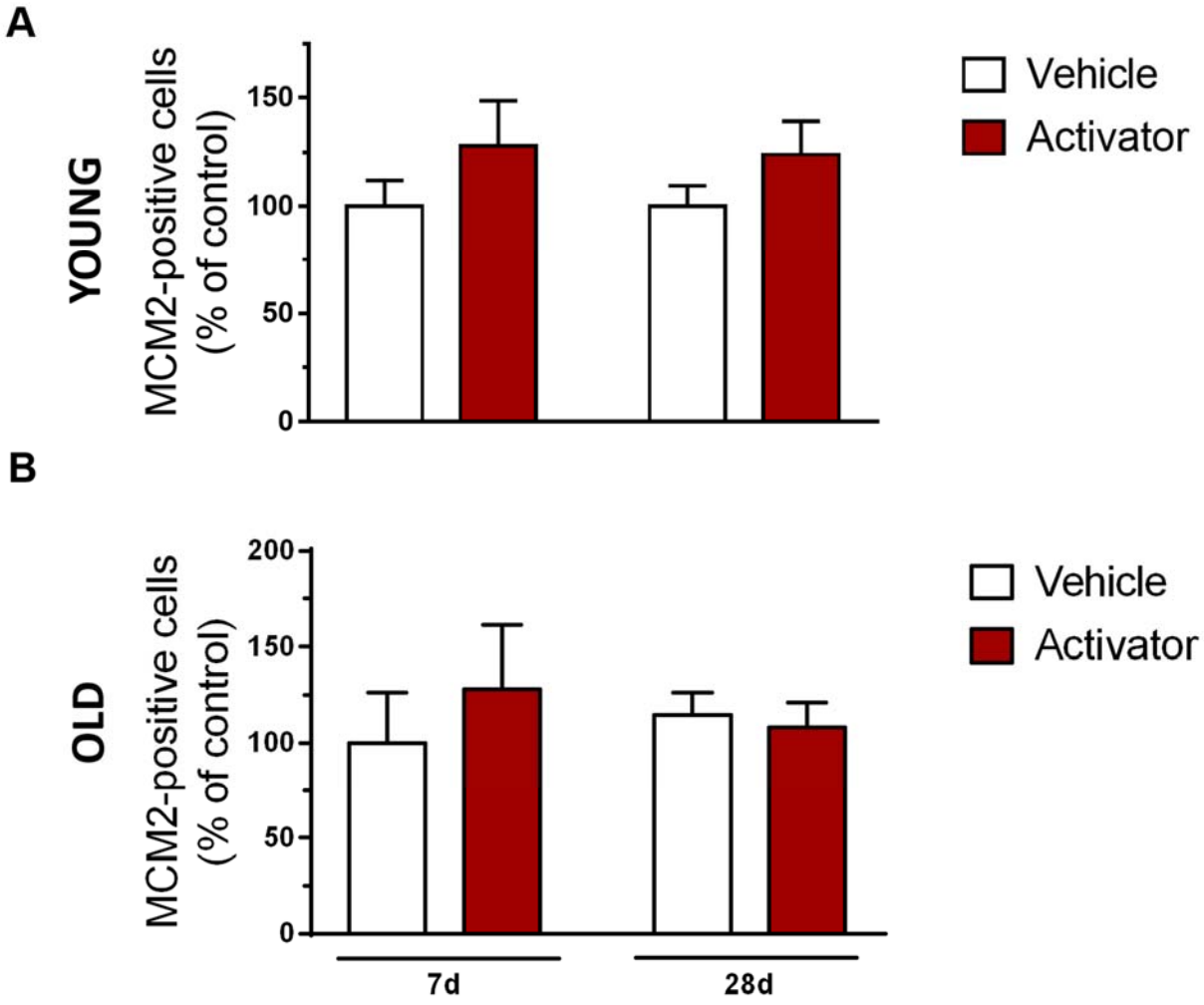

Figure 41. Effects of short- and long-term pharmacological activation of AMPK on Type II neural stem cell numbers in the young-adult and old hippocampus. Young-adult (2 months) and old (19 months) mice were subjected to intraperitoneal administration of vehicle (0.9% saline) or AMPK activator (AICAR, 500 mg/kg/day) for 7 and 28 days. Quantification of MCM2-positive cells in the young-adult (A) and old (B) SGZ after 7 and 28 days of treatment. n = 5-6 mice/group/time point, 4-6 sections per animal.

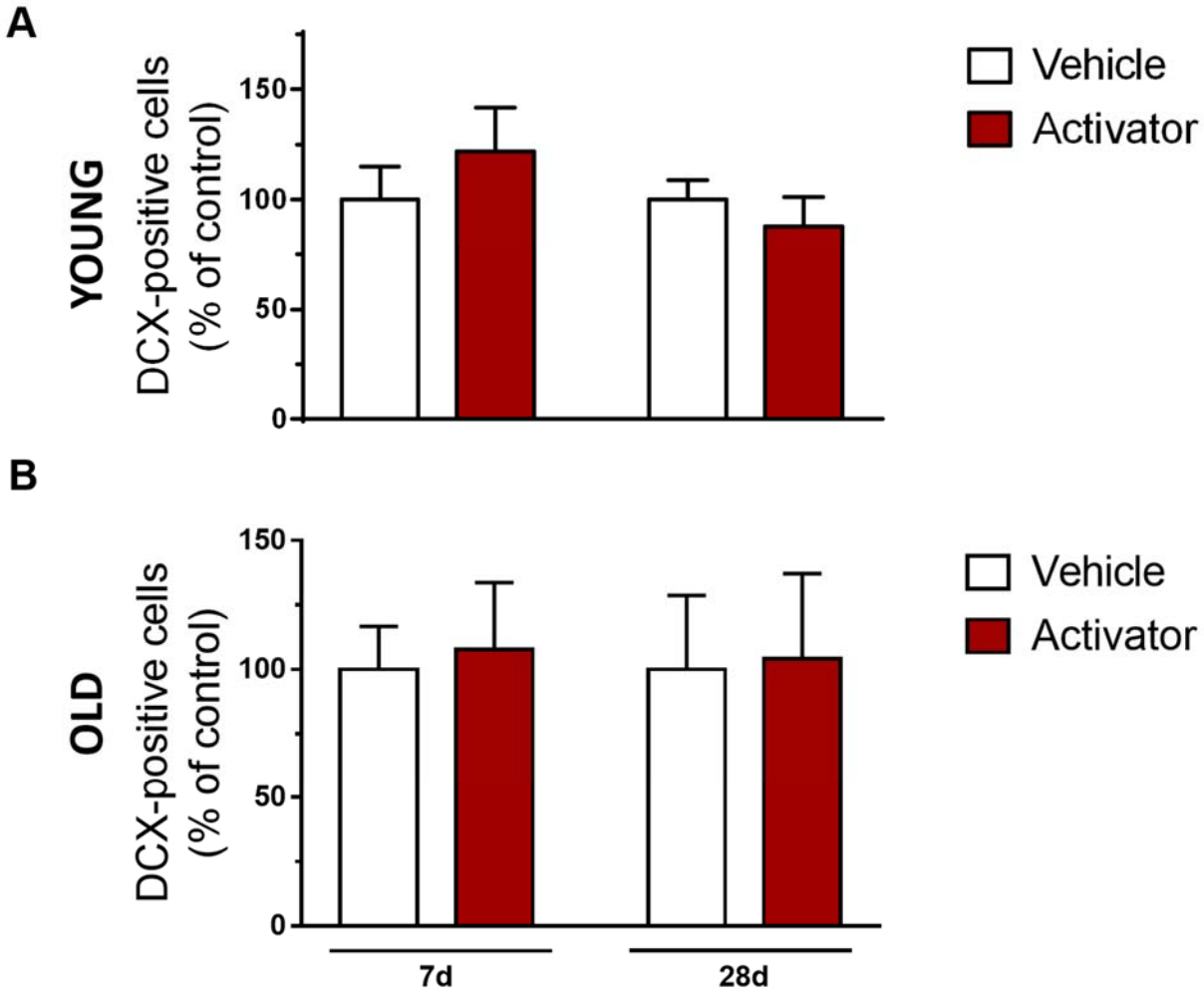

Figure 42. Effects of short- and long-term pharmacological activation of AMPK on Type III neural stem cell numbers in the young-adult and old hippocampus. Young-adult (2 months) and old (19 months) mice were subjected to intraperitoneal administration of vehicle (0.9% saline) or AMPK activator (AICAR, 500 mg/kg/day) for 7 and 28 days. Quantification of DCX-positive cells in the young-adult (A) and old (B) SGZ after 7 and 28 days of treatment. n = 5-6 mice/group/time point, 4-6 sections per animal.

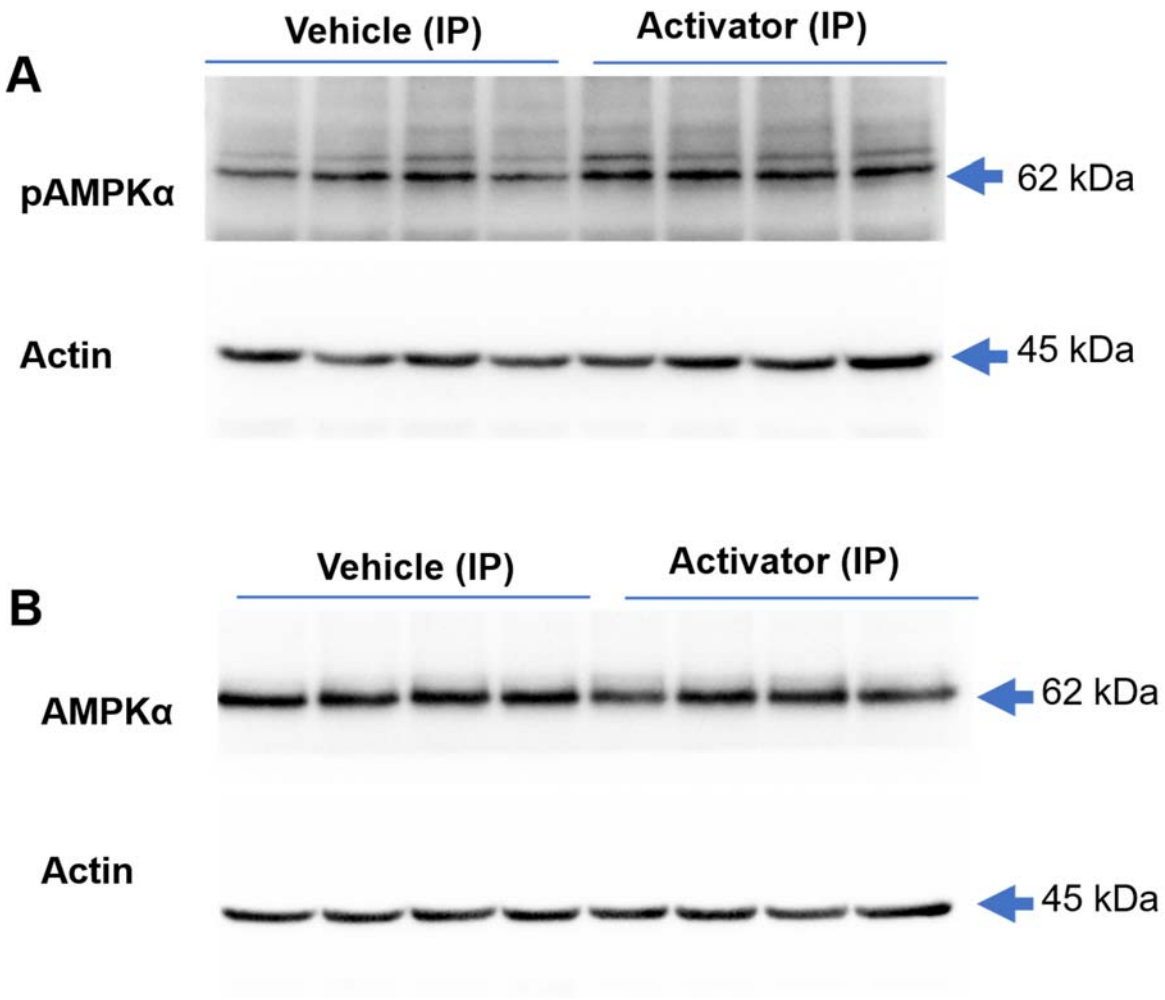

Figure 43. Forced activation of AMPK signaling in the young-adult hippocampus via IP administration. Mice were given vehicle (0.9% saline) or AMPK activator (AICAR, 500 mg/kg/day) for 7 days via the IP route. Mice were sacrificed on day 8 and their hippocampi were collected for protein analysis. Protein lysates (30 µg) from the vehicle and inhibitor groups (n = 4 per group) were resolved on 10% SDS-PAGE gels, transferred onto PVDF membranes and probed with the appropriate primary and secondary antibodies. Representative Western blots showing pAMPKα (A) and total AMPKα (B) protein levels. Actin was used as the loading control. IP: intraperitoneal.

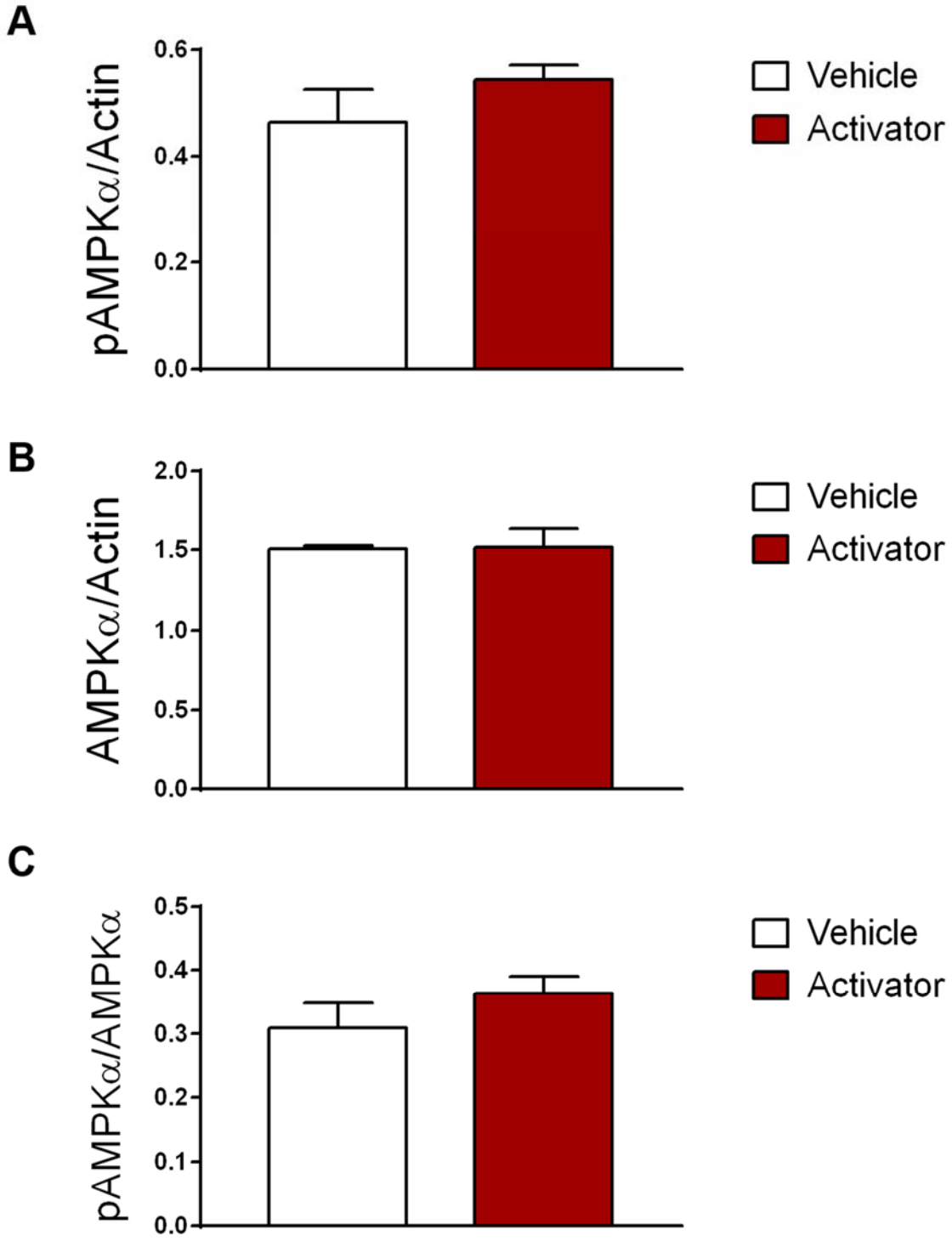

Figure 44. Statistical analysis for forced activation of AMPK signaling in the young-adult hippocampus via IP administration. Relative expressions of pAMPKα (A) and total AMPKα (B) after normalizing to Actin. Relative expression of pAMPKα versus total AMPKα content in the hippocampus. IP: intraperitoneal.

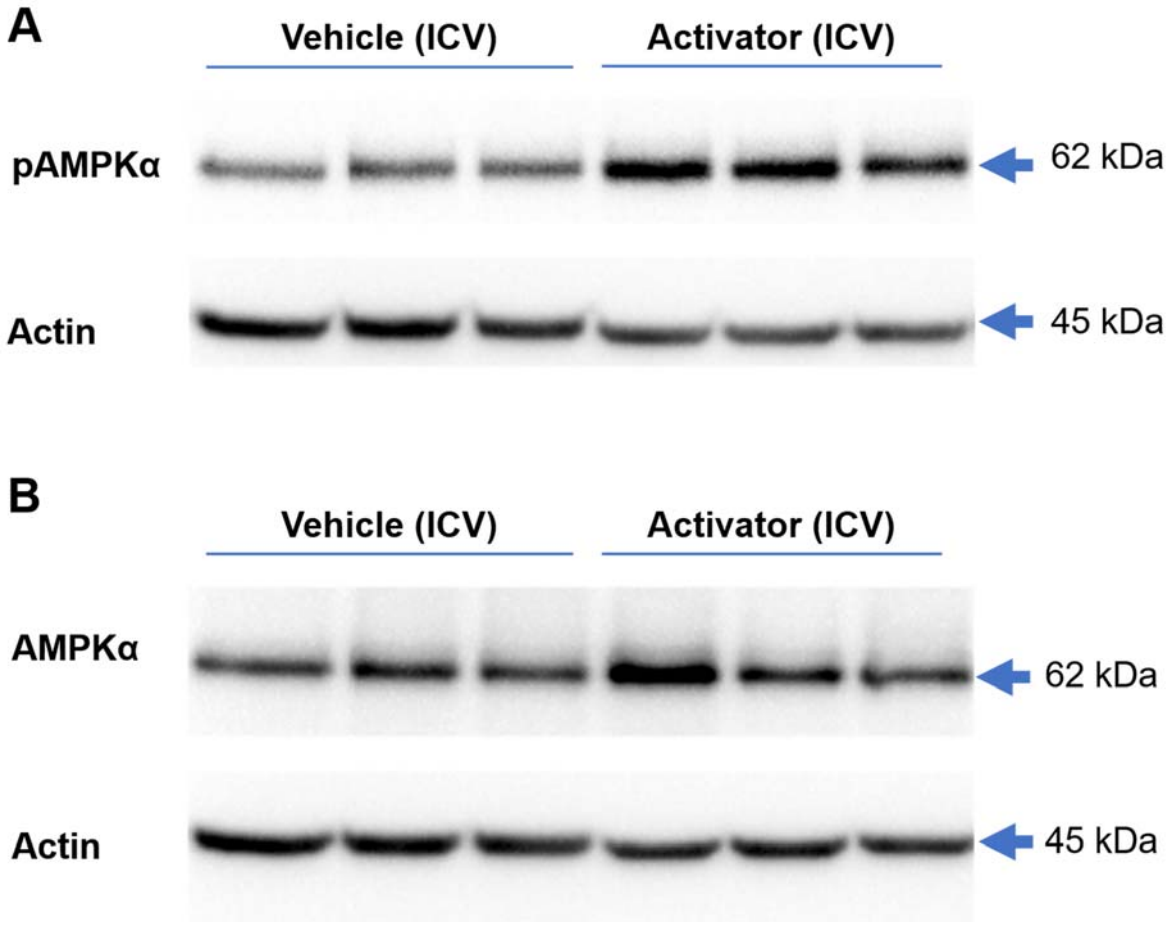

Figure 45. Forced activation of AMPK signaling in the young-adult hippocampus via ICV administration. Mice were infused via ICV administration with vehicle (0.9% saline) or AMPK activator (AICAR, 4 mM) for 3 days. Mice were sacrificed on day 4 and their hippocampi were collected for protein analysis. Protein lysates (30 µg) from the vehicle and activator groups (n = 3 per group) were resolved on 10% SDS-PAGE gels, transferred onto PVDF membranes and probed with the appropriate primary and secondary antibodies. Representative Western blots showing pAMPKα (A) and total AMPKα (B) protein levels. Actin was used as the loading control. ICV: intracerebroventricular.

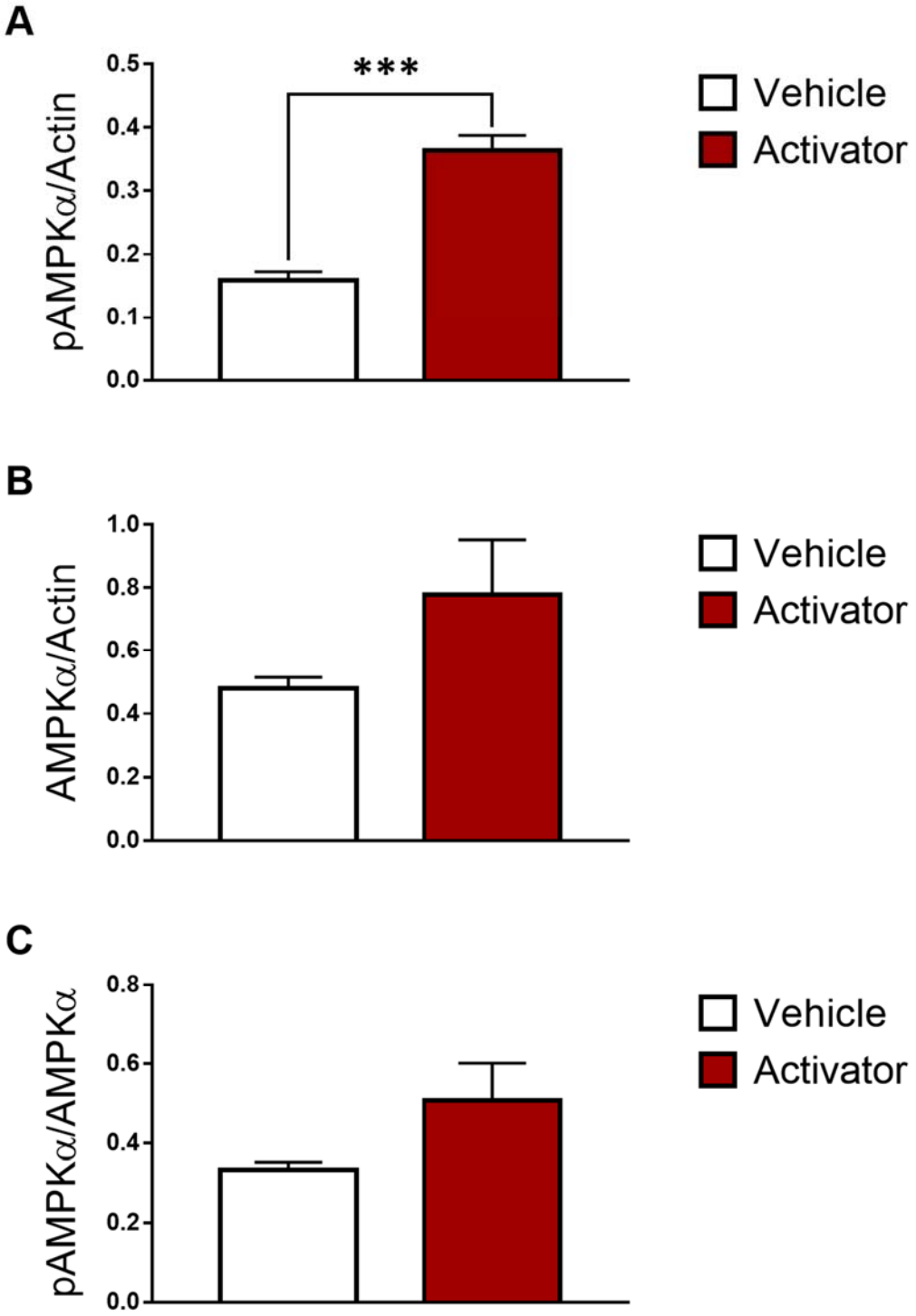

Figure 46. Statistical analysis for forced activation of AMPK signaling in the young-adult hippocampus via ICV administration. Relative expressions of pAMPKα (A) and total AMPKα (B) after normalizing to Actin. Relative expression of pAMPKα versus total AMPKα content in the hippocampus. ***$p < 0.001$. ICV: intracerebroventricular.

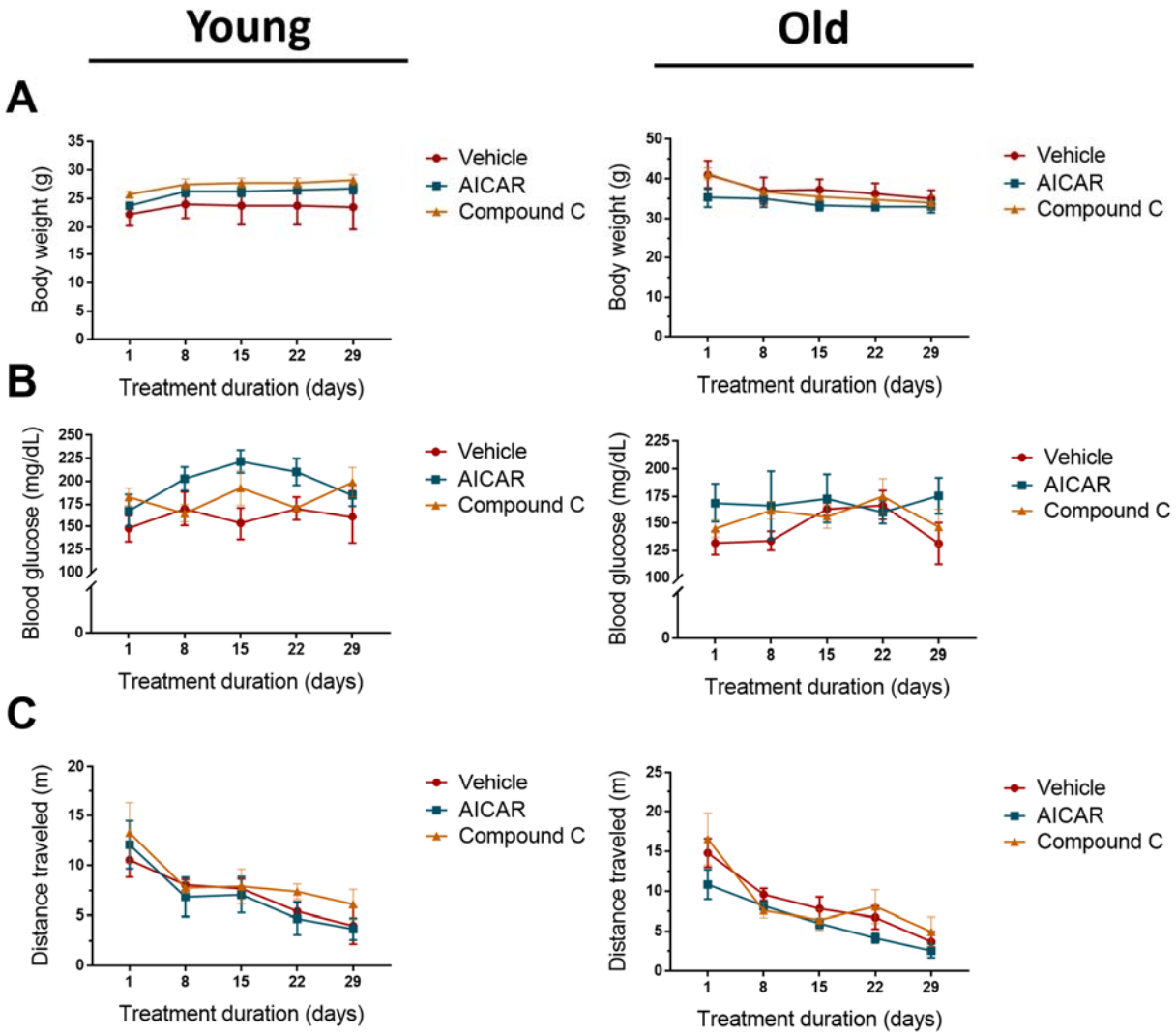

Figure 47. Effects of short- and long-term forced inhibition and activation of AMPK signaling on vital signs. Young-adult (2 months) and old (19 months) mice were subjected to intraperitoneal administration of vehicle (0.9% saline), AMPK activator (AICAR, 500 mg/kg/day) or inhibitor (Compound C, 10 mg/kg/day) for 28 days. Measurements for body weight (A), blood glucose level (B), and spontaneous locomotor activity (C) were taken every week at 9 am. n = 4 mice per group.

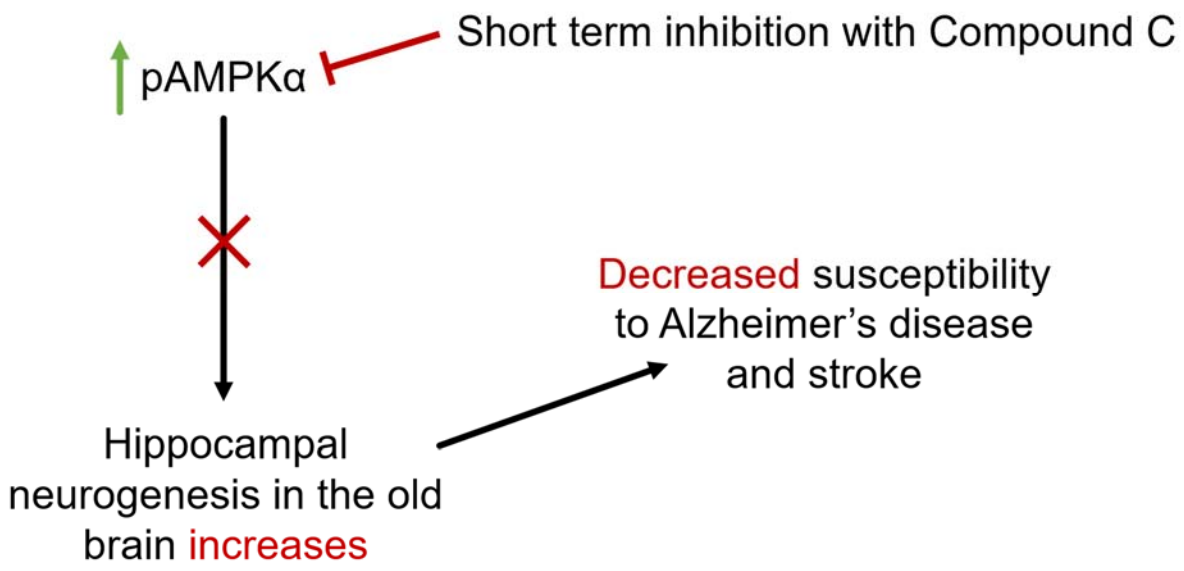

Figure 48. Working model of the short-term inhibition of AMPK signaling. Our study showed that short-term inhibition of AMPK signaling with Compound C was able to increase hippocampal neurogenesis, which could lead to decreased susceptibility to neurological diseases such as Alzheimer's disease and stroke. In other words, the increase in AMPK signaling with age is a key step in the regulation of downstream processes, leading to the age-related decline of neurogenesis. Future studies will focus on elucidating the signaling cascade responsible for decreasing neurogenesis in the old brain.

AICAR					
Purpose of study	**Animal used**	**Dose**	**Frequency**	**Duration before sacrifice**	**Ref**
Measuring tumor growth	Adult male Wistar rats weighing 200–250 g	100 mg/kg/day	Once daily	10 days	(*114*)
Measuring tumor growth	SCID mice	400 mg/kg/day	Once daily	3 days	(*115*)
Hippocampal neurogenesis	2-mo-old female C57BL/6J mice	500 mg/kg/day	Once daily	7 or 14 days	(*103*)
Hippocampal neurogenesis	5- to 7-wk-old and 23-mo-old female C57BL/6J mice	500 mg/kg/day	Once daily for 3, 7 or 14 days	26 or 33 days after the last saline or AICAR injection	(*102*)

Table 1. Compilation of studies that administered AICAR via the intraperitoneal route.

Compound C					
Purpose of study	**Animal used**	**Dose**	**Frequency**	**Duration before sacrifice**	**Ref**
Neuroprotection after focal ischemic stroke	Male C57BL/6 mice	20 mg/kg	1 x	4 h (2h MCAO + 2 h or 22 h reperfusion)	(*78*)
Neuroprotection after focal ischemic stroke	Male AMPK a1 and AMPK a2 knockout mice	20 mg/kg	1 x	24 h, 72 h	(*79*)
Neuroprotection after focal ischemic stroke	Female wild type mice and AMPK a2 KO mice (ovariectomized)	10 mg/kg	1 x	24 h	(*116*)
Neuroprotection after focal ischemic stroke	Wild-type male mice and AMPKa2-knockout (KO) mice	10 mg/kg	1 x	24 h	(*117*)
Age-related changes of AMPK's neuroprotection after focal ischemic stroke	9- to12-wk-old and 16- to 18-mo-old C57BL/6 mice	10 mg/kg	1 x	4 h, 24 h	(*54*)
Neuroprotection after ischemic preconditioning and focal ischemic stroke	Male C57BL/6 mice	10 mg/kg	1 x	24 h	(*118*)
Inflammation study	Male BALB/c mice	25 mg/kg	1 x	6 h	(*119*)

Table 2. Compilation of studies that administered Compound C via the intraperitoneal route.

Primary Antibody	Host	Clonality	Dilution	Catalog No.	Company
AMPKα1	Rabbit	Polyclonal	1:200	ab3759	Abcam
AMPKα2	Rabbit	Polyclonal	1:200	ab3760	Abcam
AMPKβ1	Rabbit	Polyclonal	1:100	orb37351	Biorbyt
AMPKβ2	Rabbit	Polyclonal	1:100	orb381985	Biorbyt
AMPKγ1	Rabbit	Polyclonal	1:50	orb247883	Biorbyt
AMPKγ2	Rabbit	Polyclonal	1:50	orb304519	Biorbyt
AMPKγ3	Rabbit	Polyclonal	1:50	orb37357	Biorbyt
Phospho-AMPKα (Thr 172)	Rabbit	Polyclonal	1:200	sc-33524	Santa Cruz
BrdU	Rat	Monoclonal	1:500	ab6326	Abcam
GFAP	Mouse	Monoclonal	1:500	3670	Cell Signaling
Sox2	Goat	Polyclonal	1:200	AF2018	R&D Systems
MCM2	Rabbit	Monoclonal	1:200	3619	Cell Signaling
Doublecortin	Goat	Polyclonal	1:200	sc-8066	Santa Cruz

Table 3. Primary antibodies used for immunostaining.

Secondary Antibody	Host	Dilution	Catalog No.	Company
Biotinylated anti-rabbit IgG	Horse	1:200	BA-1100	Vector
Biotinylated anti-goat IgG	Horse	1:200	BA-9500	Vector
Anti-goat IgG AF 488	Donkey	1:500	A-11055	Invitrogen
Anti-rabbit IgG AF 488	Donkey	1:500	R37118	Invitrogen
Anti-mouse IgG AF 594	Donkey	1:500	R37115	Invitrogen
Anti-rabbit IgG AF 647	Rabbit	1:50	A-31573	Invitrogen

Table 4. Secondary antibodies used for immunostaining.

	Subgranular zone		Subventricular zone	
AMPK isoforms	Subcellular location	Expression level in old *vs.* young	Subcellular location	Expression level in old *vs.* young
α1	Cytoplasm	↓	Cytoplasm	↓
α2	Nucleus	↓	Nucleus	↓
β1	Nucleus	↓	Nucleus	↓
β2	Cytoplasm	↓	Nucleus#	↑#
γ1	Cytoplasm	↓	Nucleus#	↑#
γ2	Cytoplasm	↓	Nucleus#	↑#
γ3	Cytoplasm	↓	Nucleus#	↑#
Phospho-α	Nucleus	↑	Nucleus	↑#

Table 5. Summary of expression pattern of AMPK subunit isoforms and activation in the SGZ and SVZ of young and old brains. # indicates different expression pattern compared with the SGZ. Green arrow indicates higher expression level. Red arrow indicates lower expression level. SGZ: subgranular zone; SVZ: subventricular zone.

	Young		Old	
Cell type	7 days	28 days	7 days	28 days
BrdU⁺	↑	⇄	↑	⇄
I	⇄	⇄	⇄	⇄
II	⇄	↑	↑	⇄
III	⇄	↑	↑	⇄

Table 6. Summary of the effects of short- and long-term inhibition of AMPK signaling on hippocampal neurogenesis in the young and old brains. Green arrow indicates significant increase. Blue arrows indicate no significant change. Type I cell: Neural stem cell; Type II cell: Neural progenitor cell; Type III cell: Immature neuron.

REFERENCES

1. C. Gemma, J. Vila, A. Bachstetter, P. C. Bickford, in *Brain Aging: Models, Methods, and Mechanisms,* D. R. Riddle, Ed. (Boca Raton (FL), 2007).
2. K. Jin, J. W. Simpkins, X. Ji, M. Leis, I. Stambler, The Critical Need to Promote Research of Aging and Aging-related Diseases to Improve Health and Longevity of the Elderly Population. *Aging and disease* **6**, 1-5 (2015).
3. E. J. Benjamin *et al.*, Heart Disease and Stroke Statistics-2018 Update: A Report From the American Heart Association. *Circulation* **137**, e67-e492 (2018).
4. J. Altman, Autoradiographic and histological studies of postnatal neurogenesis. IV. Cell proliferation and migration in the anterior forebrain, with special reference to persisting neurogenesis in the olfactory bulb. *The Journal of comparative neurology* **137**, 433-457 (1969).
5. J. Altman, G. D. Das, Autoradiographic and histological evidence of postnatal hippocampal neurogenesis in rats. *The Journal of comparative neurology* **124**, 319-335 (1965).
6. Y. Mu, F. H. Gage, Adult hippocampal neurogenesis and its role in Alzheimer's disease. *Molecular neurodegeneration* **6**, 85 (2011).
7. L. R. Zhao, A. Willing, Enhancing endogenous capacity to repair a stroke-damaged brain: An evolving field for stroke research. *Prog Neurobiol*, (2018).
8. Y. Wang, X. Ji, R. K. Leak, F. Chen, G. Cao, Stem cell therapies in age-related neurodegenerative diseases and stroke. *Ageing research reviews* **34**, 39-50 (2017).

9. S. D. Kuipers, J. E. Schroeder, A. Trentani, Changes in hippocampal neurogenesis throughout early development. *Neurobiology of aging* **36**, 365-379 (2015).

10. R. Wang, K. T. Dineley, J. D. Sweatt, H. Zheng, Presenilin 1 familial Alzheimer's disease mutation leads to defective associative learning and impaired adult neurogenesis. *Neuroscience* **126**, 305-312 (2004).

11. M. Demars, Y. S. Hu, A. Gadadhar, O. Lazarov, Impaired neurogenesis is an early event in the etiology of familial Alzheimer's disease in transgenic mice. *Journal of neuroscience research* **88**, 2103-2117 (2010).

12. X. Wang *et al.*, Conditional depletion of neurogenesis inhibits long-term recovery after experimental stroke in mice. *PloS one* **7**, e38932 (2012).

13. H. G. Kuhn, H. Dickinson-Anson, F. H. Gage, Neurogenesis in the dentate gyrus of the adult rat: age-related decrease of neuronal progenitor proliferation. *J Neurosci* **16**, 2027-2033 (1996).

14. L. B. Ngwenya, N. C. Heyworth, Y. Shwe, T. L. Moore, D. L. Rosene, Age-related changes in dentate gyrus cell numbers, neurogenesis, and associations with cognitive impairments in the rhesus monkey. *Front Syst Neurosci* **9**, 102 (2015).

15. V. Tropepe, C. G. Craig, C. M. Morshead, D. van der Kooy, Transforming growth factor-alpha null and senescent mice show decreased neural progenitor cell proliferation in the forebrain subependyma. *J Neurosci* **17**, 7850-7859 (1997).

16. E. Enwere *et al.*, Aging results in reduced epidermal growth factor receptor signaling, diminished olfactory neurogenesis, and deficits in fine olfactory discrimination. *J Neurosci* **24**, 8354-8365 (2004).

17. A. Arslan-Ergul, A. T. Ozdemir, M. M. Adams, Aging, neurogenesis, and caloric restriction in different model organisms. *Aging and disease* **4**, 221-232 (2013).

18. H. Ahlenius, V. Visan, M. Kokaia, O. Lindvall, Z. Kokaia, Neural stem and progenitor cells retain their potential for proliferation and differentiation into functional neurons despite lower number in aged brain. *J Neurosci* **29**, 4408-4419 (2009).

19. H. Tang *et al.*, Effect of neural precursor proliferation level on neurogenesis in rat brain during aging and after focal ischemia. *Neurobiology of aging* **30**, 299-308 (2009).

20. N. Shyh-Chang, G. Q. Daley, L. C. Cantley, Stem cell metabolism in tissue development and aging. *Development* **140**, 2535-2547 (2013).

21. N. Shyh-Chang, H. H. Ng, The metabolic programming of stem cells. *Genes Dev* **31**, 336-346 (2017).

22. M. H. Maurer, R. E. Feldmann, Jr., H. F. Burgers, W. Kuschinsky, Protein expression differs between neural progenitor cells from the adult rat brain subventricular zone and olfactory bulb. *BMC Neurosci* **9**, 7 (2008).

23. M. H. Maurer, R. E. Feldmann, Jr., C. D. Futterer, J. Butlin, W. Kuschinsky, Comprehensive proteome expression profiling of undifferentiated versus differentiated neural stem cells from adult rat hippocampus. *Neurochemical research* **29**, 1129-1144 (2004).

24. D. G. Hardie, F. A. Ross, S. A. Hawley, AMPK: a nutrient and energy sensor that maintains energy homeostasis. *Nature reviews. Molecular cell biology* **13**, 251-262 (2012).

25. M. M. Mihaylova, R. J. Shaw, The AMPK signalling pathway coordinates cell growth, autophagy and metabolism. *Nature cell biology* **13**, 1016-1023 (2011).

26. G. R. Steinberg, B. E. Kemp, AMPK in Health and Disease. *Physiol Rev* **89**, 1025-1078 (2009).

27. D. Stapleton *et al.*, Mammalian AMP-activated protein kinase subfamily. *The Journal of biological chemistry* **271**, 611-614 (1996).

28. A. J. Verhoeven *et al.*, The AMP-activated protein kinase gene is highly expressed in rat skeletal muscle. Alternative splicing and tissue distribution of the mRNA. *Eur J Biochem* **228**, 236-243 (1995).

29. C. S. Choi *et al.*, Suppression of diacylglycerol acyltransferase-2 (DGAT2), but not DGAT1, with antisense oligonucleotides reverses diet-induced hepatic steatosis and insulin resistance. *The Journal of biological chemistry* **282**, 22678-22688 (2007).

30. C. Thornton, M. A. Snowden, D. Carling, Identification of a novel AMP-activated protein kinase beta subunit isoform that is highly expressed in skeletal muscle. *The Journal of biological chemistry* **273**, 12443-12450 (1998).

31. M. Mahlapuu *et al.*, Expression profiling of the gamma-subunit isoforms of AMP-activated protein kinase suggests a major role for gamma3 in white skeletal muscle. *American journal of physiology. Endocrinology and metabolism* **286**, E194-200 (2004).

32. P. C. Cheung, I. P. Salt, S. P. Davies, D. G. Hardie, D. Carling, Characterization of AMP-activated protein kinase gamma-subunit isoforms and their role in AMP binding. *Biochem J* **346 Pt 3**, 659-669 (2000).

33. S. A. Hawley *et al.*, Complexes between the LKB1 tumor suppressor, STRAD alpha/beta and MO25 alpha/beta are upstream kinases in the AMP-activated protein kinase cascade. *J Biol* **2**, 28 (2003).

34. R. J. Shaw *et al.*, The tumor suppressor LKB1 kinase directly activates AMP-activated kinase and regulates apoptosis in response to energy stress. *Proc Natl Acad Sci U S A* **101**, 3329-3335 (2004).

35. A. Woods *et al.*, Ca2+/calmodulin-dependent protein kinase kinase-beta acts upstream of AMP-activated protein kinase in mammalian cells. *Cell metabolism* **2**, 21-33 (2005).

36. S. A. Hawley *et al.*, 5'-AMP activates the AMP-activated protein kinase cascade, and Ca2+/calmodulin activates the calmodulin-dependent protein kinase I cascade, via three independent mechanisms. *The Journal of biological chemistry* **270**, 27186-27191 (1995).

37. M. Xie *et al.*, A pivotal role for endogenous TGF-beta-activated kinase-1 in the LKB1/AMP-activated protein kinase energy-sensor pathway. *Proc Natl Acad Sci U S A* **103**, 17378-17383 (2006).

38. M. Momcilovic, S. P. Hong, M. Carlson, Mammalian TAK1 activates Snf1 protein kinase in yeast and phosphorylates AMP-activated protein kinase in vitro. *The Journal of biological chemistry* **281**, 25336-25343 (2006).

39. S. A. Hawley *et al.*, Characterization of the AMP-activated protein kinase kinase from rat liver and identification of threonine 172 as the major site at which it phosphorylates AMP-activated protein kinase. *The Journal of biological chemistry* **271**, 27879-27887 (1996).

40. J. Adams *et al.*, Intrasteric control of AMPK via the gamma1 subunit AMP allosteric regulatory site. *Protein Sci* **13**, 155-165 (2004).

41. D. G. Hardie, AMPK--sensing energy while talking to other signaling pathways. *Cell metabolism* **20**, 939-952 (2014).

42. A. Salminen, K. Kaarniranta, A. Kauppinen, Age-related changes in AMPK activation: Role for AMPK phosphatases and inhibitory phosphorylation by upstream signaling pathways. *Ageing research reviews* **28**, 15-26 (2016).

43. J. S. Oakhill, J. W. Scott, B. E. Kemp, AMPK functions as an adenylate charge-regulated protein kinase. *Trends Endocrinol Metab* **23**, 125-132 (2012).

44. D. G. Hardie, M. L. Ashford, AMPK: regulating energy balance at the cellular and whole body levels. *Physiology (Bethesda)* **29**, 99-107 (2014).

45. L. Chen *et al.*, Structural insight into the autoinhibition mechanism of AMP-activated protein kinase. *Nature* **459**, 1146-1149 (2009).

46. X. Li *et al.*, Structural basis of AMPK regulation by adenine nucleotides and glycogen. *Cell Res* **25**, 50-66 (2015).

47. A. Salminen, K. Kaarniranta, AMP-activated protein kinase (AMPK) controls the aging process via an integrated signaling network. *Ageing research reviews* **11**, 230-241 (2012).

48. C. M. McCay, Effect of Restricted Feeding Upon Aging and Chronic Diseases in Rats and Dogs. *American Journal of Public Health and the Nations Health* **37**, 521-528 (1947).

49. R. M. Anderson, R. Weindruch, Metabolic reprogramming, caloric restriction and aging. *Trends Endocrinol Metab* **21**, 134-141 (2010).

50. C. Canto, J. Auwerx, Caloric restriction, SIRT1 and longevity. *Trends Endocrinol Metab* **20**, 325-331 (2009).

51. E. L. Greer, A. Brunet, Different dietary restriction regimens extend lifespan by both independent and overlapping genetic pathways in C. elegans. *Aging cell* **8**, 113-127 (2009).

52. R. M. Reznick *et al.*, Aging-associated reductions in AMP-activated protein kinase activity and mitochondrial biogenesis. *Cell metabolism* **5**, 151-156 (2007).

53. V. Ljubicic, D. A. Hood, Diminished contraction-induced intracellular signaling towards mitochondrial biogenesis in aged skeletal muscle. *Aging Cell* **8**, 394-404 (2009).

54. F. Liu *et al.*, Age-related changes in AMP-activated protein kinase after stroke. *Age (Dordr)* **34**, 157-168 (2012).

55. W. Qiang, K. Weiqiang, Z. Qing, Z. Pengju, L. Yi, Aging impairs insulin-stimulated glucose uptake in rat skeletal muscle via suppressing AMPKα. *Experimental &Amp; Molecular Medicine* **39**, 535 (2007).

56. S. Turdi *et al.*, AMP-activated protein kinase deficiency exacerbates aging-induced myocardial contractile dysfunction. *Aging cell* **9**, 592-606 (2010).

57. Y. Zhang *et al.*, Mitochondrial aldehyde dehydrogenase 2 accentuates aging-induced cardiac remodeling and contractile dysfunction: role of AMPK, Sirt1, and mitochondrial function. *Free Radic Biol Med* **71**, 208-220 (2014).

58. M. Li *et al.*, Reduced AMPK-ACC and mTOR signaling in muscle from older men, and effect of resistance exercise. *Mechanisms of ageing and development* **133**, 655-664 (2012).

59. Y. Zang, L. F. Yu, F. J. Nan, L. Y. Feng, J. Li, AMP-activated protein kinase is involved in neural stem cell growth suppression and cell cycle arrest by 5-aminoimidazole-4-carboxamide-1-beta-D-ribofuranoside and glucose deprivation by down-regulating phospho-retinoblastoma protein and cyclin D. *The Journal of biological chemistry* **284**, 6175-6184 (2009).

60. H. R. Park, K. H. Kong, B. P. Yu, M. P. Mattson, J. Lee, Resveratrol inhibits the proliferation of neural progenitor cells and hippocampal neurogenesis. *The Journal of biological chemistry* **287**, 42588-42600 (2012).

61. Y. Togashi *et al.*, Evaluation of the appropriateness of using glucometers for measuring the blood glucose levels in mice. *Sci Rep* **6**, 25465 (2016).

62. J. E. Ayala *et al.*, Standard operating procedures for describing and performing metabolic tests of glucose homeostasis in mice. *Dis Model Mech* **3**, 525-534 (2010).

63. K. Jin *et al.*, Neurogenesis in dentate subgranular zone and rostral subventricular zone after focal cerebral ischemia in the rat. *Proc Natl Acad Sci U S A* **98**, 4710-4715 (2001).

64. F. Sun *et al.*, Notch1 signaling modulates neuronal progenitor activity in the subventricular zone in response to aging and focal ischemia. *Aging cell* **12**, 978-987 (2013).

65. X. Wang, X. Mao, L. Xie, D. A. Greenberg, K. Jin, Involvement of Notch1 signaling in neurogenesis in the subventricular zone of normal and ischemic rat brain in vivo. *J Cereb Blood Flow Metab* **29**, 1644-1654 (2009).

66. F. Ortega *et al.*, Using an adherent cell culture of the mouse subependymal zone to study the behavior of adult neural stem cells on a single-cell level. *Nat Protoc* **6**, 1847-1859 (2011).

67. D. L. Williamson, D. R. Bolster, S. R. Kimball, L. S. Jefferson, Time course changes in signaling pathways and protein synthesis in C2C12 myotubes following AMPK activation by AICAR. *American journal of physiology. Endocrinology and metabolism* **291**, E80-89 (2006).

68. A. M. Turnley *et al.*, Cellular distribution and developmental expression of AMP-activated protein kinase isoforms in mouse central nervous system. *Journal of neurochemistry* **72**, 1707-1716 (1999).

69. G. Gao *et al.*, Catalytic subunits of the porcine and rat 5'-AMP-activated protein kinase are members of the SNF1 protein kinase family. *Biochimica et biophysica acta* **1266**, 73-82 (1995).

70. C. Culmsee, J. Monnig, B. E. Kemp, M. P. Mattson, AMP-activated protein kinase is highly expressed in neurons in the developing rat brain and promotes neuronal survival following glucose deprivation. *J Mol Neurosci* **17**, 45-58 (2001).

71. B. Dasgupta *et al.*, The AMPK beta2 subunit is required for energy homeostasis during metabolic stress. *Molecular and cellular biology* **32**, 2837-2848 (2012).

72. E. K. Kim *et al.*, C75, a fatty acid synthase inhibitor, reduces food intake via hypothalamic AMP-activated protein kinase. *The Journal of biological chemistry* **279**, 19970-19976 (2004).

73. J. Mu, E. R. Barton, M. J. Birnbaum, Selective suppression of AMP-activated protein kinase in skeletal muscle: update on 'lazy mice'. *Biochem Soc Trans* **31**, 236-241 (2003).

74. M. C. Towler, D. G. Hardie, AMP-activated protein kinase in metabolic control and insulin signaling. *Circ Res* **100**, 328-341 (2007).

75. I. Salt *et al.*, AMP-activated protein kinase: greater AMP dependence, and preferential nuclear localization, of complexes containing the alpha2 isoform. *Biochem J* **334 (Pt 1)**, 177-187 (1998).

76. H. Ai *et al.*, Effect of fiber type and nutritional state on AICAR- and contraction-stimulated glucose transport in rat muscle. *American journal of physiology. Endocrinology and metabolism* **282**, E1291-1300 (2002).

77. T. Quentin *et al.*, Different expression of the catalytic alpha subunits of the AMP activated protein kinase--an immunohistochemical study in human tissue. *Histol Histopathol* **26**, 589-596 (2011).

78. L. D. McCullough *et al.*, Pharmacological inhibition of AMP-activated protein kinase provides neuroprotection in stroke. *The Journal of biological chemistry* **280**, 20493-20502 (2005).

79. J. Li, Z. Zeng, B. Viollet, G. V. Ronnett, L. D. McCullough, Neuroprotective effects of adenosine monophosphate-activated protein kinase inhibition and gene deletion in stroke. *Stroke* **38**, 2992-2999 (2007).

80. V. Vingtdeux, P. Davies, D. W. Dickson, P. Marambaud, AMPK is abnormally activated in tangle- and pre-tangle-bearing neurons in Alzheimer's disease and other tauopathies. *Acta neuropathologica* **121**, 337-349 (2011).

81. M. Domise *et al.*, AMP-activated protein kinase modulates tau phosphorylation and tau pathology in vivo. *Sci Rep* **6**, 26758 (2016).

82. T. Ma *et al.*, Inhibition of AMP-activated protein kinase signaling alleviates impairments in hippocampal synaptic plasticity induced by amyloid beta. *J Neurosci* **34**, 12230-12238 (2014).

83. S. L. Peng *et al.*, Age-related increase of resting metabolic rate in the human brain. *Neuroimage* **98**, 176-183 (2014).

84. J. D. Mulligan, A. A. Gonzalez, R. Kumar, A. J. Davis, K. W. Saupe, Aging elevates basal adenosine monophosphate-activated protein kinase (AMPK) activity and eliminates hypoxic activation of AMPK in mouse liver. *J Gerontol A Biol Sci Med Sci* **60**, 21-27 (2005).

85. Q. Jin *et al.*, Differential regulation of phosphatidylinositol 3-kinase/Akt, mitogen-activated protein kinase, and AMP-activated protein kinase pathways during menadione-induced oxidative stress in the kidney of young and old rats. *Biochem Biophys Res Commun* **315**, 555-561 (2004).

86. M. C. Schmidt, R. R. McCartney, beta-subunits of Snf1 kinase are required for kinase function and substrate definition. *The EMBO journal* **19**, 4936-4943 (2000).

87. A. Suzuki *et al.*, Leptin stimulates fatty acid oxidation and peroxisome proliferator-activated receptor alpha gene expression in mouse C2C12 myoblasts by changing the subcellular localization of the alpha2 form of AMP-activated protein kinase. *Molecular and cellular biology* **27**, 4317-4327 (2007).

88. S. Krishan, D. R. Richardson, S. Sahni, Adenosine monophosphate-activated kinase and its key role in catabolism: structure, regulation, biological activity, and pharmacological activation. *Molecular pharmacology* **87**, 363-377 (2015).

89. Z. Chen *et al.*, Expression of the AMP-activated protein kinase beta1 and beta2 subunits in skeletal muscle. *FEBS letters* **460**, 343-348 (1999).

90. B. Dasgupta, J. Milbrandt, AMP-activated protein kinase phosphorylates retinoblastoma protein to control mammalian brain development. *Developmental cell* **16**, 256-270 (2009).

91. A. Takano, T. Endo, T. Yoshihisa, tRNA actively shuttles between the nucleus and cytosol in yeast. *Science* **309**, 140-142 (2005).

92. R. B. Kopito, M. Elbaum, Reversibility in nucleocytoplasmic transport. *Proc Natl Acad Sci U S A* **104**, 12743-12748 (2007).

93. L. Zhang, S. Borthakur, M. Buck, Dissociation of a Dynamic Protein Complex Studied by All-Atom Molecular Simulations. *Biophysical journal* **110**, 877-886 (2016).

94. T. K. Lee *et al.*, A dynamically assembled cell wall synthesis machinery buffers cell growth. *Proc Natl Acad Sci U S A* **111**, 4554-4559 (2014).

95. P. J. Marangos *et al.*, Adenosinergic modulation of homocysteine-induced seizures in mice. *Epilepsia* **31**, 239-246 (1990).

96. G. Zhou *et al.*, Role of AMP-activated protein kinase in mechanism of metformin action. *J Clin Invest* **108**, 1167-1174 (2001).

97. N. Handa *et al.*, Structural basis for compound C inhibition of the human AMP-activated protein kinase alpha2 subunit kinase domain. *Acta Crystallogr D Biol Crystallogr* **67**, 480-487 (2011).

98. P. van Wijngaarden, R. J. Franklin, Ageing stem and progenitor cells: implications for rejuvenation of the central nervous system. *Development* **140**, 2562-2575 (2013).

99. S. Lugert *et al.*, Quiescent and active hippocampal neural stem cells with distinct morphologies respond selectively to physiological and pathological stimuli and aging. *Cell stem cell* **6**, 445-456 (2010).

100. J. Kim, G. Yang, Y. Kim, J. Kim, J. Ha, AMPK activators: mechanisms of action and physiological activities. *Exp Mol Med* **48**, e224 (2016).

101. B. Xiao *et al.*, Structural basis for AMP binding to mammalian AMP-activated protein kinase. *Nature* **449**, 496-500 (2007).

102. T. Kobilo *et al.*, AMPK agonist AICAR improves cognition and motor coordination in young and aged mice. *Learn Mem* **21**, 119-126 (2014).

103. T. Kobilo, C. Yuan, H. van Praag, Endurance factors improve hippocampal neurogenesis and spatial memory in mice. *Learn Mem* **18**, 103-107 (2011).

104. P. Bi, S. Kuang, Notch signaling as a novel regulator of metabolism. *Trends Endocrinol Metab* **26**, 248-255 (2015).

105. P. Bi *et al.*, Inhibition of Notch signaling promotes browning of white adipose tissue and ameliorates obesity. *Nature medicine* **20**, 911-918 (2014).

106. U. B. Pajvani *et al.*, Inhibition of Notch signaling ameliorates insulin resistance in a FoxO1-dependent manner. *Nature medicine* **17**, 961-967 (2011).

107. U. B. Pajvani *et al.*, Inhibition of Notch uncouples Akt activation from hepatic lipid accumulation by decreasing mTorc1 stability. *Nature medicine* **19**, 1054-1060 (2013).

108. C. Y. Ma *et al.*, SIRT1 suppresses self-renewal of adult hippocampal neural stem cells. *Development* **141**, 4697-4709 (2014).

109. T. Prozorovski *et al.*, Sirt1 contributes critically to the redox-dependent fate of neural progenitors. *Nature cell biology* **10**, 385-394 (2008).

110. K. D. Tipton, Gender differences in protein metabolism. *Current opinion in clinical nutrition and metabolic care* **4**, 493-498 (2001).

111. C. Roepstorff *et al.*, Higher skeletal muscle alpha2AMPK activation and lower energy charge and fat oxidation in men than in women during submaximal exercise. *The Journal of physiology* **574**, 125-138 (2006).

112. Y. Lipovka *et al.*, Oestrogen receptors interact with the alpha-catalytic subunit of AMP-activated protein kinase. *Biosci Rep* **35**, (2015).

113. G. S. Kim *et al.*, Critical role of sphingosine-1-phosphate receptor-2 in the disruption of cerebrovascular integrity in experimental stroke. *Nat Commun* **6**, 7893 (2015).

114. R. Rattan, S. Giri, A. K. Singh, I. Singh, 5-Aminoimidazole-4-carboxamide-1-beta-D-ribofuranoside inhibits cancer cell proliferation in vitro and in vivo via AMP-activated protein kinase. *The Journal of biological chemistry* **280**, 39582-39593 (2005).

115. D. Guo *et al.*, The AMPK agonist AICAR inhibits the growth of EGFRvIII-expressing glioblastomas by inhibiting lipogenesis. *Proc Natl Acad Sci U S A* **106**, 12932-12937 (2009).

116. J. Li, S. E. Benashski, C. Siegel, F. Liu, L. D. McCullough, Adenosine monophosphate activated protein kinase inhibition is protective in both sexes after experimental stroke. *Neurosci Lett* **482**, 62-65 (2010).

117. R. M. Koffie *et al.*, Nanoparticles enhance brain delivery of blood-brain barrier-impermeable probes for in vivo optical and magnetic resonance imaging. *Proc Natl Acad Sci U S A* **108**, 18837-18842 (2011).

118. V. R. Venna, J. Li, S. E. Benashski, S. Tarabishy, L. D. McCullough, Preconditioning induces sustained neuroprotection by downregulation of adenosine 5'-monophosphate-activated protein kinase. *Neuroscience* **201**, 280-287 (2012).

119. Y. Guo *et al.*, AMPK inhibition blocks ROS-NFkappaB signaling and attenuates endotoxemia-induced liver injury. *PloS one* **9**, e86881 (2014).